University of Stavanger

Faculty of Science and Technology

MASTER'S THESIS

Study program: MSc in Offshore Technology Specialization: Marine and Subsea Technology	Spring semester, 2015 Open access
Writer: Velarasan Masilamani	…… (Writer's signature)
Faculty supervisor: Ove Tobias Gudmestad External supervisor(s):	
Thesis title: Vortex Induced Vibration (VIV) Analysis of Subsea Jumper Spools	
Credits (ECTS): 30	
Key words: Vortex Induced Vibration (VIV) Subsea Jumper Spools Finite Element Analysis ANSYS DNV-RP-F105 DNV-RP-C203 Fatigue Life Assessment	Pages: 75 + enclosure: 125 Stavanger, June 15, 2015

ABSTRACT

Subsea rigid jumpers are usually rigid steel pipe sections that provide the interface between subsea structures, such as pipelines to manifolds, trees to flowlines and pipelines to risers. Each jumper shall be designed such that it is flexible enough to allow the expansion and contraction of the flowline or the pipeline due to the change in pressure rating and/or end thermal expansion and to accommodate the installation misalignment. In addition, the subsea jumper design should also be rigid enough to meet the external environmental loads.

The ability of the jumper system to accommodate these loads is achieved through its design procedure, which includes strength and fatigue analysis. The former defines the required configuration of the jumper system based on the end displacement tolerance requirements, with the least flexibility possible and the latter helps to determine the fatigue life of the system to satisfy the design life. Based on the field specific conditions and end displacement requirements, any geometry of the jumper can be used in the field architecture. The usual types of jumper configurations used in the industry are free span, M-shape, Z-shape and inverted U-shaped.

Although some designers consider these jumper systems as static elements, they are in fact susceptible to fatigue loading. This arises from the complex jumper configurations with longer unsupported lengths of the pipe section. Though the complexity is advantageous with regard to the displacement tolerance, they bring their own unique challenges from a fatigue loading perspective.

The objective of this project is to perform a sensitivity study, of the fatigue damage due to vortex induced vibration (VIV), on the typical subsea jumper system. Even though there are other modes, which can cause fatigue damage to the jumpers, like the thermal cyclic loading from flowlines, slugging effect and fluid induced vibrations, this report is confined only to the fatigue damage due to VIV. A comprehensive study of a specific case has been carried out to demonstrate the effects of VIV on a subsea jumper spool. The results are extended to general spool geometries whenever possible. The sensitivity study will assess the key parameters, like the jumper configuration, seabed current velocity and the angle of the current flow to understand the case specific severity of the fatigue damage. This analysis is performed based on the background principle followed in DNV-RP-F105 and using the finite element analysis (FEA) tool ANSYS.

Based on the observations from the sensitivity study, we understand that from the fatigue life of the typical jumper system, we can define the case specific critical length of the jumper. This critical length identification helps to understand the cases that require the use of the VIV mitigation measures. It is also observed that for the same jumper configuration under the same seabed current condition, the fatigue life would be different based on the angle of current flow and the yearly probability of occurrence of the seabed current velocity.

ACKNOWLEDGEMENT

I take this opportunity to express my sincere gratitude to the following persons for their valuable contribution and support, in helping me to turn this thesis thought into a valuable piece of work.

First and foremost, my heartfelt gratitude to my supervisor Professor **Ove T. Gudmestad,** who in-spite of being extraordinarily busy with his duties, took time out to hear and guide my thesis throughout the period. The tasks that are accomplished in this work would have never been possible without his advice and suggestions. Without his comments and remarks, the presentation of this report could have never been perfected. Of all the above, he has always been a person of inspiration to me, to challenge the challenges in life.

Secondly, I would like to express my deepest thanks to **Dr. Daniel Karunakaran** for his suggestions on the documents to refer, to understand the physics behind the work and also for his advice on framing the work. My special thanks to **Mr. Goutam Marath** of J P Kenny, who introduced me to this topic and also supported me all the way to accomplish the tasks.

Furthermore, I express my radiant sentiment of thanks to my parents, for their love, affection, moral support and guidance throughout my life. Last but not least, I thank all my friends of Stavanger, who made my stay in Norway a fun-filled and magnificent one, with lots of memories to carry for the rest of my life.

Finally, I would like to devote all my credits of this thesis work to GOD, who provided me good health and living, throughout the way in completing this thesis.

ABBREVIATIONS

ROV	Remotely Operated Vehicle
DP	Dynamic Positioning
RAO	Response Amplitude Operator
NB	Nominal Bore
O.D	Outside Diameter
SMYS	Specified Minimum Yield Strength
CDF	Cumulative Density Function
IL	In-Line

Table of Contents

List of Tables

List of Figures

CHAPTER-1

INTRODUCTION

1.1 Background

In the oil and gas industry, pipelines are used to transport the hydrocarbons from the source to the destination. Based on the type of the function involved, these pipelines can vary from a small bore inter-field flowline to a large bore trunk export pipeline. Normally, when these pipelines are installed in the field, the final connection between the pipeline end termination (PLET) and the destination is performed through the use of a Tie-in spool. This is due to the pipeline installation limitations from the various field specific factors.

Therefore, these tie-in spools should also satisfy the design life requirement of the pipelines, in order to ensure that it performs its intended purpose, without any hydrocarbon leakage, though out the service life. Even though, the mechanical design of the jumper, which depends on the following factors like,

- Pipeline end thermal movement
- Pipeline installation misalignment and
- Connecting hubs reaction force limitations

satisfies the design life of the system, through proper selection of the jumper configuration and integrity checks. It is also necessary to make sure that the fatigue life of the jumper satisfies the design life requirement. This is because, the occurrence of seabed current, makes the large unsupported configuration of the jumpers, more prone to vibrations, which can result in fatigue damage of the system.

Based on the jumper configuration and the seabed current profile involved, the severity of the jumper fatigue life would differ. Therefore, it is always a must to make sure that the jumper system satisfies the fatigue life requirements in addition to the mechanical design integrity checks for design life.

1.2 Motivation

Even though VIV assessment of long, slender structures may be considered sufficiently mature, it is noted lately that the industry is increasingly considering complex jumper systems, wherein the structure may comprise of pipe sections of various orientations. However, there are currently neither a guideline for the design like the DNV-RP-F105, which presents the free spanning analysis for the subsea pipelines, nor a prominent software such as FatFree (DNV software) or Shear7, which are specially designed for the riser systems, that may directly be used to estimate

the VIV fatigue damage for the non-straight pipe configurations like in the case of subsea jumpers.

1.3 Scope

As mentioned in the section-1 of DNV-RP-F105,

"Basic principles may also be applied to more complex cross sections such as pipe-in-pipe, bundles, flexible pipes and umbilicals"

"The fundamental principles given in this RP may also be applied and extended to other offshore elements such as cylindrical structural elements of the jacket….."

This thesis is performed based on the basic free spanning principle, as mentioned in DNV-RP-F105 and it also using the finite element analysis (FEA) tool ANSYS.

The purpose of this thesis is to,

- Perform a sensitivity study on the fatigue life of the typical jumper system due to the VIV phenomenon.
- Observe the fatigue life variation based on the assessment of the key parameters like jumper configuration, seabed current and the angle of the current flow.
- Compare the fatigue life of the same system under the same seabed current condition, but based on the difference in the yearly probability of current velocity occurrence.
- Discuss about the variation in the critical length of the jumper based on the case specific conditions with respect to the angle of the current flow.
- Conclude the results from the sensitivity study and make future recommendations of possible work extension.

1.4 Limitation

Since, this thesis is performed for a typical M-shaped jumper configuration the results of this work involve the following limitations,

- Percentage of occurrence of the in-line oscillation under a cross-flow excitation mode (or) the cross-flow oscillation under an in-line excitation mode.
- Any change in the angle of current flow, from either pure in-plane (or) out-of-plane current flow.
- Any change in the field specific environmental condition, content of transport and configuration of the jumper, from the assumed conditions in this work.
- Any change in the safety zone classification, based on the location of operation.

1.5 Organization of the Report

Since, the phenomenon of the VIV on a complex structure like the subsea jumpers is not focused much on the academic section. This report will help to understand not only the physics behind the VIV phenomenon, but also the method of its application for the jumper systems based on the industrial available sources. This report has been organized such that, it starts from the overview of the pipelines to understand the usage of the tie-in spools and it gradually proceeds to how the fatigue damage due to the VIV varies based on the probability of occurrence. The synopsis of core chapters, before deriving the discussion and conclusion from the sensitivity analysis observations are given below.

Chapter-2 Overview of the Pipelines & Tie-in Spools

- Usage & Classification of the Pipelines.
- Design requirements & Installation types of the Pipelines.
- Usage & types of the Tie-in spools.
- Sequence of Installation of the Tie-in spool connection to the seabed structure.

Chapter-3 VIV Phenomenon

- Physics & the factors influencing the vortex formation & its intensity.
- Parameters that defines the intensity of the vortices.
- Physics behind the "Lock-in" phenomenon.
- Possible types of VIV & its range of occurrence.

Chapter-4 Analysis Methodology

- Performance of the modal analysis using the FEA tool ANSYS.
- Performance of the VIV Analysis, which includes,
  - Modelling of the Environment.
  - Modelling of the response amplitude based on the DNV-RP-F105 guidelines.
  - Selection of the criterion which demands the detailed fatigue analysis.
  - Detailed fatigue life assessment based on the DNV-RP-C203 guidelines.

Chapter-5 Assumptions

- Defines the limitations that the considered system has, from that of the real case scenario.

Chapter-6 Sensitivity Analysis

- Check the cases & the configuration of the jumpers that satisfies the "Lock-in" condition.
- Comparison of the oscillation type difference based on the type of the current flow.
- Evaluate the variation in the fatigue life based on the jumper configuration & the type of the seabed current involved.
- Observe the difference in the fatigue life based on the yearly probability of the current occurrence.

CHAPTER-2

OVERVIEW OF THE PIPELINES AND TIE-IN SPOOLS

2.1 Pipelines

In the oil and gas industry, Pipelines are one of the ways to transport a fluid that is chemically stable like the crude (or) refined petroleum, from one place to the other, that are physically separated by a long distance. In general, the industry uses three essential ways of transportation, which includes,

- Tanker/Shuttle – Here, the fluid is filled and sealed in the tanks and transported to the required destination.
- Pipelines – Here, the fluid is pumped along the pipeline that is constructed between the source and the destination.
- Combination – This works in combination with either of the above two methods, here the fluid is transformed into either a solid or to another fluid form and then it is transported through either of the above two methods.

The preference to choose the pipelines, over any other types of transportation is due to the advantages listed below,

- The oil spill rate in the case of the pipelines is less than any other type of transportation.
- The cost involved in the oil and gas transported through the pipeline is less in comparison to the others.
- Pipelines are much safe and environment friendly.
- Least energy requirement.
- Low maintenance cost.
- High reliability and
- Minimal impact on the land use pattern.

2.2 Classification of Offshore Pipelines

Based on the nature of the fluid that is transported, pipelines can be termed as, (see figure: 1) (Bai & Bai, 2012 & Guo, Song, Chacko & Ghalambor, 2005),

- Export pipelines – These transport either refined (or) crude products (oil and gas) from the production facility platforms to the shore terminal facilities.
- Flow-lines – These transport oil and/or gas from the satellite subsea wells to the subsea manifolds, from subsea manifolds to production facility platforms and also between production facility platforms.

- Water or chemical injection flow-lines – These transport either water or flow assurance chemicals, from the production facility platforms to the injection wellheads, through the subsea injection manifolds.
- Pipeline bundles.

2.3 Pipeline Design

Since, the primary purpose of the pipeline in the oil and gas industry, is to transport the fluids from the source to the destination, then the main objective is to make sure that the pipeline is designed to meet all its requirements throughout its service life, like the integrity check for the internal and external pressure condition, on-bottom stability and free span assessment, pressure drop evaluation across the flow and all its operating condition stresses satisfying the allowable limits specified by the industry standards. The analysis performed to verify that the stresses experienced by the pipeline are within allowable includes, (Bai & Bai, 2005)

- Hoop stress
- Longitudinal stress
- Equivalent stress
- Span analysis and vortex shedding
- Expansion analysis
- Buckling analysis
- Crossing analysis

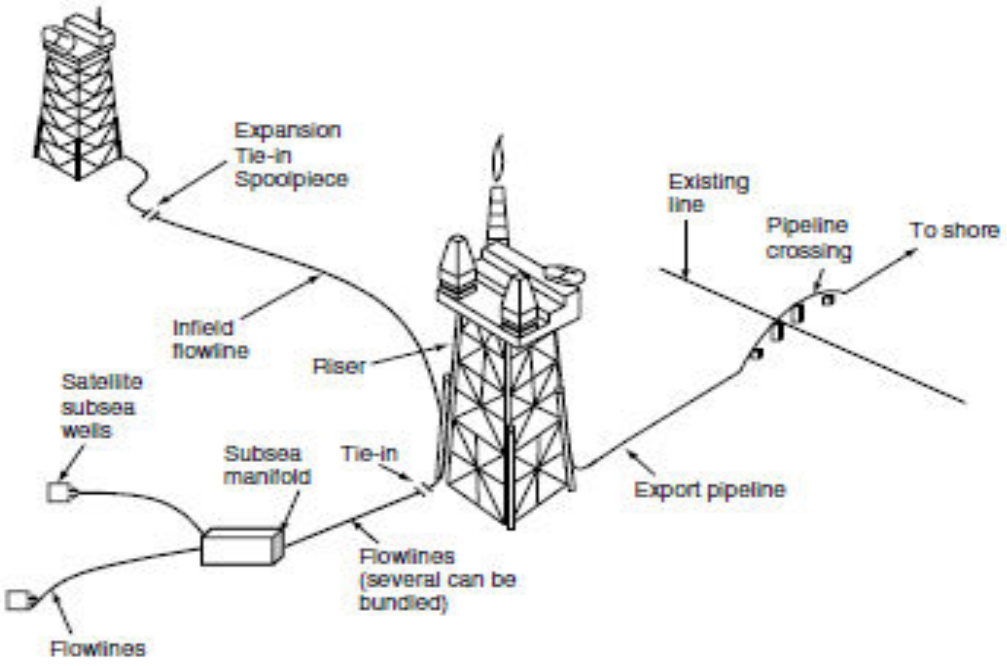

Figure 1 - Types of Pipelines (Guo et al., 2005)

2.4 Pipeline Installation

Once the pipeline is designed, constructed and fabricated. It is then transported and installed at the site by one of the several installation methods available, which includes, (Guo et al., 2005)

- S-lay
- J-lay
- Reel barge and
- Tow-in

2.4.1 S-lay

In this type, the laying barge has its own, several welding stations on the deck, enabling the crew to weld together 40 to 80 foot lengths of insulated pipe in a dry environment which is away from the wind and rain. As the barge moves forward, the welded length of the pipe starts to ease off the stern of the barge. The lay vessel continues to move until the pipe moves down the sea and reaches the touchdown point. Once it reaches the touchdown point, more pipe been laid out the stern with the installation generating a normal S-shape along the pipeline (See figure: 2). In order to avoid damage to the pipeline while installation, due to excess bending stress, a stringer is used on the stern layout position and a tensioning roller with controlled forward thrust is also used to avoid the damage caused by the buckling of the pipe. This method of pipe lay been used over a range of water depths from shallow to deep.

2.4.2 J-lay

Here, the pipe is welded along a tall tower on the stern of the lay vessel and then the welded section of the pipe is dropped vertically down through the sea until it reaches the touchdown point. As the vessel moves further, once after the touchdown, the pipeline along its length generates the profile of the normal J-shape (See figure: 3). Since, this method avoids some difficulties, such as tensile load and forward thrust as in S-lay type, this can be used in deep water conditions.

2.4.3 Reel barge

For smaller diameter pipelines, this method is economical, as the pipe can be constructed, fabricated and wound around the reel, on the onshore facility. This method is employed in combination with the above two methods, where the horizontal reel is coupled with the S-lay type and the vertical reel is coupled with the J-lay type.

2.4.4 Tow-in

There are four types of tow-in method of installation, they are,

- Surface tow
- Mid-depth tow
- Off-bottom tow and
- Bottom tow

2.4.4.1 Surface tow

In this type, the pipeline is towed to the site between the two towboats with the buoyancy modules being added to the pipeline so that it floats on the surface while towing. Once it arrives to the site, the modules are removed (or) the pipeline is flooded so that the pipeline settles to the sea floor (See figure: 4).

2.4.4.2 Mid-depth tow

Here, the pipeline settles to the sea floor on its own, when the forward progress of the tow-boat ceases. It requires, lesser buoyancy modules than in the case of surface tow (See figure: 5).

2.4.4.3 Off-bottom tow

It involves a combination of buoyancy modules and chains, as added mass on the pipeline. Once the pipeline is towed to the location, the buoyancy modules are removed and it automatically settles on the bottom, due to the added mass of the chains (See figure: 6).

2.4.4.4 Bottom tow

In this case, the pipeline is allowed to sink and settle on the sea floor, it is then towed all the way along the sea bottom up to the site location. This method is usually practiced for flat and soft sea floors in shallow waters (See figure: 7).

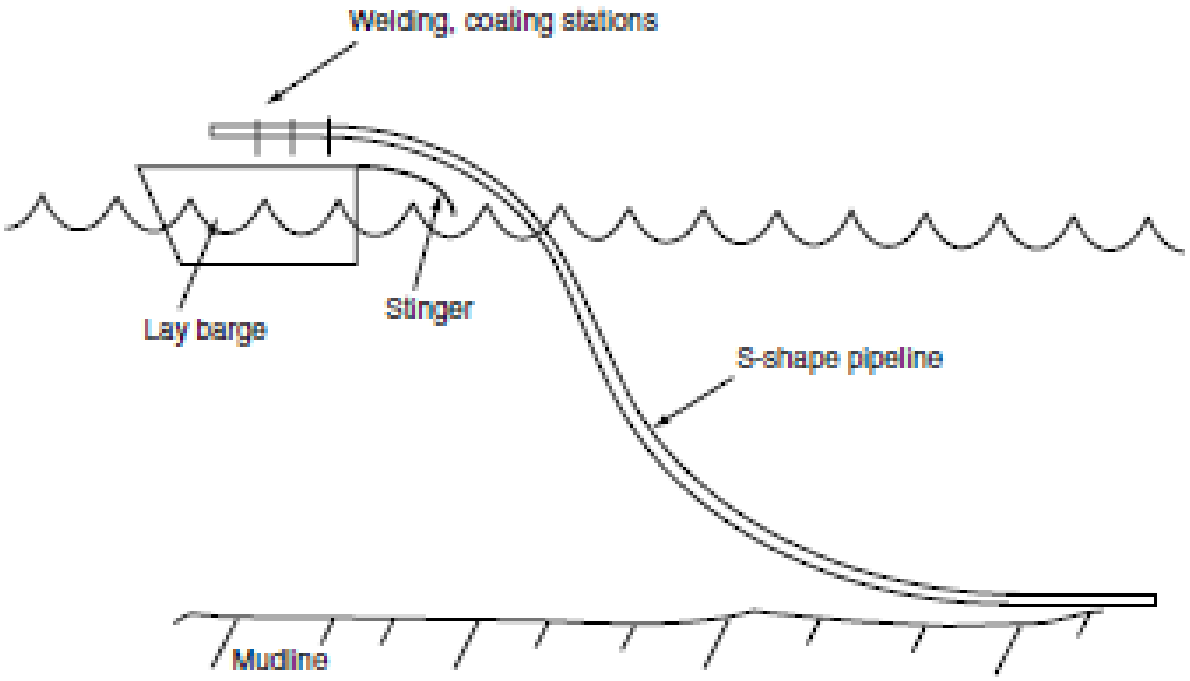

Figure 2- S-Lay Method of Pipeline Installation (Guo et al., 2005)

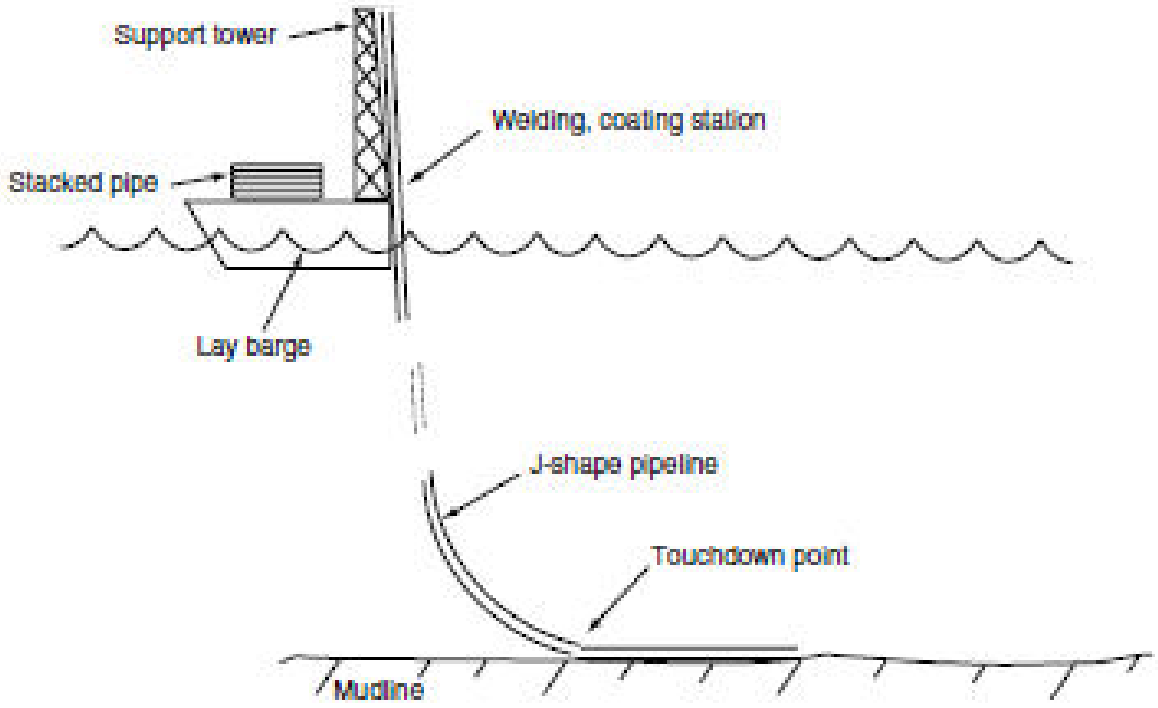

Figure 3 - J-Lay Method of Pipeline Installation (Guo et al., 2005)

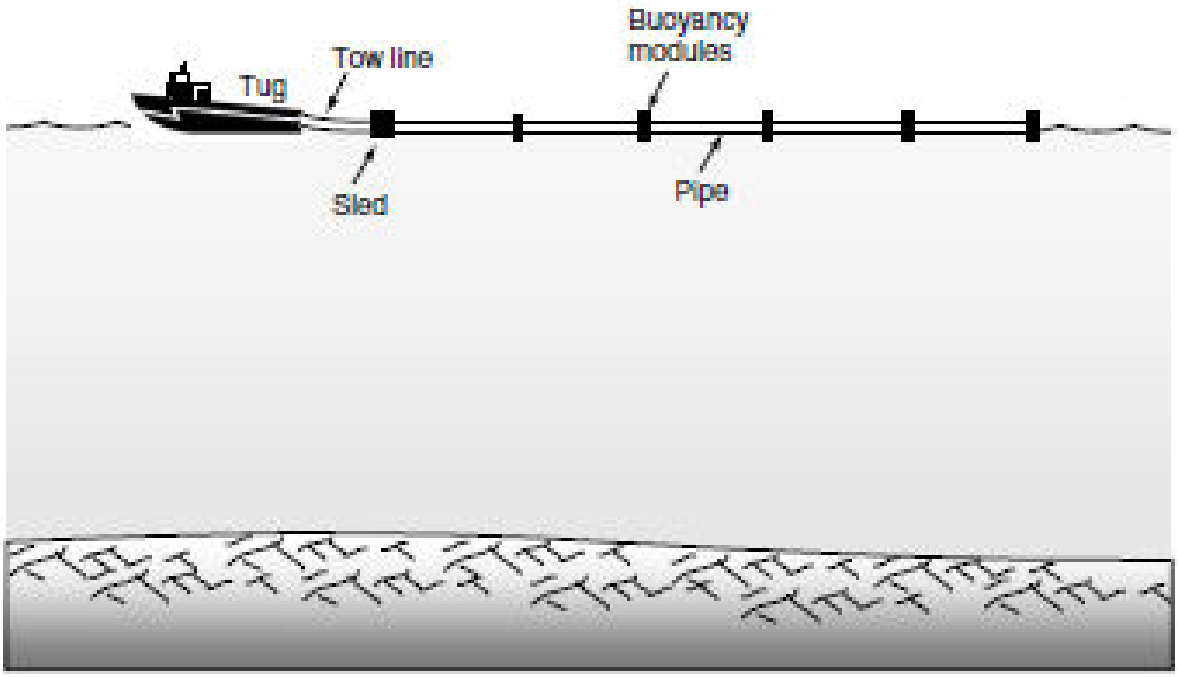

Figure 4 - Surface Tow Method of Pipeline Installation (Guo et al., 2005)

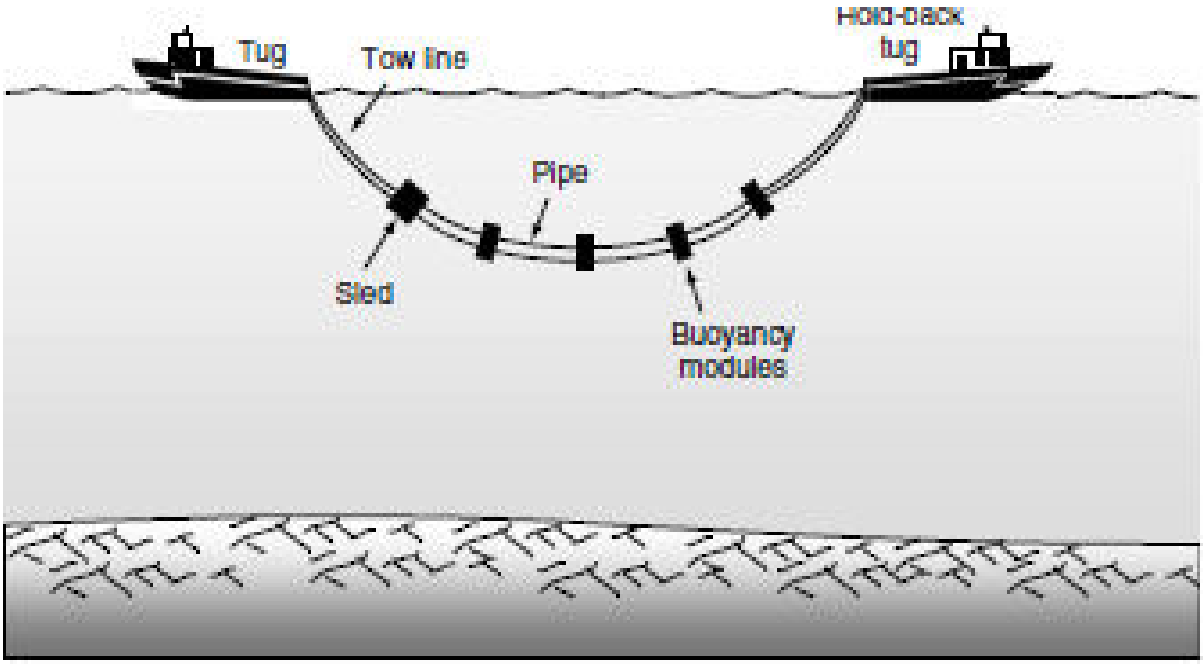

Figure 5 - Mid-Depth Tow Method of Pipeline Installation (Guo et al., 2005)

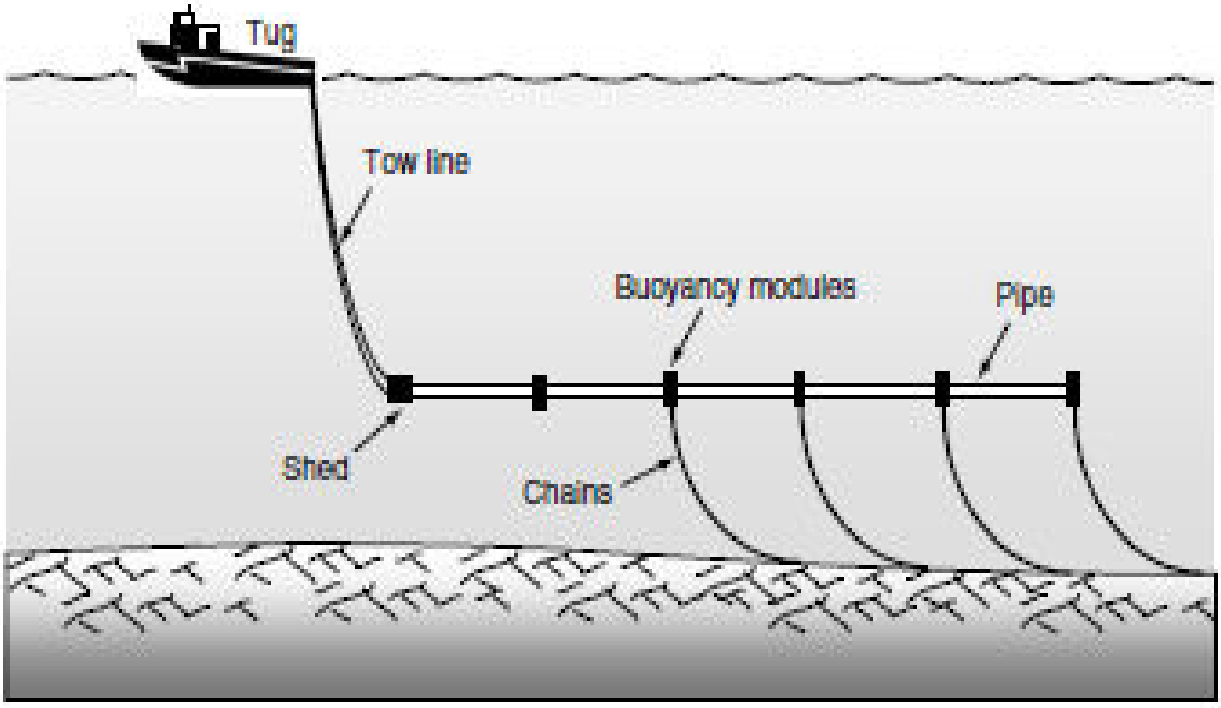

Figure 6 - Off-Bottom Tow Method of Pipeline Installation (Guo et al., 2005)

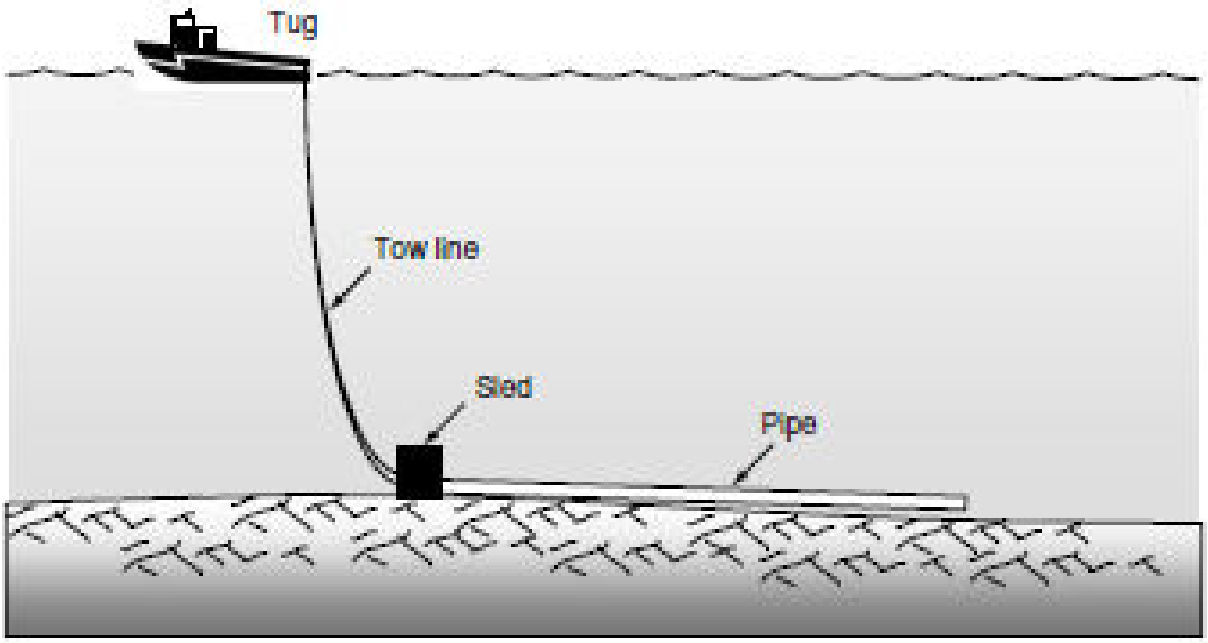

Figure 7 - Bottom Tow Method of Pipeline Installation (Guo et al., 2005)

2.5 Pipeline Stresses

Once the installed pipeline comes into operation, the pipeline, which is a form of a pressure vessel, will experience some stresses due to differential pressure and temperature, between the pipeline operating condition and the surrounding medium. These stresses act both circumferential and longitudinal to the pipeline. The component of the stress acting along the circumference is due to the pressure differential in the pipeline. This stress buildup is usually restrained by the integrity of the pipeline. This also helps to understand that to which category does the pipeline belongs to, whether is it thin walled (or) thick walled pipeline. Another component of the stress acting along the longitudinal axis of the pipeline arises from the temperature gradient between the maximum operating temperature in the pipeline and the minimum installed temperature. The longitudinal strain of the pipeline in general is given by equation 2.5 (a), (Palmer & King, 2004 & Guo et al., 2005)

$$\varepsilon_t = \alpha_t * \Delta T \ldots\ldots\ldots\ldots\ldots \text{Eqn 2.5 (a)}$$

Here,

$\alpha_t = Co.efficient\ of\ Thermal\ Expansion\ of\ the\ pipeline\ material\ at\ operating\ temp.$

$\Delta T = Differential\ temperature\ between\ operating\ and\ installed\ condition = T_2 - T_1$

$\varepsilon_t = Longitudinal\ Strain$

If incase, the generated longitudinal strain due to temperature difference is restrained ($\varepsilon_t = 0$) by the boundary conditions of the pipeline then the corresponding longitudinal stress generated is represented by equation 2.5 (b),

$$\sigma = -E * \alpha_t * \Delta T \ldots\ldots\ldots\ldots\ldots \text{Eqn 2.5 (b)}$$

Here,

$\sigma = Longitudinal\ Stress\ due\ to\ thermal\ expansion$

$E = Young'sModulus\ of\ the\ material$

The negative sign of stress indicates that for an increase in the temperature of the system under restrained condition, the stress developed at the boundary conditions is compressive in nature. If the system involves a decrease in temperature, then the type of stress turns to be tensile. Based on the type of system boundary condition (unrestrained, partially restrained (or) restrained), an effect due to soil friction (Soft, loose, clay, etc.,), degree of restrains involved (1/2/3 directional restrained) and the end cap effect, the magnitude of the above general longitudinal stress and strain differs.

2.6 Tie-in Spools

Usually the installed pipelines will not be in direct connection with the tie-in structures due to the following constraints,

- Installation limitations due to existing facilities like platforms/semi-submersibles/drilling rigs.
- Installation inaccuracy due to uncertainty from the seabed bathymetry.
- Installation limitations from the seabed conditions like the existing pipelines, seabed structures like manifolds, wellheads, mooring lines etc.,
- Pipeline thermal expansion forces under operation.

Due to the above mentioned constraints, the pipelines are connected to the target tie-in structures of the platform, through a special piece of pipe arrangement termed “Tie-in spool”. These Tie-in spools are usually made from steel pipes, connecting subsea architectures such as, pipelines, Pipeline End Termination (PLET), Subsea trees, flowlines, manifolds and riser base via subsea connectors. The functional requirement of each of the jumper involved shall differ based on the fluid internal pressure rating, longitudinal thermal expansion involved, external environmental pressure, installation requirements etc.,

Once the pipeline end is laid on the seabed, subsea metrology study is conducted to establish, the connecting distance between the terminal and the tie-in structure, seabed trench details, horizontal and the vertical orientation of the connecting hubs, pitch, roll and azimuth angle details. In addition to the above details, pipeline thermal expansion data are also required for the design of the tie-in spools.

The ultimate purpose of using the tie-in spool will include the following,

- Accommodate the pipeline installation inaccuracy.
- Reduced/allowable reaction forces on the connecting hubs.
- Hydrocarbon leak prevention due to excessive reaction forces that can lead to damage.
- Accommodate the pipeline longitudinal strain due to differential temperature.

In order to meet the above requirements, the installed tie-in spool should be flexible enough. But, the rigidity of the tie-in spools (Jumpers) also becomes a critical factor of consideration, as the additional length of doglegs to the jumper configuration may result in an increased unsupported length condition this causes the jumpers to have a low Eigen frequency, even though it improves the flexibility of the system. This increased unsupported length of the system, makes it more prone to vortex induced vibration (VIV), due to the existence of sea bottom current. This VIV can account for one of the possible fatigue damage in the system, lowering its expected service life.

2.7 Types of Tie-in Spools

The subsea oil and gas industry have developed using a variety of tie-in spool systems in the past decades, ranging from horizontal tie-in systems with bolted flange connections to until collet connected vertical tie-in's. From an installation perspective, the horizontal types are installed using diver dominated activities in shallow water conditions, whereas the same are being installed using the remote (ROV) systems in case of deep water applications, in order to connect the pipeline with the fixed riser nearby the platform, whereas in the case of the vertical spools, they are always installed using the guideline deployment method with the help of ROV's.

2.7.1 Vertical Tie-in Systems

These types of jumpers are mainly adopted in the Gulf of Mexico region, with relatively simple deployment, operation involving short tie-in duration and low reliance on the ROV to perform the task. Since, the guideline method is used to deploy these types of jumpers the dependence on the weather to perform the operation is relatively high. Maximizing the operational window can be achieved through the use of relatively high specification DP vessel with stable RAO characteristics. The vertical nature, size and connection type of these spools may demand higher accuracy on metrology data, higher connector complexity due to increased tooling, involving heavier connection and higher crane height to deploy using the guided mechanism.

These jumpers can usually be characterized by either an inverted U (or) M-shaped configuration. In addition, there is also horizontal Z-shaped style and so on. The configuration of the jumper to be used depends on the following characteristics,

- Design parameters of the field.
- Type of interface with the subsea structure and
- The different operational modes

Even after finalizing the configuration, the change of direction of the profile can be achieved either by using the bend structures (or) elbows. This option again depends on certain requirements like,

- Stress based flexibility.
- Span based rigidness.
- Space constraint, etc.,

2.7.2 Horizontal Tie-in Systems

These types of jumpers involve relatively complex deployment, operation involving long tie-in duration and high reliance on the ROV to perform the task. Since, the spreader beam method is used to deploy these jumpers the dependence on the weather to perform the operation is

relatively low. As, the operation is independent of the vessel motion, this result in the usage of the low specification DP vessel with a large deck space and a crane vessel of lower capacity and height requirement for the spool deployment. The horizontal nature, smaller size and the connection type of these spools may demand medium accuracy on metrology data. Any possibility of error on the seabed measurement can be compensated through stroking length adjustments of the spool, once it lands on the seabed, with the help of the simple and lighter connecting flanges.

The various steps involved in the installation of the horizontal jumper are listed below,

- The horizontal tie-in system is hooked up to a spreader beam and then it is deployed, to until it is lowered up to a few meters above the target area seabed as shown in figure 8.
- The spool is lowered until the stab on the first termination head enters the stab receptacle on the tie-in porch as shown in the figure 9 (a).
- The second termination head will align horizontally as the spool continues to be lowered until the stab enters the stab receptacle and lands on the tie-in porch.
- The connector actuation tool (CAT) is landed and locked on the first termination head by the ROV as shown in figure 9 (b).
- The termination head is leveled and locked in the horizontal position. The protection caps are removed from the connector and the inboard hub as shown in the figure 9 (c).
- The termination head is stroked against the inboard hub and the connection is closed as shown in the figure 9 (d).
- A pressure test is carried out to check for the integrity of the connector seal and then the CAT is unlocked and lifted from the termination head and inboard hub.
- The connection procedure is repeated for the second termination head to the inboard hub without returning the CAT to the surface vessel.

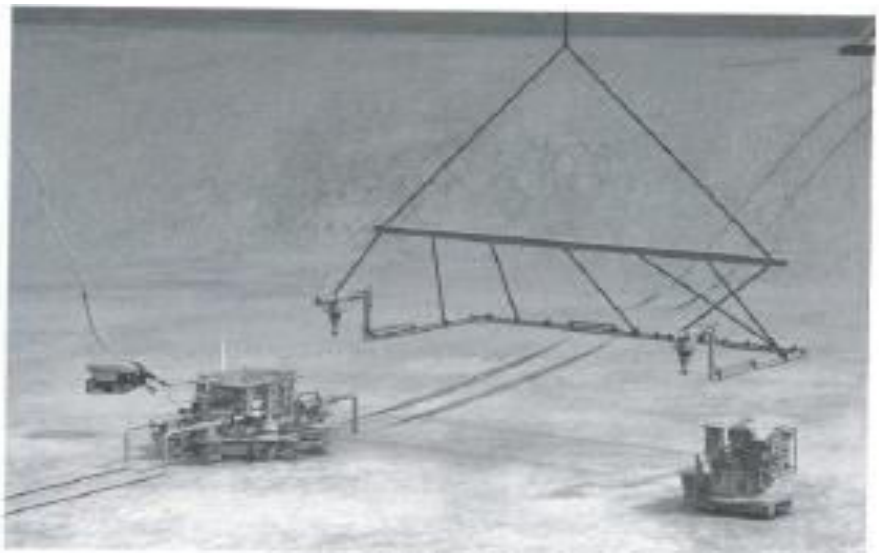

Figure 8 – Horizontal tie-in system (Bai & Bai, 2012)

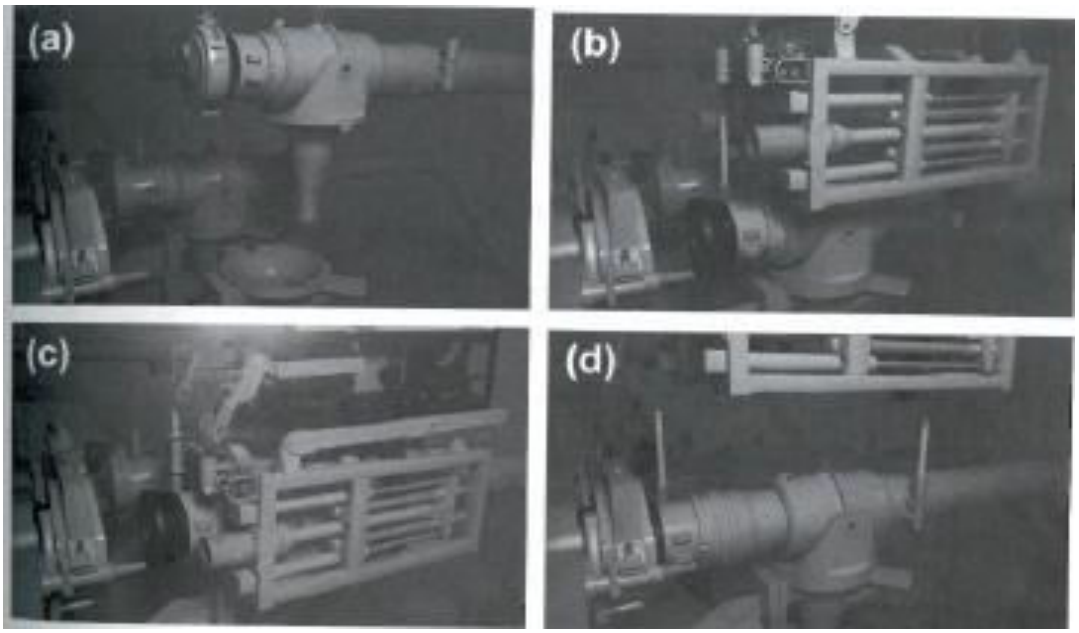

Figure 9 – Sequence of installation for horizontal tie-in system (Bai & Bai, 2012)

Thus, this chapter has provided an insight into the usage based classification of the pipelines, their design requirements and the different pipeline installation methods available. Even though, we understand from this chapter that, the installation limitations of the pipeline have introduced the use of the tie-in spools, their design requirements are mainly the pipeline thermal expansion and the pipeline installation inaccuracy data. This chapter has also provided information about the types of tie-in spools available and a comparison between them to understand the case specific use of the type.

CHAPTER 3

VIV PHENOMENON

3.1 Vortex Formation

Whenever a structure is introduced into a flowing medium, it disturbs the regular (undisturbed) medium flow as an obstacle along its path. This makes the medium to exert some force on the structure based on the water particle velocity and acceleration. Just like the fluid force, the structure will also exert an equal and opposite force to the fluid. The level of the resistive force and the impact made by the fluid force on the structure depends on the material strength of the structure. For a structure with light weight material of construction, the resistance to the applied force will be less and eventually they deform more compared with the structures that are made of heavy material. As they deform they change their orientation with respect to the fluid medium resulting in different magnitude of force acting on them. On the other hand when the structure resistive force is high enough to the fluid exerted force, then it results in the generation of stronger wakes on the downstream side. The phase and pattern of generation of these wakes depends on the fluid characteristics under consideration and also to some extent on the considered structure roughness. These wakes (vortices) formed on the downstream will generate low pressure zone on the side of the vortex formation and tend the structure to oscillate (vibrate) based on the flow of energy principle from high pressure to low pressure. These are termed as Vortex Induced Vibrations (VIV). These vibrations are usually considered as the secondary design load conditions with the life condition of up to least until damage has been made. With the progress of the oil discovery to remote, harsh and deep water depths, the installation limitations influence the engineers to utilize the maximum material limit of the structure, making them more lighter, flexible and more prone to vortex induced vibrations.

3.1.1 Factors Influencing Vortex Induced Vibrations

The occurrence and level of impact due to the vortex induced vibrations depends on the following factors,

- Upstream fluid characteristics
- Fluid-Structure interface criterions and
- Structural properties

3.1.2 Physics behind Vortex Formation

When the fluid particles flow from a free stream towards the leading edge of the stationary structure (in our case it is the jumper cylinder), its pressure will develop from its free stream pressure to its stagnation pressure. This high pressure of the fluid particle will impel the fluid to

flow across the cylinder forming a boundary layer zone on the fluid cylinder interface, as a result of the viscous friction. Normally, the velocity profile on the boundary layer will increase gradually from zero at the contact point to until upstream free flow velocity far away from the boundary layer the fluid is usually treated as in-viscid at this region (Prandtl, 1904). This distribution of velocity intensity depends on the boundary layer thickness which depends on the viscosity of the fluid involved. As the viscosity increases, the boundary layer becomes thicker. The boundary layer usually tends to develop along the transverse length (x) of the fluid flow and is usually a function proportional to √x. The boundary layer thickness is the distance normal to the fluid flow from the point of contact to until the flow velocity would be 99% of the upstream undisturbed free stream velocity (Newman, 1977). This is given in the equation 3.1.2,

$$U\,(y) = 0.99\,U_c \ldots\ldots\ldots\ldots\ldots Eqn.\,3.1.2$$

Here,

$U\,(y) = Current\ velocity\ at\ the\ outer\ limit\ of\ the\ boundary\ layer\ thickness\ \left(\frac{m}{s}\right)$

$U_c = Free\ stream\ steady\ current\ velocity\ on\ the\ upstream\ \left(\frac{m}{s}\right)$

However, the pressure developed based on the upstream free stream velocity is not high enough to get the flow to until the back of the cylinder forming a complete boundary zone even at high Reynolds number condition. Thus, the flow starts to separate from the cylinder at the widest possible section of the cylinder (Blevins, 2001). This sheared flow of the fluid will have two different velocity zones once it is sheared off, one near the cylinder shear off point where the velocity is less and another one at a distance from the sheared off flow along the stream behind the cylinder where the velocity is much higher compared to the former. This difference in velocity makes the vortices on the downstream to swirl and form vortices and circulation into large discrete vortices which form alternatively on opposite sides of the considered cylinder (Perry, Chong & Lim (1982), Williamson & Roshko, (1988)). At one certain stage of this vortex development on the downstream, the strength of the vortex becomes sufficiently large to pull the opposite sided vortex to shed from the cylinder. From then the increase in strength of the vortices stops as it get utilized for vortices shedding further and the phenomenon of vortex shedding on the downstream continues alternatively (Kenny, 1993).

3.1.3 Factors Influencing Vortices Intensity

Based on the vortex formation physics, the main characteristics determining the vortex intensity and their pattern of formation on the downstream are,

- Velocity of the fluid (defining the free stream pressure)
- Viscosity of the fluid (defining the differential velocity)

- Diameter of the cylinder (defining both the stagnation pressure impact, resistive force and the differential pressure)
- Cylinder roughness (defining the differential pressure)

3.2 Parameters to define the vortex significance

There are three categories of parameters that are used to define the significance of the vortex being shed on the downstream. They are,

i. Fluid Parameters
ii. Fluid-Structure Interface (FSI) Parameters and
iii. Structure Parameters

The individual parameters and their influence on vortices intensities are detailed in the following sections.

3.2.1 Fluid Parameters

The parameters that involve the properties and characteristics of the upstream fluid medium which can impact change on the vortex shedding on the downstream are included under this.

3.2.1.1 Reynolds Number (Re)

The parameter that relates the first three vortex intensity characteristics in section 3.1.3 being the Reynolds number, which helps in describing the flow pattern under various flow conditions for a steady flow with similar streamlines around the cylinder (Schlichting, 1968).The expression is given in equation 3.2.1.1,

$$Re = \frac{Inertia\ Force}{Viscous\ Force} = \frac{U_c * D}{\nu} (Dimensionless) \dots\dots\dots\dots\dots\dots Eqn\ 3.2.1.1$$

Here,

$D = Outer\ Diameter\ of\ the\ circular\ cylinder\ (m)$

$\nu = Kinematic\ viscosity\ of\ the\ fluid\ \left(\frac{m^2}{s}\right)$

The difference in the vortex pattern as a function of the Reynolds number is represented in the figure 10.

3.2.1.2 Keulegen-Carpenter Number (KC)

If the system is exposed to a harmonic oscillating flow (i.e., waves) then the influence of the added mass on the vortex shedding pattern of the system due to the acceleration of the fluid

particle around the cylinder is to be taken into account. The addition of this acceleration component to the constant velocity case like in Reynolds number case makes the understanding of vortex pattern more complex as the wave induced current velocity changes with time and this leads to a new parameter called "Keulegen-Carpenter" number to understand the vortex pattern under combined case (Keulegan & Carpenter, 1958).

$$KC = \frac{U_m}{f_w * D} (Dimensionless) \dots\dots\dots\dots\dots Eqn\ 3.2.1.2$$

Here,

$U_m = U_c + U_w = Maximum\ water\ particle\ Velocity\ (\frac{m}{s})$

$U_w = Wave\ Velocity\ (\frac{m}{s})$

$f_w = Wave\ Frequency\ (\frac{1}{s})$

In other words, for steady current condition Reynolds number (Re) can define the vortex pattern of the given system, but under combination of steady current and wave induced current condition Keulegen-Carpenter number been used to define the vortex pattern on the downstream.

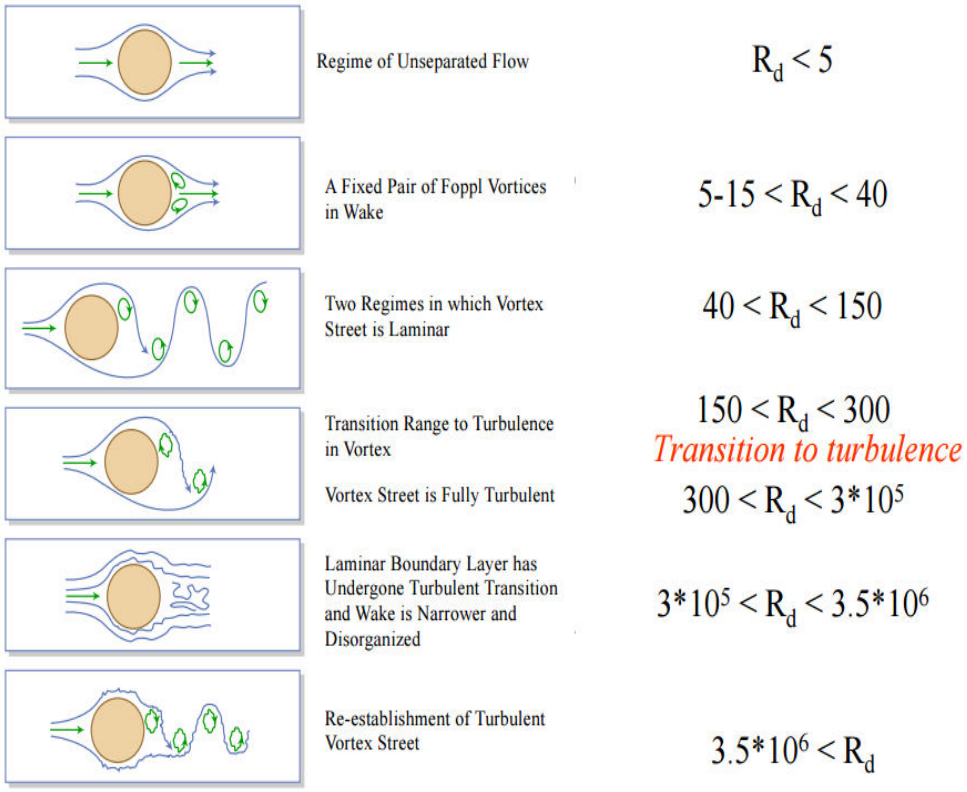

Figure 10 - Variation in vortex pattern based on Reynolds number (Re) (Leinhard, 1966).

3.2.1.3 Current Flow Velocity ratio

In a real sea state, it is not just either wave or current scenario it is always a combination of both. But, in our area of concern near the seabed, the level of wave influence over the current gradually decreases, while moving from a shallow water case to that of ultra-deep water. This current-wave percentage of influence in a considered environment can be determined based on the "Current Flow Velocity" ratio.

$$\alpha = \frac{U_c}{U_c + U_w}(Dimensionless) \dots\dots\dots\dots\dots Eqn\ 3.2.1.3$$

3.2.1.4 Turbulence Intensity

Any fluctuation from the mean fluid flow velocity under considered environmental conditions is defined by the turbulence intensity and is represented by the equation 3.2.1.4,

$$Turbelence\ Intensity = \frac{u_{rms}}{U} \dots\dots\dots\dots\dots Eqn\ 3.2.1.4$$

Here,

$u_{rms} = root\ mean\ square\ of\ flutuating\ velocity = U(t) - U\ (\frac{m}{s})$

$U = Mean\ free\ stream\ fluid\ velocity\ (\frac{m}{s})$

3.2.1.5 Shear Fraction of Flow Profile

The amount of shear in the considered non-uniform fluctuating current profile is usually represented as a fraction to that of the mean velocity case and is defined by the equation 3.2.1.5,

$$Shear\ Fraction = \frac{\Delta U}{U_m}(dimensionless) \dots\dots\dots\dots\dots Eqn.\ 3.2.1.5$$

Here,

$\Delta U = Variation\ of\ the\ velocity = U_m - U_{min}\ (\frac{m}{s})$

$U_{min} = Minimum\ current\ velocity\ in\ the\ current\ profile\ (\frac{m}{s})$

3.2.2 Fluid Structure Interface (FSI) Parameters

Those parameters that define the structural response due to the variation in shedding pattern based on the Fluid Structure Interface (FSI) are listed below.

3.2.2.1 Reduced Velocity

Based on the environmental scenario involved, either it is steady current or a combination of steady current and time dependent wave induced current, the vortices generated on the downstream will influence the system to oscillate based on the differential pressure zone. The velocity at which the vortices are shed on the downstream induce vibration on the system is given by the "Reduced Velocity". This vibration amplitude path length per cycle of oscillation for the given model conditions is given by equation 3.2.2.1 (a) (DNV-RP-F105, 2006).

$$V_r = \frac{U_m}{f_n * D}(Dimensionless) \dots\dots\dots\dots\dots Eqn\ 3.2.2.1\ (a)$$

Here,

$f_n = Natural\ frequency\ of\ the\ system\ vibrational\ mode\ \left(\frac{1}{s}\right)$

The equation 3.2.2.1 (a) makes it clear that in additional to the environmental condition the amplitude of oscillation attains its maximum (critical) state, when the frequency of vibration matches with the natural frequency. This natural frequency of the system depends on the system stiffness, end support conditions, unsupported span length and effective mass of the system. It is represented by equation 3.2.2.1 (b),

$$f_n = \frac{C_e}{2\pi}\sqrt{\frac{E * I}{M_e * {L_s}^4}}\left(\frac{1}{s}\right) \dots\dots\dots\dots\dots Eqn\ 3.2.2.1\ (b)$$

Here,

$C_e = End\ condition\ constant$

$= 9.87\ (Pinned - Pinned)$

$= 15.5(Clamped - Pinned)$

$= 22.2(Clamped - Clamped)$

$E = Modulus\ of\ Elasticity\ \left(\frac{N}{m^2}\right)$

$I = Mass\ Moment\ of\ Inertia\ (m^4)$

$= \frac{\pi}{64}\left({D_o}^4 - {D_i}^4\right)$

$M_e = Effetive\ unit\ mass\ \left(\frac{kg}{m}\right)$

$= M_p + M_c + M_w$

$M_p = Unit\ pipe\ mass\ including\ coating\ \left(\frac{kg}{m}\right)$

$M_c = Unit\ content\ mass\ \left(\frac{kg}{m}\right)$

$M_w = Unit\ mass\ of\ water\ displaced\ by\ the\ system\ \left(\frac{kg}{m}\right)$

$L_s = Unsupported\ net\ span\ length\ of\ the\ system\ (m)$

Depending on the end conditions and the net span length involved in the system under consideration, the natural (Eigen) frequency of the system would differ and the same can be observed from the figure 11.

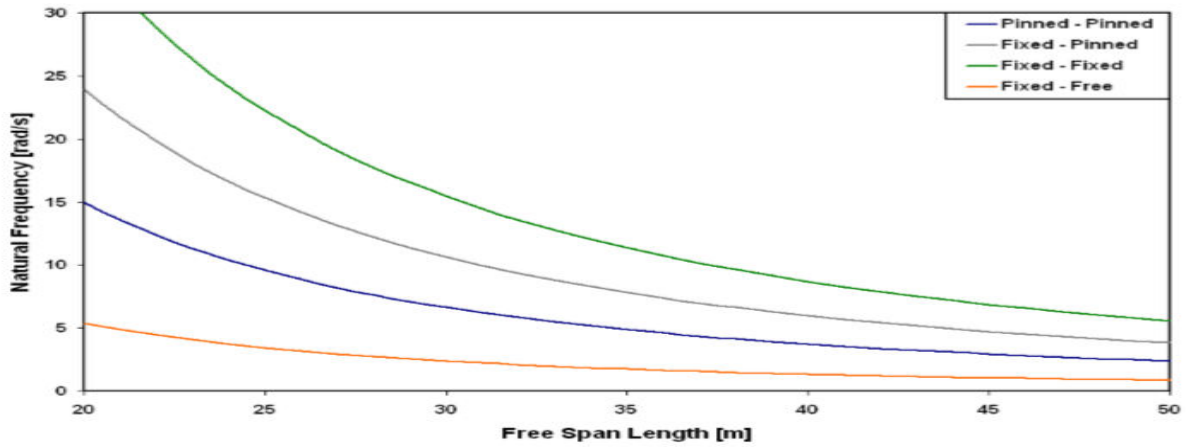

Figure 11 - Variation of the Eigen frequency w.r.t span length under different boundary conditions for a cylinder of O.D = 500 mm (Abeele, Voorde & Goes, 2008).

3.2.2.2 Stability Parameter

The significance of the reduced velocity that will induce motion on the given system is defined by the "Stability Parameter". The developed reduced velocity will not be the same respective of the structural parametric dependence. This influence of the structural factors on the system motion is defined by the "Stability Parameter" (Blevins, 2001). The expression for the same is,

$$K_s = \frac{4 * \pi * M_e * \zeta_t}{\rho * D^2} (Dimensionless) \dots\dots\dots\dots\dots Eqn\ 3.2.2.2$$

Here,

$\rho = water\ density\ \left(\frac{kg}{m^3}\right)$

VIV ANALYSIS OF SUBSEA JUMPER SPOOLS

$\zeta_t = Total\ modal\ damping\ ratio\ (Dimensionless)$

$= \zeta_{str} + \zeta_{soil} + \zeta_h$

$\zeta_{str} = Structural\ damping$

$= 0.005\ (without\ any\ coating)$

$= 0.01 - 0.02\ (with\ coating)$

$\zeta_{soil} = Soil\ damping\ (not\ included\ in\ case\ of\ Jumpers)$

$\zeta_h = Hydrodynamic\ damping$

Based on the above observation, the relation between the reduced velocity and Reynolds number for a cross-flow vibration condition and the relation between the reduced velocity and stability parameter for an in-line flow vibration condition are represented in the figure 12 and 13 respectively.

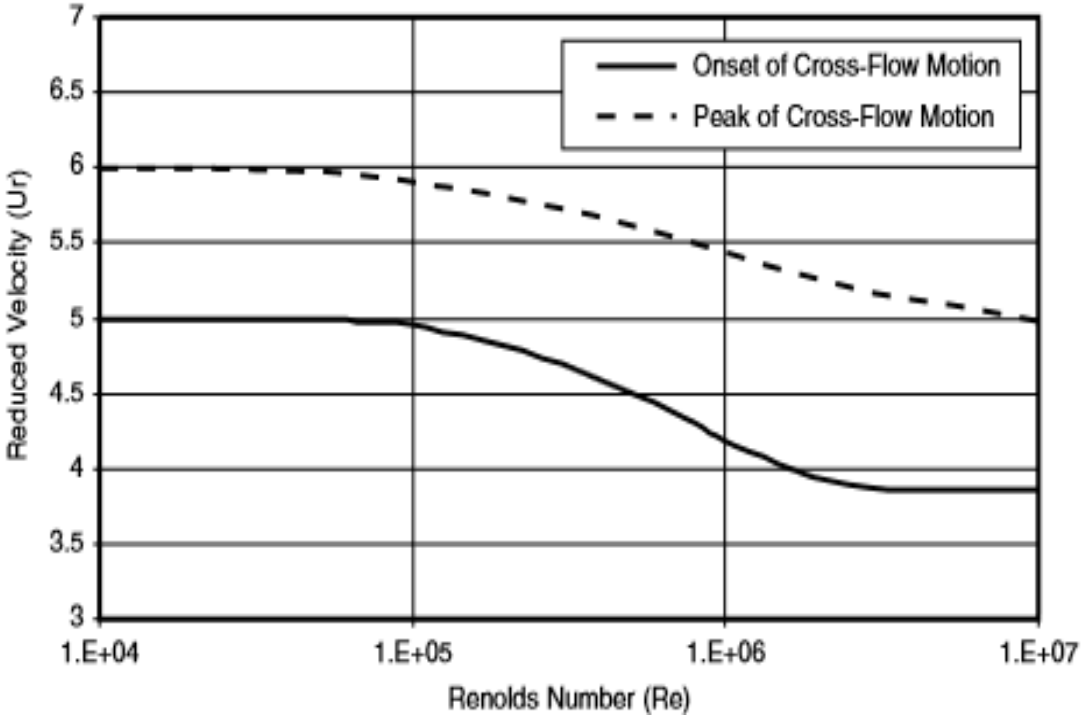

Figure 12 - Cross-Flow Reduced Velocity variation w.r.t Reynolds number (Blevins, 2001)

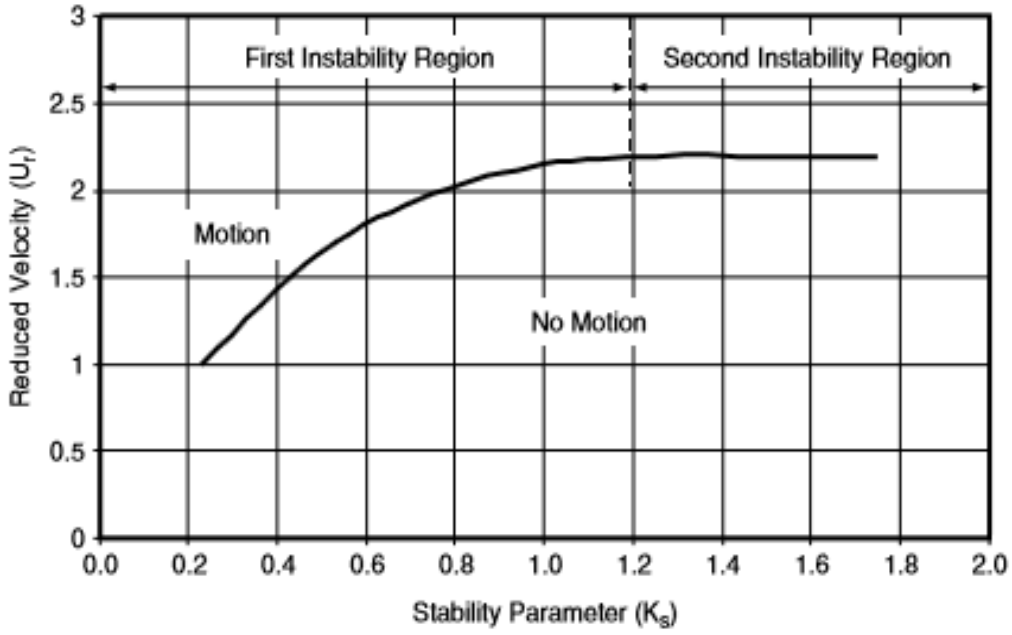

Figure 13 - In-line Reduced Velocity variation w.r.t Stability Parameter (Blevins, 2001)

3.2.2.3 Strouhal Number (S)

The pattern of the vortex shedding also depends to some extent on the cylinder surface roughness as it has some impact on the boundary layer viscous force generation. The frequency of the vortex shedding based on the surface roughness and fluid flow parameters is defined by Strouhal Number (S). It generally brings a relation between the flow velocity, diameter of the structure and frequency of shedding is given in equation 3.2.2.3 (Strouhal, 1878).

$$S = \frac{f_v * D}{U_c} (Dimensionless) \dots\dots\dots\dots\dots\dots Eqn\ 3.2.2.3$$

Here,

$f_v = Vortex\ shedding\ frequency\ (\frac{1}{S})$

The variation in the Strouhal number based on the surface roughness factor for the same Reynolds number can be observed from the figure 14.

In the figure 14, though the Strouhal number corresponding to the transitional regime of the Reynolds number is different based on the roughness factor as a result of the wake instability, usually the vortex induced vibrations of a circular cylinder under transitional regime occurs at a Strouhal number of 0.2 (represented as dotted line in the figure 14) (Coder, 1982).This makes it clear that the vortex shedding pattern on the downstream of the cylinder will remain the same, as the impact due to the surface roughness on pattern is negligible.

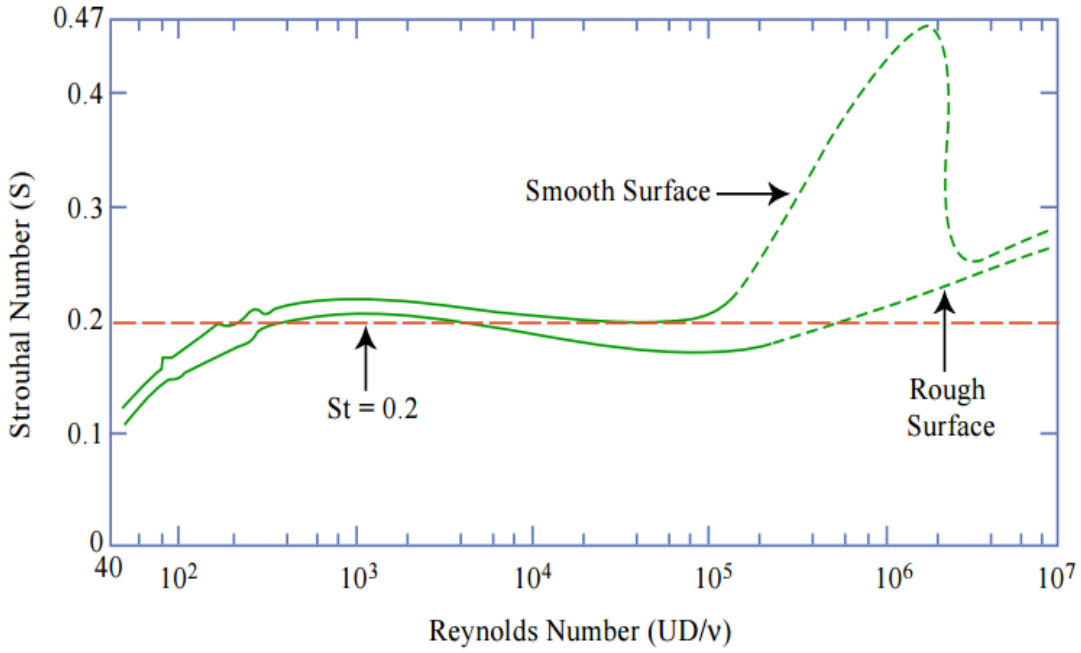

Figure 14 - Variation in Strouhal Number (S) w.r.t Reynolds Number (Re) (Lienhard, 1966; Achenbach & Heinecke, 1981), S ≈ 0.21 (Roshko, 1954).

3.2.3 Structure Parameters

The parameters related to the geometry of the system involved, with its impact on vortex shedding are listed below.

3.2.3.1 Geometry

The geometry of the structure involved is an important parameter as it defines the fluid force been exerted on the object. Usually it is measured in "fineness ratio" which is the ratio of the structure length to its width. The expression is given in equation 3.2.3.1,

$$Fineness\ ratio = \frac{Length}{width/diameter}(dimensionless) \dots\dots\dots\dots\dots Eqn.\ 3.2.3.1$$

3.2.3.2 Mass Ratio

It is usually the ratio of mass of the structure per unit length to the fluid it displaced per unit length. This parameter is important from the categorization of the structure perspective, as lightweight structures are more prone to vibrations. In short, lesser the mass ratio, higher the possibility of flow induced vibrations. The expression for mass ratio is given in equation 3.2.3.2,

$$Mass\ ratio = \frac{m}{\rho D^2} = \frac{Structure\ mass\ per\ length}{fluid\ mass\ per\ length}(dimensionless) \dots\dots Eqn.\ 3.2.3.2$$

3.2.3.3 Damping Factor

It is usually the ratio of the energy dissipated by the structure upon oscillations induced by the vortices to the energy imposed by the fluid upon the structure. It is usually expressed in multiples of the critical damping factor. If the energy imposed by the fluid on the structure is less than the energy it has expended in damping, then the structure will eventually diminish oscillations. The expression of it is given in equation 3.2.3.3,

$$\zeta = \frac{energy\ dissipated\ per\ cycle}{4\pi * total\ energy\ of\ the\ structure} \dots\dots\dots\dots\dots Eqn.\ 3.2.3.3$$

3.3 "Lock-in" Phenomenon

As the system starts to vibrate at a specified frequency and amplitude based on the reduced velocity condition in the initial stage, its Eigen frequency alters due to the change in the system effective mass based on the added mass difference. This Eigen frequency difference is compensated by the change in the vibration frequency of the system which has control over the shedding frequency. When this vibration frequency becomes near, equal or multiples of the stationary shedding frequency, then it results in a critical phenomenon of importance called the "Lock-in" (Blevins, 2001).

Usually every system has a range of reduced velocity for which it has the ability to adjust its Eigen frequency with control over the shedding frequency based on vibration frequency compensation. This range within which the system vibration frequency has the control over the shedding frequency is called the "Lock-in Range".

The phenomenon of "Lock-in" can be mathematically expressed as follows,

The Eigen frequency of the system in terms of reduced velocity is given by,

$$f_n = \frac{U_m}{V_r * D}(Hertz) \dots\dots\dots\dots\dots Eqn\ 3.3\ (a)$$

The shedding frequency of the system in terms of stationary Strouhal number is given by,

$$f_v = \frac{S * U_c}{D}(Hertz) \dots\dots\dots\dots\dots Eqn\ 3.3\ (b)$$

Under the condition of the vibration frequency with control over the shedding frequency the equations 3.3 (a) and (b) are related by,

$$f_n \cong f_v \,(or)\, \frac{U_m}{f_n * D} = \frac{U_c}{f_v * D} => \frac{1}{S} = 5 \ldots\ldots\ldots\ldots\ldots Eqn\ 3.3\ (c)$$

Based on the section 3.2.2.3 input that, vortex induced vibrations for a transitional regime starts around a Strouhal number of 0.2, the reduced velocity corresponding to the onset of the lock-in range will be around 5. But, there are also low frequency regions where this lock-in phenomenon can be observed when the vibration frequency is a sub-multiple of the stationary shedding frequency.

3.4 Types of Vortex Induced Vibrations

The two types of vortex induced motions the system gets exposed to based on the direction of fluid attack relative to the cylindrical axis are,

- In-line VIV
- Cross-Flow VIV

3.4.1 In-line VIV

When the vibration induced in the system for a given modal shape based on the vortex shedding pattern, is translational and along the direction of the fluid attack is defined as “In-line” VIV (Carruth & Cerkovnik, 2007).

Though the amplitude involved in this type of oscillations is only 10% of that in case of cross-flow oscillations due to the force components difference (Guo et al., 2005), these oscillations will take place at a lower vibration frequency than that of the critical frequency in the cross-flow condition. Usually, the system will start to oscillate along the flow direction when the vibration frequency is 1/3rd of its Eigen frequency. The expression for the same is given in equation 3.4.1,

$$f_v = \frac{1}{3} f_n \ldots\ldots\ldots\ldots\ldots Eqn.\ 3.4.1$$

This in-line oscillation frequency gradually increase with increase in the reduced velocity (The theory behind is explained in section the 3.5 in this chapter) and it will reach the lock-in condition when the vibration frequency is one-half of the Eigen frequency.

The first two modes of instability under this type of oscillation have their maximum amplitude response at a reduced velocity of 1.9 and 2.6 respectively and the possibility to prevent them will be by maintaining the stability parameter above 1.8 (Wootton, 1991).

The amplitude response corresponding to a reduced velocity of less than 2.2 makes the shedding remain symmetric and on the other hand for a reduced velocity above 2.2 the shedding changes into alternate type.

3.4.2 Cross-Flow VIV

When the vibration induced in the system for a given modal shape based on the vortex shedding pattern is in two different translational directions and being perpendicular to that of the fluid attack, then it is defined as "Cross-Flow" VIV (Carruth & Cerkovnik, 2007).

Since, these oscillations take place at a vibration frequency much higher than that of the in-line oscillation case, though the amplitude associated are high, these cannot turn into the governing criterion for design in our case as the span length is limited for jumpers. This type of oscillations approach lock-in phenomenon as the vibration frequency is near, equal to (or) multiple of the Eigen frequency.

Normally, when a vortex is shed from the system under an alternate wake pattern, which remain the typical case with transition regime of Reynolds number, forces are generated both in the in-line and cross-flow directions. The amplitude of these in-line and cross-flow oscillation, once a vortex is shed is governed by the dimensionless parameters drag and lift coefficients respectively. The frequency of the cross-flow oscillation is equal to that of the shedding frequency, whereas it is twice the shedding frequency for the in-line oscillations. This is because, inline oscillation are experienced for every single vortex being shed from the cylinder, whereas cross-flow oscillation requires a complete cycle of vortex to be shed. This can be observed in the figure 15 below.

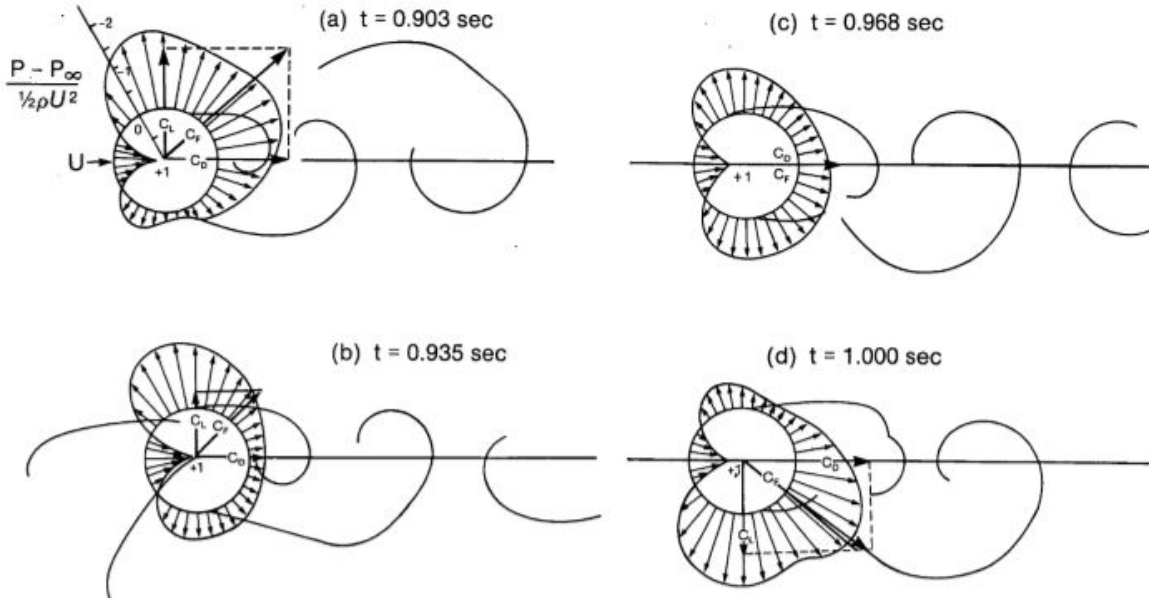

Figure 15 - Wake formation pattern for 1/3rd of the vortex shedding cycle (Drescher, 1956).

Usually systems tend to trace an “8” shaped motion due to vortex induced vibrations (Jauvtis & Williamson, 2003). Under fully developed vortex shed pattern condition, the amplitude of the cross-flow oscillations are much higher when compared to that of the in-line oscillations, but the average force for the cross-flow oscillations are zero as they tend to experience the lift force about the centre of flow to the system, whereas it is not the case for the in-line oscillations, the average force of drag is not zero as it always needs some resistive force against the fluid flow force and the frequency of oscillation is also twice in case of drag when compared to that of the lift forces. .

Based on the type of current involved, whether it is an out-of-plane current or an in-plane current, the nature of the portion of the system geometry exposed to the VIV influence differs. The principle is that, only the portion of the system with its cylindrical axis perpendicular to the flow direction is exposed to VIV.

The difference in the system VIV exposure area based on the out-of-plane and in-plane current for an M-shaped jumper is represented in figure 16 and 17 respectively.

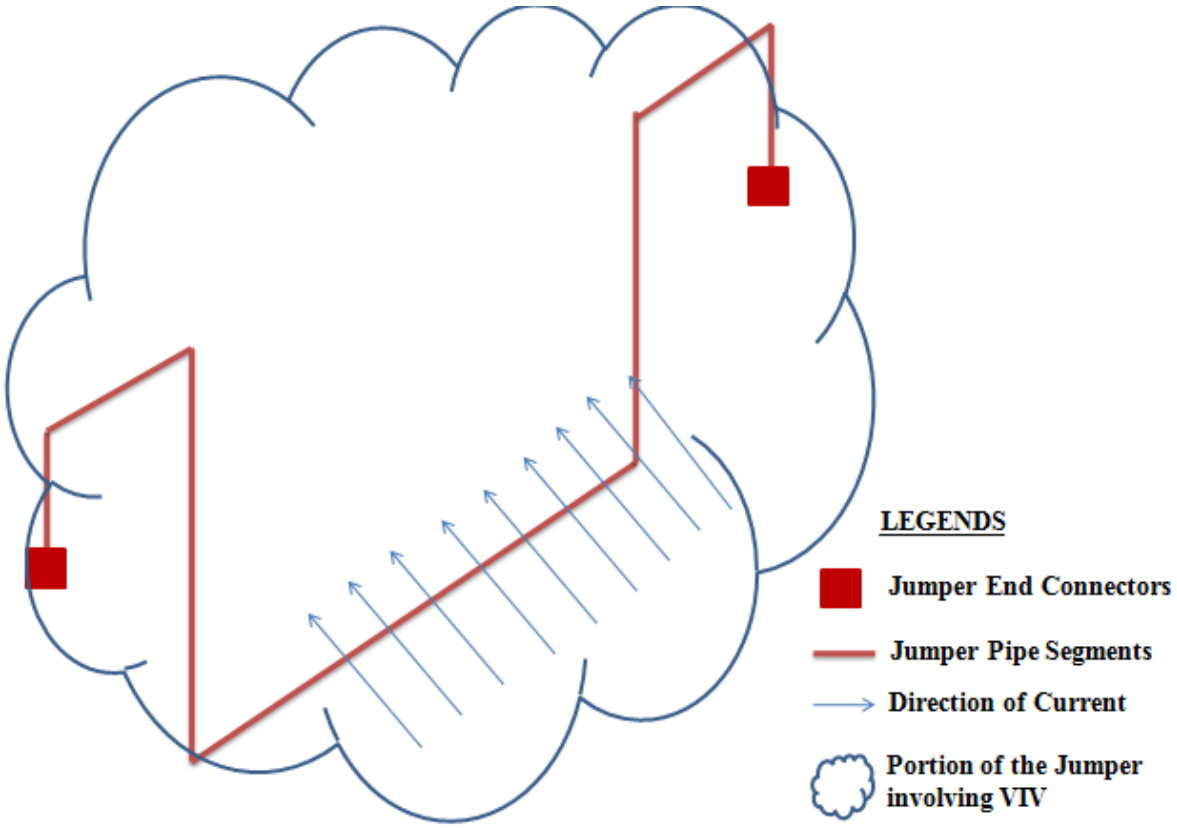

Figure 16 – VIV exposure area of the Jumper for the Out-of-Plane current condition

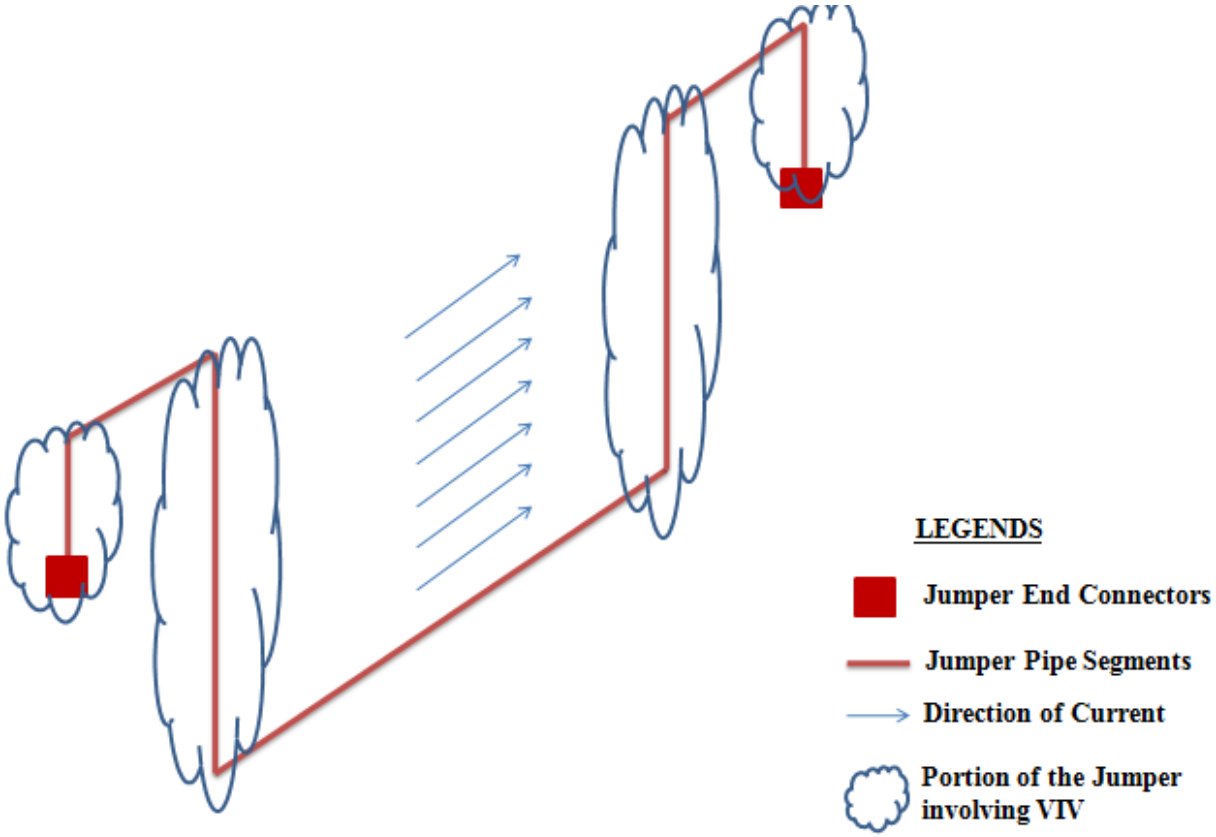

Figure 17 - VIV exposure area of the Jumper for the In-Plane current condition

3.5 Impact of the cylinder oscillatory motion on wakes

Once the shed vortices has induced significant amount of oscillatory motion in the system, the amplitude of these oscillations can bring measurable impact on the wakes pattern generated further and also widen the possibility of "lock-in" which is crucial.

It is conceptual that the oscillatory motion of the system will increase the effective mass of the system through increase in the added mass. This change will bring down the natural frequency of the system from that of the stationary case. It further becomes obvious that structures with lower Eigen frequency are more prone to vibrations, hence it will increase the frequency of the vibration based on increase in their reduced velocity. As the motion induced increases the vibration frequency and decreases the Eigen frequency, the possibility of "Lock-in" gets close. This makes the system more prone to lock-in than predicted based on the stationary case. With increase in the amplitude of oscillation the onset of the "Lock-in" is quicker and the Lock-in range is wider. The figure 18 shows that for higher amplitude cases this lock-in band range is ±40% from that of the stationary condition. This becomes a point of focus for determining the

fatigue damage in the concerned system, as the amplitude of oscillation increases, the stress induced will subsequently increase and reduce the system life drastically.

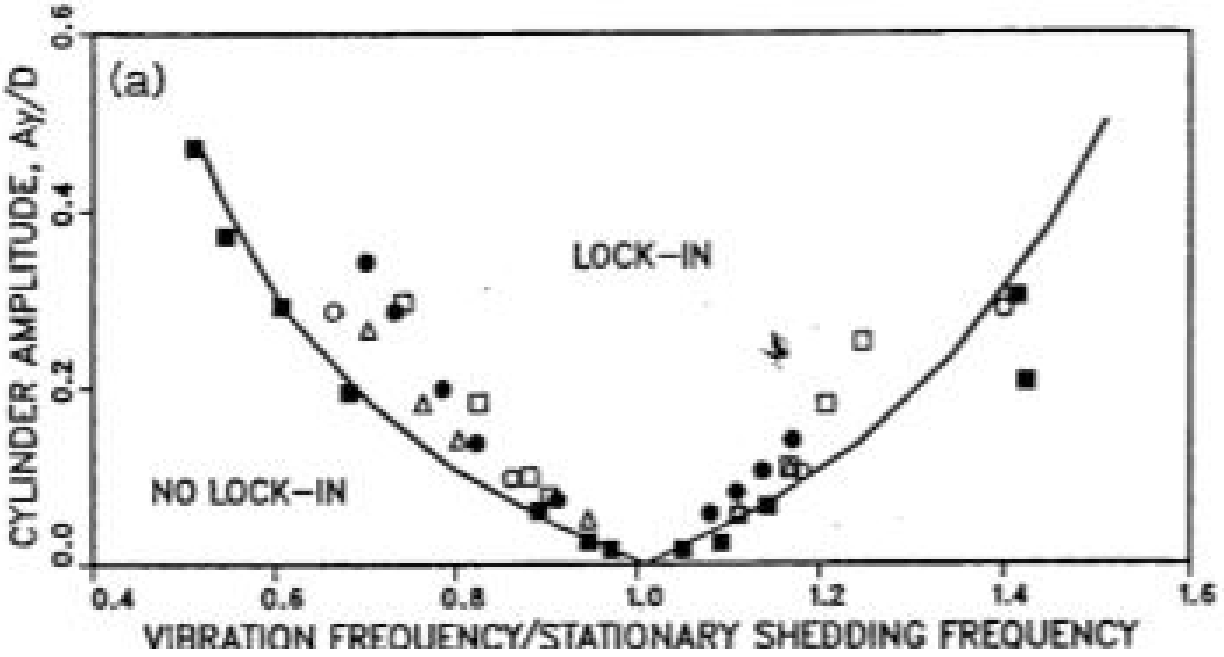

Figure 18 - Variation of the "Lock-in" range based on Cylinder Amplitude (A_y) Experimental data: Koopman (1967) & Stansby (1976), • for Re 200, o for Re 9200, □ for Re 100, ■ for Re 3600 &Δ for Re 300

As we observed from the figure 18 above, the lock-in band usually is found on both the sides of the vibration and stationary shedding frequency match point. Significant changes in the phase of shedding (Stansby (1976), Ongoren & Rockwell (1988)) and the pattern of shedding (Williamson & Roshko, 1988) are observed through the lock-in band transition across the match point.

When the vibration frequency is slightly below the stationary shedding frequency, the vortices will shed from the side opposite to the side of the cylinder that is experiencing maximum amplitude. But, when the vibration frequency is above the natural shedding frequency, the vortices will shed from the same side experiencing the maximum amplitude (Zdravkovich, 1982).

On the other hand, based on the experiments by Griffin & Ramberg (1974), the pattern of the vortices also becomes a function of the amplitude of oscillation. They found that for amplitude of 0.5 times the cylinder diameter the vortex shed are stable with symmetric pattern of alternate vortex shedding and for amplitude equal to the diameter of the cylinder the pattern of the vortex been shed are unstable with three vortices are formed per cycle of oscillation instead of the condition at the lower amplitude with two alternate shed pattern. This can be noted from the figure 19 and 20 the stable and unstable vortex shedding pattern.

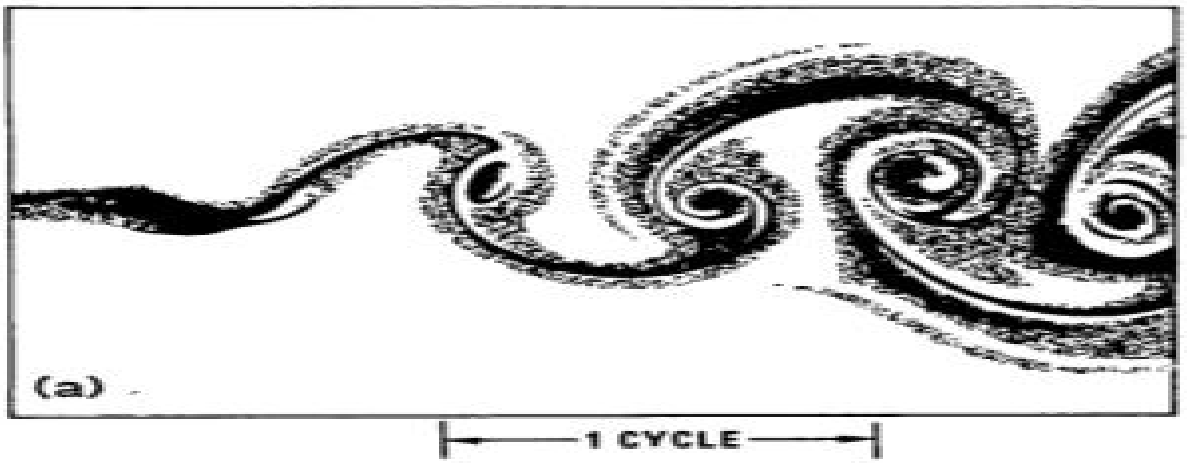

Figure 19 - Stable vortex shedding pattern for Re = 190 and when $\frac{A_y}{D} = 0.5$(Griffin & Ramberg, 1974)

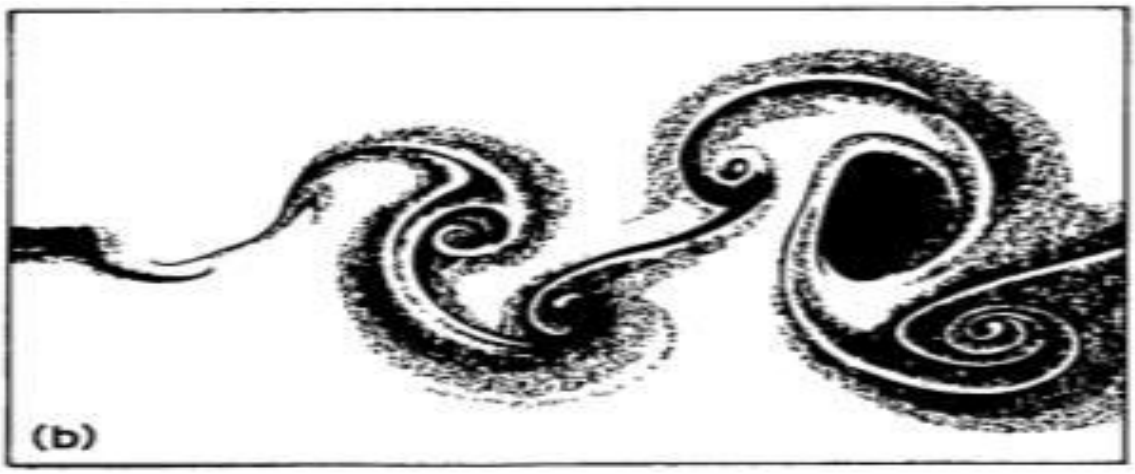

Figure 20 - Unstable vortex shedding pattern for Re = 190 and when $\frac{A_y}{D} = 1.0$(Griffin & Ramberg, 1974)

Based on the amplitude of the vibration, the average drag force exerted by the cylinder would differ. Different experimental work has found different expressions to determine the drag coefficient (C_D) based on the amplitude of oscillation involved but the difference in the value between the expression remain between 15% to one another under resonance condition.

Based on the data of Sarpkaya (1978), Tanida, Okajima & Watanabe (1973), & Torum & Anand (1985) a curve to fit the drag coefficient based on the amplitude was found. The expression behind the curve to find the drag coefficient for the defined amplitude is,

$$C_D = \left\{1 + 2.1\left(\frac{A_y}{D}\right)\right\} C_{D0} \ldots\ldots\ldots\ldots\ldots Eqn\ 3.5.1$$

Here,

$A_y = Amplitude\ i.e\ one\ half\ of\ the\ peak\ to\ peak\ transverse\ cylinder\ motion\ (m)$

$D = Diameter\ of\ the\ Cylinder\ (m)$

$C_{D0} = Drag\ Coeffieicent\ when\ A_y = 0\ (ref.fig.22)$

The respective figure defining the graph of drag increase based on the data satisfying the equation 3.5.1 is given below in figure 21.

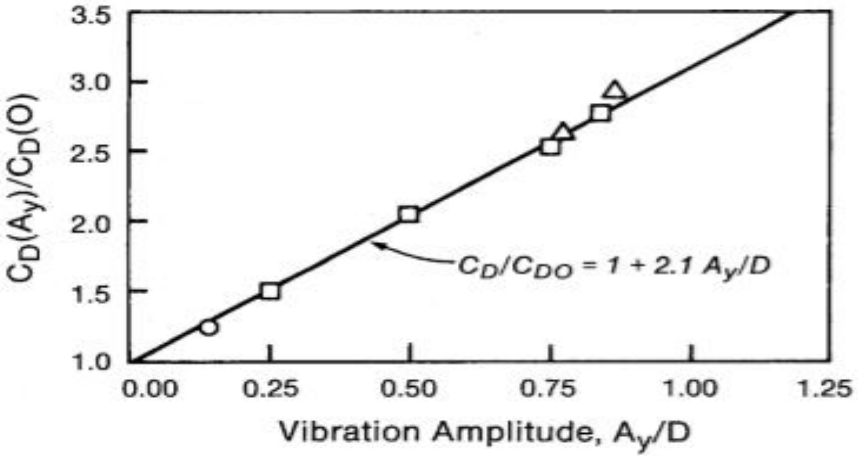

Figure 21 - Drag Coefficient increase based on Vibration Amplitude at a frequency equal to the shedding frequency, Experimental Data:o for Re 4000 by Tanida et al, □ for Re 8000 by Sarpkaya (1978) and Δ for Re 15000 by Torum & Anand (1985)

The drag coefficient when there is no vibration amplitude on the considered smooth cylinder in a steady flow is found from the figure 22.

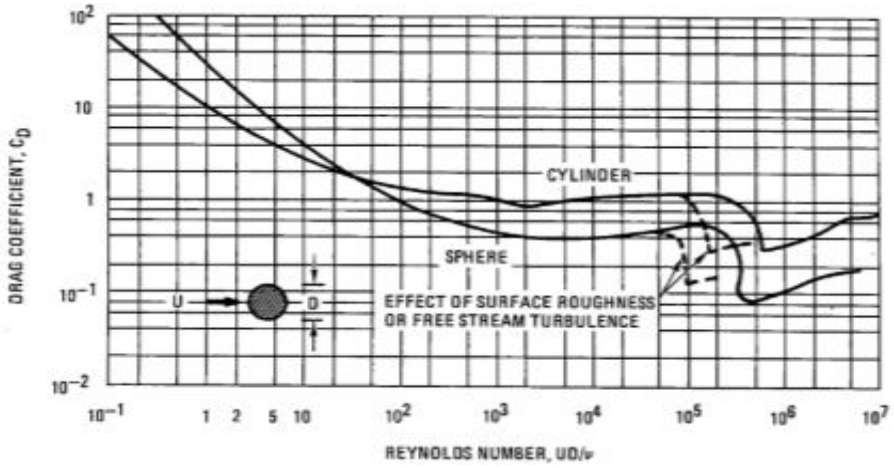

Figure 22 - Drag coefficient variation based on Reynolds number in a steady flow for smooth circular cylinder (Massey, 1979)

VIV ANALYSIS OF SUBSEA JUMPER SPOOLS

Vandiver (1983) found that the drag experienced marine cables vibrating due to vortex shedding can be predicted using the formula 3.5.2.

$$C_D = \left\{1 + 1.043 \left(\left(\frac{2 * Y_{rms}}{D}\right)^{0.65}\right)\right\} C_{D0} \dots\dots\dots\dots\dots Eqn\ 3.5.2$$

Here,

$Y_{rms} = Root\ square\ of\ the\ time\ average\ of\ the\ Amplitude\ square$

Whereas, Skop, Griffin & Ramberg (1977), found another expression for the same drag increase prediction based on his finding as represented in equation 3.5.3.

$$C_D = \left\{1 + 1.16 \left(\left\{\langle\left(\frac{1 + 2 * A_y}{D}\right) * \left[\frac{f_n}{f_v}\right]\rangle - 1\right\}^{0.65}\right)\right\} C_{D0} \dots\dots\dots\dots\dots Eqn\ 3.5.3$$

The interesting fact between all the above three equations (Eqn. 3.5.1, 3.5.2 and 3.5.3) is that at the resonance condition the difference in the drag coefficient outcome from individual case study doesn't deviate from the other by more than 15%.

Based on the value of drag coefficient determined through the expression for the considered condition of vibration, the average drag force per unit length acting on the system is given by,

$$F_D = \frac{1}{2}\rho D C_D {U_m}^2 \left(\frac{N}{m}\right) \dots\dots\dots\dots\dots Eqn.\ 3.5.4$$

Here,

$F_D = Drag\ Force\ per\ unit\ length\ (\frac{N}{m})$

$\rho = Density\ of\ Sea\ water\ (\frac{kg}{m^3})$

Thus, the impact of the system vibration oscillation on further generation of wakes has the following effects,

i. Increase the strength of the vortices based on higher separation force and enhanced velocity of separation (Davies (1976), Griffin & Ramberg (1974)).
ii. Cause the vibration frequency to shift towards the stationary shedding frequency (Bishop & Hassan (1964)), increasing the possibility of lock-in phenomenon with widening of lock-in band based on the amplitude of oscillation involved.
iii. It alters the phase, sequence and pattern of the vortex generated based on the amplitude (Zdravkovich (1982), Ongoren & Rockwell (1988), Williamson & Roshko (1988)).

iv. Increases the mean drag force acting on the system based on drag coefficient increase with respect to the amplitude (Bishop & Hassan (1964), Tanida et al., (1973), Sarpkaya (1978)).

3.6 VIV Mitigation

The consequences of the "Lock-in" phenomenon, like the magnification of the amplitude of vibration and the drag force experienced by the system can be suppressed by modifying either the structure (or) the flow associated with the system (Blevins, 2001).

3.6.1 Increased Stability Parameter

As we observe from the fig. 13 above, that any increase in the stability parameter will increase the requirement of the reduced velocity for the system to fall in the "lock-in" zone. This increase in the stability parameter of the system can be achieved through either increasing the effective unit mass of the system (or) increasing the total modal damping ratio (see equation 3.2.2.2). Both of these possibilities can be achieved only through the material parameter of the structure, as all the other associated parameters of the system remains fixed. Use of other materials such as viscoelastic, rubber and wood with high internal damping (or) any external damping devices will help to achieve increased stability parameter. In particular, if the stability parameter exceeds about a specific value, then the associated amplitude of resonance will be less than 1% of the system diameter, this can usually be neglected in comparison to the drag force experienced by the system (Blevins, 2001).

3.6.2 Avoiding Resonance

Resonance possibility can be avoided by maintaining the reduced velocity (See equation 3.2.2.1 (a)) of the system less than 1. From the equation 3.2.2.1 (a), we can observe that except for the Eigen frequency of the system all other parameters remain fixed. Therefore, the reduction in the reduced velocity is possible only through increasing the Eigen frequency of the system. System with higher Eigen frequency means that the system is rigid. Therefore, the increase in the Eigen frequency requires proper stiffening of the system through improving the rigidity of the system configuration. This is the most practical case for the slender structures (Blevins, 2001).

3.6.3 Streamline Cross Section

Once the flow separation from the structure at the downstream is decreased, then the intensity of the vortices that are shed gets reduced, this in turn reduces the drag force experienced by the system. Streamlining the vortices on the downstream of a structure normally requires a taper of 6 longitudinal for every unit lateral (or) an included angle of the taper not more than 8-10 degrees. This method of streamlining the structure downstream would be effective in the cases with fixed

direction of current flow relative to the system that has sufficient rigidity in order to avoid any further fluttering (Blevins, 2001).

3.6.4 Add a Vortex Suppression Device

The physics behind these vortex suppression devices is that, they interrupt the proper boundary layer formation in the generation of an organized, two dimensional vortex streets on the downstream of the system. This is usually achieved through the introduction of an artificial turbulence on the downstream (Blevins, 2001).

From this chapter, we understood the physics behind the vortex shedding phenomenon, the factors that influence their generation, the factors that can alter the intensity of the vortices formed & the parameters that can be used to quantify those intensities. It also helps to understand the most crucial part of the vortex shedding, the “Lock-in” phenomenon & also the severity the system would face with a further wakes generation during resonance. Furthermore, it also explains the types of oscillations that the system will experience, their range of occurrence & also the possible ways to suppress them.

CHAPTER 4

ANALYSIS METHODOLOGY

4.1 Modal Analysis on ANSYS

The ANSYS finite element analysis computer program was used to perform the static analysis of the jumper to verify the structural integrity of the system. The modal analysis is then conducted on the static analyzed model to account for the pre-stress and to extract the Eigen frequencies and their corresponding unit amplification stresses based on the mode shapes.

Accuracy of the extracted result depends on the correlation of the modeled system to the real field specific load case conditions. It includes the following input provision,

- Material properties of the system like type of material, minimum specified yield strength, material density, young's modulus and Poisson ratio.
- Dimensional properties of the system like outside diameter, thickness, segmental length, elbow bend radius, coating and lining etc.,
- Boundary conditions like type of restrains at the ends, stroking tolerance to mate the flanges, metrological and fabrication tolerance for jumper positioning etc.,
- Operational parameters like design pressure, design temperature, longitudinal displacement due to thermal expansion etc.,
- Transported fluid properties like density to account for added mass effect.

Based on the extracted mode shape, the jumper oscillation can be categorized into two types relative to the current flow direction as shown in figure 23, they are

- In-line oscillation (along the direction of current)
- Cross-flow oscillation (perpendicular to the direction of current)

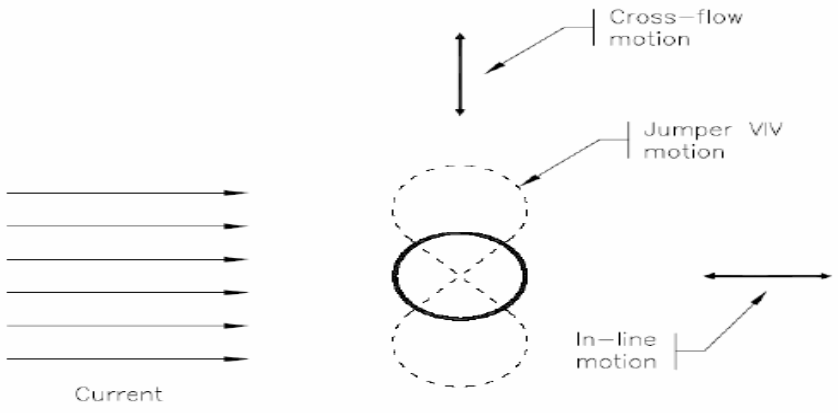

Figure 23 - Types of Jumper Oscillations (Carruth & Cerkovnik, 2007)

4.2 VIV Analysis

In addition to the above list of inputs to perform the modal analysis in ANSYS, the following inputs are also required for a complete VIV analysis of the system.

- Environmental data like significant wave height, wave period, current velocity at the sea surface, wave and current heading relative to the system.
- Seabed bathymetry details.
- Water depth of operation involved.

4.2.1 Environmental Modeling

As specified in section.3 of DNV-RP-F105, the environment to which the jumper system is exposed to, be modeled based on a return period of 100 year with a long term distribution statistics both for the steady state current and wave induced velocity and period of oscillation at the pipe level. The characteristics of the current and wave is usually extrapolated from the free surface to the pipe level to study the jumper characteristics as they govern the response.

4.2.1.1 Current

The variation of the current velocity relative to the water depth is considered relative and the total current velocity from the components of tidal and wind induced current and its variation along the water depth from the reference surface is modeled as per section D-301 of DNV-OS-J101.

Based on section D-301 from DNV-OS-J101,

$$\vartheta\,(z) = \vartheta_{tide}\,(z) + \vartheta_{wind}\,(z) \ldots\ldots\ldots\ldots\ldots Eqn.\,4.2.1.1\,(a)$$

Where,

$$\vartheta_{tide}\,(z) = \vartheta_{tide0}\left(\frac{h+z}{h}\right)^{1/7} for\ z \le 0 \ldots\ldots\ldots\ldots\ldots Eqn.\,4.2.1.1\,(b)$$

$$\vartheta_{wind}\,(z) = \vartheta_{wind0}\left(\frac{h_0+z}{h_0}\right) for - h_0 \le z \le 0 \ldots\ldots\ldots\ldots\ldots Eqn.\,4.2.1.1\,(c)$$

Here,

$\vartheta\,(z) = Total\ current\ velocity\ at\ level\ z\ (\frac{m}{s})$

$z = Distance\ from\ still\ water\ level\ negative\ downward\ (m)$

$\vartheta_{tide0}\ = Tidal\ velocity\ at\ still\ water\ level\ (m)$

ϑ_{wind0} $= Wind\ generated\ current\ at\ still\ water\ level\ (m)$

h $= Water\ depth\ from\ still\ water\ level\ positive\ downward\ (m)$

h_0 $= Reference\ depth\ for\ wind\ generated\ current\ (50\ m)$

Based on the condition mentioned in equation 4.2.1.1 (c), the equation 4.2.1.1 (a) for water depth's beyond 50 meters can be modified as,

$$\vartheta\ (z) = \vartheta_{tide}\ (z) \ldots\ldots\ldots\ldots\ldots Eqn.\ 4.2.1.1\ (d)$$

As most of the wind induced component of current for deeper cases can be contributed from the waves with an exponential decay method.

Since, no information is available related to the intensity of current turbulence, the value is taken as 5% as mentioned in section 3.2.12 of DNV-RP-F105.

4.2.1.2 Waves

As the intended system is exposed to the environment throughout its service life, a long term based environmental analysis is preferred instead of the short term sea state condition. For modeling the significant wave height (Hs) on a long term statistical basis a 3-parameter Weibull distribution is often appropriate as per section 3.5 of DNV-RP-F105 and the Weibull distribution is given by,

$$F_x(x) = 1 - \exp(-(\frac{x-\gamma}{\alpha})^{\beta}) \ldots\ldots\ldots\ldots\ldots eqn.\ 4.2.1.2\ (a)$$

Here,

$F_x(x) = Alternatecumulative\ density\ function\ = \dfrac{n}{N+1}$

$n = no.of\ observation\ for\ the\ particular\ condition$

$N = Total\ no.of\ observation\ under\ the\ given\ sea\ state$

$\alpha = Scale\ parameter$

$\beta = Shape\ parameter$

$\gamma = Location\ parameter = zero\ (assumed)$

All these Weibull distribution parameters are linked to the statistical moments (μ: mean value, σ: standard deviation, δ: skewness) as follows:

$$\mu = \alpha\tau\left(1+\frac{1}{\beta}\right)+\gamma \ldots\ldots\ldots\ldots\ldots Eqn.\ 4.2.1.2\ (b)$$

$$\sigma = \alpha\sqrt{\tau\left(1+\frac{2}{\beta}\right)-\tau\left(1+\frac{1}{\beta}\right)^{2}} \ldots\ldots\ldots\ldots\ldots Eqn.\ 4.2.1.2\ (c)$$

$$\delta = \frac{\alpha^{3}}{\sigma} * \left[\tau\left(1+\frac{3}{\beta}\right)-3\tau\left(1+\frac{1}{\beta}\right)*\tau\left(1+\frac{2}{\beta}\right)+2\tau(1+\frac{1}{\beta})^{3}\right] \ldots\ldots\ldots\ldots\ldots Eqn.\ 4.2.1.2\ (d)$$

Here,

$\tau = Gamma\ function$

$$\tau(x) = \int_{0}^{\infty} t^{x-1} * e^{-t} * dt \ldots\ldots\ldots\ldots\ldots Eqn.\ 4.2.1.2\ (e)$$

Upon developing the equation 4.2.1.2 (a), with the assumption that $\gamma = 0$, it will result in,

$$\ln\big(\ln\big(1-F(x)\big)\big) = \beta lnx - \beta ln\alpha \ldots\ldots\ldots\ldots\ldots Eqn.\ 4.2.1.2\ (f)$$

From the above equation.4.2.1.2 (f), if we plot the histogram data from a storm of 3 hours duration on a Weibull probability paper with lnx as the x-axis and $\ln\big(\ln\big(1-F(x)\big)\big)$ as the y-axis following the alternative cumulative distribution function. The significant wave height relative to the return period required can be obtained from the plot through extrapolation of the plot fitted straight line which follows the Weibull distribution. The accuracy of the extrapolated result depends on the fitness level of the plot to the Weibull distribution.

For a Weibull distributed variable the return period value (x_c) is given by,

$$x_c = \alpha(\ln(N))^{1/\beta}+\gamma \ldots\ldots\ldots\ldots\ldots Eqn.\ 4.2.1.2\ (g)$$

Where,

$$F(x_c) = 1-\frac{1}{N} \ldots\ldots\ldots\ldots\ldots Eqn.\ 4.2.1.2\ (h)$$

Here

N = number of independent events in the return period (e.g. 100 years)

This will result in the determination of the extreme sea state significant wave height for the assumed storm duration based on the probability of exceedance considered. Once we determined the significant wave height for the extreme sea state involved in the considered return period, its relative time period can be obtained through the extrapolation of the linear plot fitted between

the average time periods involved for each interval of wave height recorded in the histogram data.

Based on the Hs and Tp value of the extreme sea state for an assumed probability of exceedance 10^{-2}, the relative zero up-crossing period (Tz) for the peak period (Tp) can be calculated using the relation in equation.4.2.1.2 (i),

$$T_z = T_p \sqrt{\frac{5+\gamma}{11+\gamma}} \ldots\ldots\ldots\ldots\ldots Eqn.\ 4.2.1.2\ (i)$$

Here,

$\gamma = peak\ enhancement\ factor.$

$= 5\ for\ \frac{T_p}{\sqrt{H_s}} \leq 3.6$

$= e^{5.75-1.15\frac{T_p}{\sqrt{H_s}}}\ for\ 3.6 < \frac{T_p}{\sqrt{H_s}} \leq 5$

$= 1\ for\ \frac{T_p}{\sqrt{H_s}} > 5$

From the zero up-crossing period, we can calculate the total number of waves ($\bar{n}$) observed within the storm duration considered as shown in equation.4.2.1.2 (j),

$$\bar{n} = \frac{Storm\ duration\ in\ seconds}{T_z} \ldots\ldots\ldots\ldots\ldots Eqn.\ 4.2.1.2\ (j)$$

Based on the Gaussian process to define the surface of the sea, the corresponding highest wave crest is given by

$$\epsilon_0 = \bar{y} = \sigma_E \sqrt{2ln\bar{n}} \ldots\ldots\ldots\ldots\ldots Eqn.\ 4.2.1.2\ (k)$$

Here,

$\sigma_E = Standard\ deviation\ of\ the\ significant\ wave\ height = \frac{H_s}{4}$

Based on the value of $\epsilon_0\ and\ T_z$, the determination of the involved case study being shallow/intermediate/deep water can be done through calculating the wavelength (L) using the dispersion relation shown in equation.4.2.1.2 (l)

$$\omega^2 = g * k * \tanh(kd) \ldots\ldots\ldots\ldots\ldots Eqn.\ 4.2.1.2\ (l)$$

Here,

VIV ANALYSIS OF SUBSEA JUMPER SPOOLS

$\omega = angular\ frequency = \frac{2\pi}{T_z}\ (\frac{1}{s})$

$g = acceleration\ due\ to\ gravity = 9.81\ (\frac{m}{s^2})$

$k = \frac{2\pi}{L}\ (1/m)$

$L = wave\ length\ (m)$

$d = water\ depth\ of\ operation\ (m)$

The categorization of shallow/intermediate/deep water condition is based on the satisfaction of the condition mentioned in table 1 below.

Table 1 - Condition for Water Depth Categorization (Gudmestad, 2014)

Type of Water Depth	Condition
Shallow	d/L <1/20
Intermediate	1/20<d/L<1/2
Deep	d/L>1/2

Once, the water depth category is fixed, the decay of the horizontal water particle velocity from the highest wave crest to the pipe level near the seabed is calculated using the category specific formulae listed in table 2 below,

Table 2 - Horizontal Water Particle Velocity based on Water Depth category (Gudmestad, 2014)

Type of Water Depth	Horizontal Water Particle Velocity (m/s)
Shallow	$\frac{\varepsilon_0 kg}{\omega}\sin(\omega t - kx)$
Intermediate	$\frac{\varepsilon_0 kg}{\omega}\frac{\cosh k(z+d)}{\cosh(kd)}\sin(\omega t - kx)$
Deep	$\frac{\varepsilon_0 kg}{\omega}e^{kz}\sin(\omega t - kx)$

Thus, the total maximum horizontal water particle velocity present at the pipe level consists of two components in it. It includes the steady state current velocity and the oscillatory wave induced velocity. It is given by

$$U_m = U_c + U_w \dots\dots\dots\dots\dots Eqn.\ 4.2.1.2\ (m)$$

4.2.2 Response Modeling

The amplitude response models are empirical models in agreement with the generally accepted concept of VIV providing the maximum steady state VIV amplitude responses as a function of the basic hydrodynamic and structural parameters mentioned and detailed in chapter.3. The response models can possibly be generated for the following conditions

- Inline VIV in steady state current and current dominated conditions.
- Cross-flow VIV induced inline motion.
- Cross-flow VIV in steady state current and combined wave and current conditions.

In the response models the possible two types of oscillations like the inline and cross-flow are considered separately. But, the inline instability from the first two inline oscillation are considered implicit, there is also a possibility of increased fatigue damage from the inline oscillations due to the additional inline motion induced from the cross-flow oscillations under all reduced velocity range. But, the possible potential of inline induced cross-flow oscillations are usually neglected for reduced velocity range of 2-3. Under conditions where several modes of the same type (either inline (or) cross-flow) are excited simultaneously then the principle of multi-mode response shall be applicable to account the total fatigue damage.

4.2.2.1 Inline Response Modeling

The inline response model of a system free span under current dominated conditions is associated with either alternating (or) symmetric vortex shedding and it applies for all inline vibration modes.

The parameters that define the inline response amplitude for the concerned inline modes are

- Reduced Velocity (Vr)
- Stability Parameter (Ks)
- Turbulence Intensity (Ic) and
- Flow angle relative to the pipe (θ_{rel})

The inline VIV induced stress range S_{IL} is calculated using the equation 4.2.2.1 (a) below,

$$S_{IL} = 2 * A_{IL} * \left(\frac{A_Y}{D}\right) * \psi_{\alpha,IL} * \gamma_s \ldots\ldots\ldots\ldots\ldots Eqn.\ 4.2.2.1\ (a)$$

Here,

$A_{IL} = Unit\ stress\ amplitude\ (defined\ by\ ANSYS\ for\ unit\ diameter\ deflection)$

$\frac{A_Y}{D} = Maximum\ inline\ VIV\ response\ amplitude\ as\ a\ function\ of\ V_r\ and\ K_s.$

$\psi_{\alpha,IL} = Correlation\ factor\ for\ current\ flow\ ratio\ \alpha$

$\gamma_s = Safety\ factor\ to\ be\ multiplied\ to\ the\ stress\ range$

The value of Maximum inline VIV response amplitude ($\frac{A_Y}{D}$), is determined from the generated response model as a function of $V_r\ and\ K_s$. The general response model generation principle is given in figure 24 below,

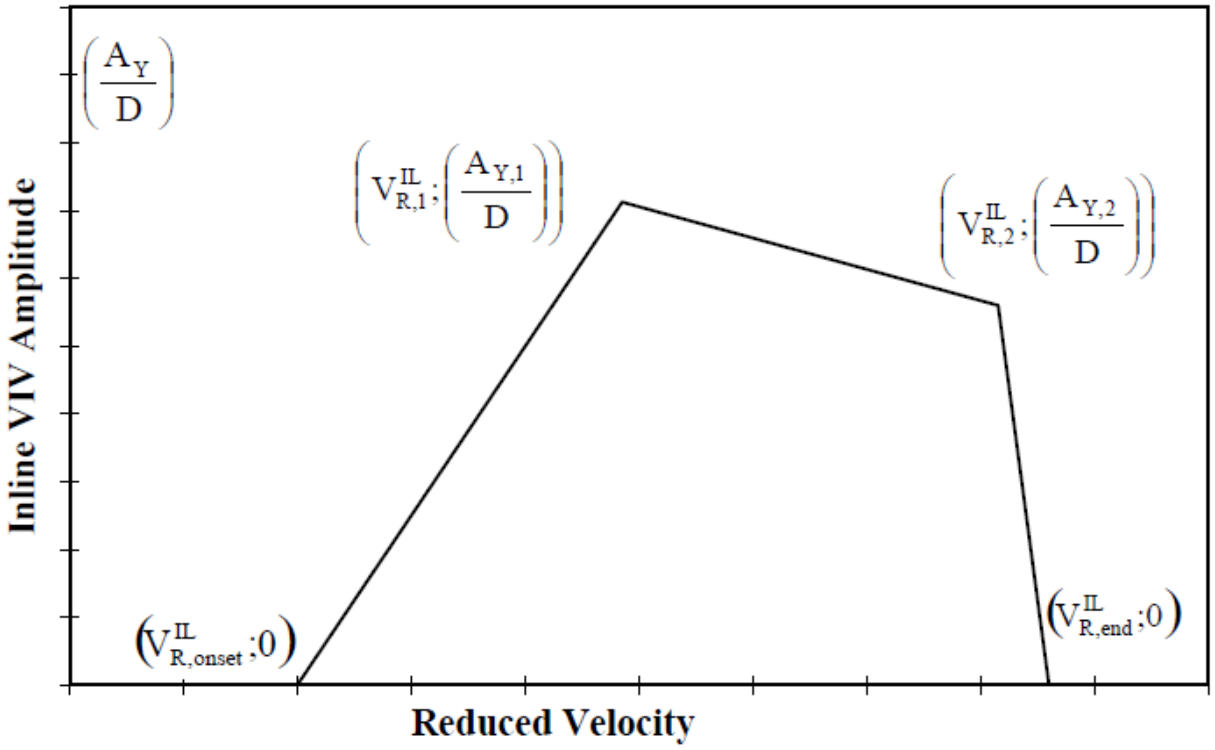

Figure 24 - Inline Response Model Generation Principle (DNV-RP-F105, 2006)

The construction of response model mentioned above in figure 24, involves the following equations and conditions.

$$V_{R,onset}{}^{IL} = \left\{ \begin{array}{c} \frac{1.0}{\gamma_{on,IL}}\ for\ K_{sd} < 0.4 \\ \frac{0.6 + K_{sd}}{\gamma_{on,IL}}\ for\ 0.4 < K_{sd} < 1.6 \\ \frac{2.2}{\gamma_{on,IL}}\ for\ K_{sd} > 1.6 \end{array} \right\} \ldots\ldots\ldots\ldots\ldots Eqn.\ 4.2.2.1\ (b)$$

$$V_{R,1}{}^{IL} = 10 * \left(\frac{A_{Y,1}}{D}\right) + V_{R,onset}{}^{IL} \ldots\ldots\ldots\ldots\ldots Eqn.\ 4.2.2.1\ (c)$$

$$V_{R,2}{}^{IL} = V_{R,end}{}^{IL} - 2 * \left(\frac{A_{Y,2}}{D}\right) \ldots\ldots\ldots\ldots\ldots Eqn.\ 4.2.2.1\ (d)$$

$$V_{R,end}{}^{IL} = \begin{Bmatrix} 4.5 - 0.8K_{sd}\ for\ K_{sd} < 1.0 \\ 3.7\ for\ K_{sd} \geq 1.0 \end{Bmatrix} \dots\dots\dots\dots\dots Eqn.\ 4.2.2.1\ (e)$$

$$\frac{A_{Y,1}}{D} = \max\left(0.18 * \left(1 - \frac{K_{sd}}{1.2}\right) * R_{I\theta,1};\ \left(\frac{A_{Y,2}}{D}\right)\right) \dots\dots\dots\dots\dots Eqn.\ 4.2.2.1\ (f)$$

$$\frac{A_{Y,2}}{D} = 0.13 * \left(1 - \frac{K_{sd}}{1.8}\right) * R_{I\theta,2} \dots\dots\dots\dots\dots Eqn.\ 4.2.2.1\ (g)$$

$$K_{sd} = \frac{K_s}{\gamma_k} \dots\dots\dots\dots\dots Eqn.\ 4.2.2.1\ (h)$$

The reduction factors $R_{I\theta,1}\ and\ R_{I\theta,2}$ based on the turbulence intensity and angle of flow relative to the pipe is given by,

$$R_{I\theta,1} = 1 - \pi^2\left(\frac{\pi}{2} - \sqrt{2} * \theta_{rel}\right) * (I_c - 0.03) for\ 0 \leq R_{I\theta,1} \leq 1 \dots\dots\dots\dots\dots Eqn.\ 4.2.2.1\ (i)$$

$$R_{I\theta,2} = 1 - \left(\frac{I_c - 0.03}{0.17}\right) for\ 0 \leq R_{I\theta,2} \leq 1 \dots\dots\dots\dots\dots Eqn.\ 4.2.2.1\ (j)$$

The reduction function ($\psi_{\alpha,IL}$) to account for the reduction in the inline VIV relative to the wave dominated conditions is given by,

$$\psi_{\alpha,IL} = \begin{Bmatrix} 0.0\ for\ \alpha < 0.5 \\ \dfrac{\alpha - 0.5}{0.3}\ for\ 0.5 < \alpha < 0.8 \\ 1.0\ for\ \alpha > 0.8 \end{Bmatrix} \dots\dots\dots\dots\dots Eqn.\ 4.2.2.1\ (k)$$

The general safety factors for the natural frequencies and fatigue based on section 2.6 of DNV-RP-F105 is given in table 3 and 4 below.

Table 3 - Safety factors for Natural Frequencies (DNV-RP-F105, 2006)

Safety Factors for Natural Frequencies, γ_f			
Free Span Type	Safety Class		
	Low	Normal	High
Very well defined	1.0	1.0	1.0
Well defined	1.05	1.1	1.15
Not well defined	1.1	1.2	1.3

Table 4 - General Safety factors for Fatigue (DNV-RP-F105, 2006)

General Safety Factors for Fatigue			
Safety Factor	Safety Class		
	Low	Normal	High
η	1.0	0.5	0.25
γ_k	1.0	1.15	1.30
γ_s	1.3		
$\gamma_{on,IL}$	1.1		
$\gamma_{on,CF}$	1.2		

4.2.2.2 Cross-flow Response Modeling

The onset of the cross-flow VIV for a system free span under steady state current dominated condition is typically at a value between 3.0 and 4.0, whereas maximum vibrations occur at larger reduced velocity range. But, for low specific mass systems under wave dominated flow situations, the onset of the cross-flow VIV will be shifted between 2.0 and 3.0.

The parameters that affect the cross-flow VIV amplitude for the concerned cross-flow modes are,

- Reduced Velocity (Vr)
- Keulegan Carpenter number (KC)
- Current flow velocity ratio (α)
- Stability Parameter (Ks)
- Seabed gap ratio (e/D)
- Strouhal number (St) and
- Pipe roughness (k/D)

The cross-flow VIV induced stress range S_{CF} is calculated using the equation 4.2.2.2 (a) below,

$$S_{CF} = 2 * A_{CF} * \left(\frac{A_Z}{D}\right) * R_k * \gamma_s \ldots\ldots\ldots\ldots\ldots Eqn.\ 4.2.2.2\ (a)$$

Here,

$A_{CF} = Unit\ stress\ amplitude\ (defined\ by\ ANSYS\ for\ unit\ diameter\ deflection)$

$\frac{A_Z}{D} = Maximum\ cross-flow\ VIV\ response\ amplitude\ as\ a\ function\ of\ \alpha\ and\ KC.$

$R_k = Amplitude\ reduction\ factor\ due\ to\ damping$

$\gamma_s = Safety\ factor\ to\ be\ multiplied\ to\ the\ stress\ range$

The value of Maximum cross-flow VIV response amplitude ($\frac{A_Z}{D}$), is determined from the generated response model as a function of $\alpha\ and\ KC$. The general response model generation principle is given in figure 25 below,

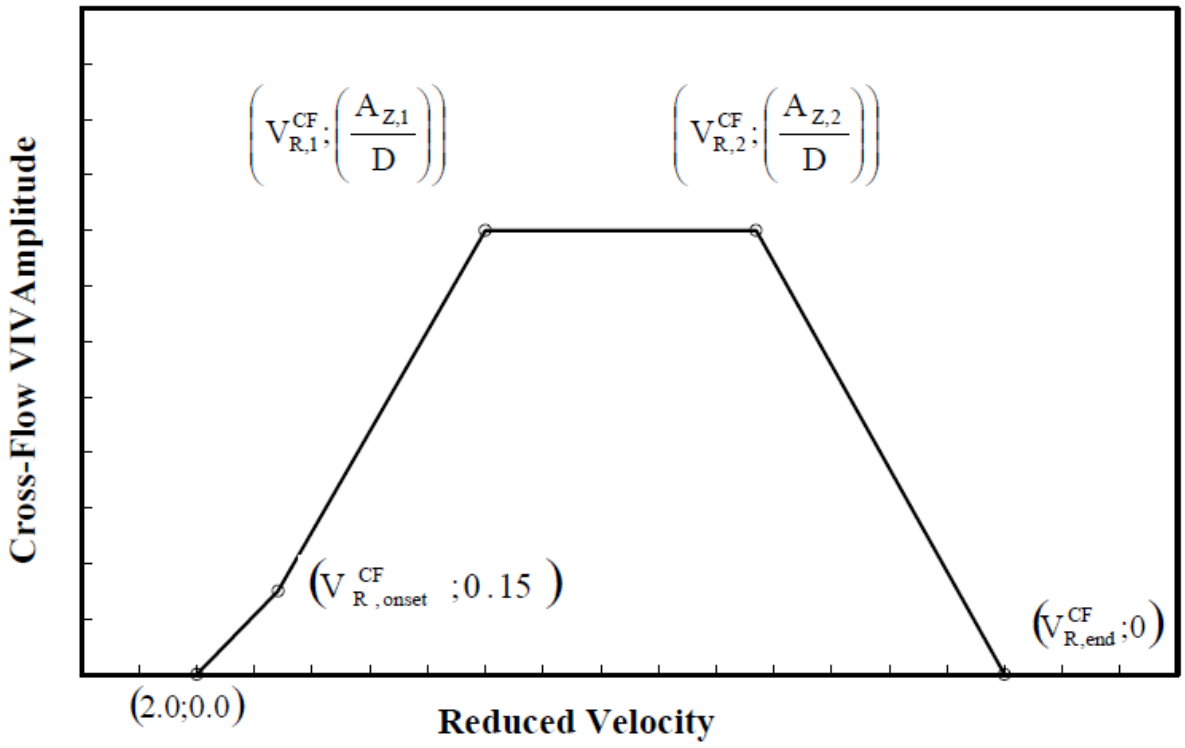

Figure 25 - Cross-flow Response Model Generation Principle (DNV-RP-F105, 2006)

The construction of response model mentioned above in figure 25, involves the following equations and conditions.

$$V_{R,onset}{}^{CF} = \frac{3 * \psi_{proxi,onset} * \psi_{trench,onset}}{\gamma_{on,CF}} \dots\dots\dots\dots\dots Eqn.\ 4.2.2.2\ (b)$$

$$V_{R,1}{}^{CF} = 7 - \frac{(7 - V_{R,onset}{}^{CF})}{1.15} * (1.3 - \frac{A_{Z,1}}{D}) \dots\dots\dots\dots\dots Eqn.\ 4.2.2.2\ (c)$$

$$V_{R,2}{}^{CF} = V_{R,end}{}^{CF} - \frac{(7)}{1.3} * (\frac{A_{Z,1}}{D}) \dots\dots\dots\dots\dots Eqn.\ 4.2.2.2\ (d)$$

$$V_{R,end}{}^{CF} = 16 \dots\dots\dots\dots\dots Eqn.\ 4.2.2.2\ (e)$$

$$\frac{A_{Z,2}}{D} = \frac{A_{Z,1}}{D} \dots\dots\dots\dots\dots Eqn.\ 4.2.2.2\ (f)$$

$$\frac{A_{Z,1}}{D} = \begin{Bmatrix} 0.9 & for\ \alpha > 0.8\ and\ \left(\frac{f_{n+1,CF}}{f_{n,CF}}\right) < 1.5 \\ 0.9 + 0.5\left(\frac{f_{n+1,CF}}{f_{n,CF}} - 1.5\right) & for\ \alpha > 0.8\ and\ 1.5 \leq \frac{f_{n+1,CF}}{f_{n,CF}} \leq 2.3 \\ 1.3 & for\ \alpha > 0.8\ and\ \left(\frac{f_{n+1,CF}}{f_{n,CF}}\right) > 2.3 \\ 0.9 & for\ \alpha \leq 0.8\ and\ KC\ > 30 \\ 0.7 + 0.01(KC - 10) & for\ \alpha \leq 0.8\ and\ 10 \leq KC \leq 30 \\ 0.7 & for\ \alpha \leq 0.8\ and\ KC\ < 10 \end{Bmatrix} \dots Eqn.\ 4.2.2.2\ (g)$$

Here,

$\frac{f_{n+1,CF}}{f_{n,CF}}$, is the cross-flow frequency ratio for two consecutive cross-flow modes.

Even though, the maximum cross-flow amplitude response is a function of α and KC, the onset of the cross-flow VIV is dependent on the seabed proximity and trench geometry. These parameters are calculated as follows,

$$\psi_{proxi,onset} = \begin{Bmatrix} \frac{1}{5}\left(4 + \frac{1.25e}{D}\right) for\ \frac{e}{D} < 0.8 \\ 1 \quad elsewhere \end{Bmatrix} \dots\dots\dots\dots\dots Eqn.\ 4.2.2.2\ (h)$$

$$\psi_{trench,onset} = 1 + \frac{0.5\Delta}{D} \dots\dots\dots\dots\dots Eqn.\ 4.2.2.2\ (i)$$

Here

$$\frac{\Delta}{D} = \frac{1.25d - e}{D}\ for\ 0 \leq \frac{\Delta}{D} \leq 1$$

The relation between the trench depth (d), eccentricity (e) and pipe diameter (D) can be found from the figure 26 below,

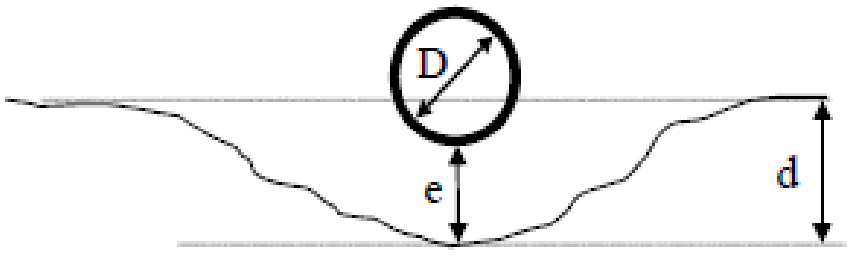

Figure 26 - Relation between d, e and D (DNV-RP-F105, 2006)

The characteristics reduction factor R_k of the cross-flow VIV due to the effect of damping is given by,

$$R_k = \begin{Bmatrix} 1 - 0.15K_{sd} \ for\ K_{sd} \ \leq 4.0 \\ 3.2{K_{sd}}^{-1.5} \ for\ K_{sd} \ > 4.0 \end{Bmatrix} \dots\dots\dots\dots\dots Eqn.\ 4.2.2.2\ (j)$$

4.3 VIV Analysis Criterion

The vibrations induced by the vortex shedding on the considered system shall be acceptable if it satisfies the fatigue damage acceptance criterion specified in section 2.4 of DNV-RP-F105, as mentioned in equation 4.3 (a) below,

$$\eta * T_{life} \ \geq T_{exposure} \dots\dots\dots\dots\dots Eqn.\ 4.3\ (a)$$

Here

$\eta = allowable\ fatigue\ damage\ ration\ as\ per\ Table\ 4\ above$

$T_{life} = Fatigue\ life\ capacity\ in\ years$

$T_{exposure} = Design\ life\ capacity\ in\ years$

If the system has the potential to be excited by several vibration modes at a given flow velocity, then the effect of additional fatigue can be determined by multi-mode vibration analysis. The main aim of the fatigue design assessment is to ensure that the fatigue life is within the subjected design life of the system.

4.3.1 Inline VIV fatigue criterion

The criterion to be satisfied for the inline VIV involved fatigue in the concerned system to be considered acceptable is given in equation 4.3.1 (a) below,

$$\frac{f_{n,IL}}{\gamma_{IL}} > \frac{U_{c,100\ year}}{{V_{R,onset}}^{IL} * D}\left(1 - \frac{\frac{L}{D}}{250}\right) * \frac{1}{\bar{\alpha}} \dots\dots\dots\dots\dots Eqn.\ 4.3.1\ (a)$$

Here,

$\gamma_{IL} = Screening\ factor\ for\ inline\ VIV\ as\ per\ Table\ 5\ below$

$\bar{\alpha} = Current\ flow\ ratio = \dfrac{U_{C,100\ year}}{U_{w,1\ year} + U_{C,100\ year}}$

$D = Outer\ Diameter\ of\ the\ Pipe\ including\ coating$

$L = Free\ span\ length$

$V_{R,onset}{}^{IL} = Inline\ onset\ value\ for\ the\ reduced\ velocity\ see\ section$ 4.2.2.1

$U_{c,100\ year} = 100\ year\ return\ period\ value\ for\ the\ current\ velocity\ at\ the\ pipe\ level$

$U_{w,1\ year} = 1\ year\ return\ period\ value\ for\ the\ wave\ induced\ velocity\ at\ pipe\ level$

Table 5 - Safety factors for Screening Criterion (DNV-RP-F105, 2006)

Safety factors for screening criteria	
γ_{IL}	1.4
γ_{CF}	1.4

4.3.2 Cross-flow VIV fatigue criterion

The criterion to be satisfied for both the inline and cross-flow VIV involved fatigue in the concerned system to be considered acceptable is given in equation 4.3.2 (a) below,

$$\frac{f_{n,CF}}{\gamma_{CF}} > \frac{U_{c,100\ year} + U_{w,1\ year}}{V_{R,onset}{}^{CF} * D} \dots\dots\dots\dots\dots Eqn.\ 4.3.2\ (a)$$

Here,

$\gamma_{CF} = Screening\ factor\ for\ cross - flow\ VIV\ as\ per\ Table\ 5\ above$

$V_{R,onset}{}^{CF} = Cross - flow\ onset\ value\ for\ the\ reduced\ velocity\ see\ section$ 4.2.2.2

4.3.3 Direct Wave Induced VIV fatigue criterion

The criterion to be satisfied for the direct wave involved fatigue in the concerned system to be considered acceptable is given in equation 4.3.3 (a) below in addition to that of the Inline VIV fatigue criterion mentioned in the section 4.3.1 above,

$$\frac{U_{c,100\ year}}{U_{c,100\ year} + U_{w,1\ year}} > 2/3 \dots\dots\dots\dots\dots Eqn.\ 4.3.3\ (a)$$

4.4 Workflow for VIV Assessment

The flow of work for the assessment of considered system with respect to the VIV induced fatigue damage with the main components involved in the assessment, to make sure that the system satisfies the criterion mentioned in equation 4.3 (a) based on the system and environmental details available is mentioned in figure 27 and 28 below.

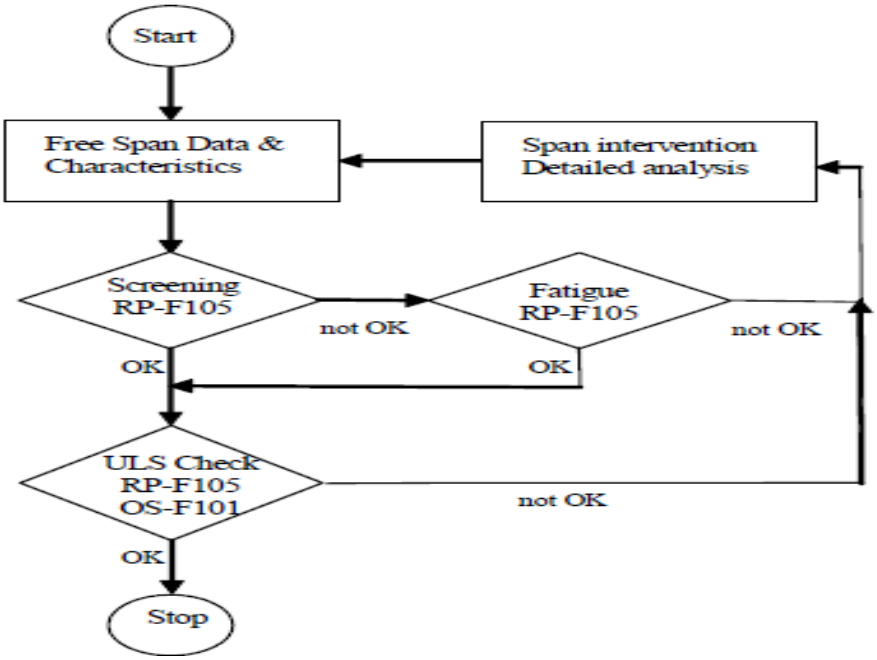

Figure 27 - Flowchart over design checks for a free span (DNV-RP-F105, 2006)

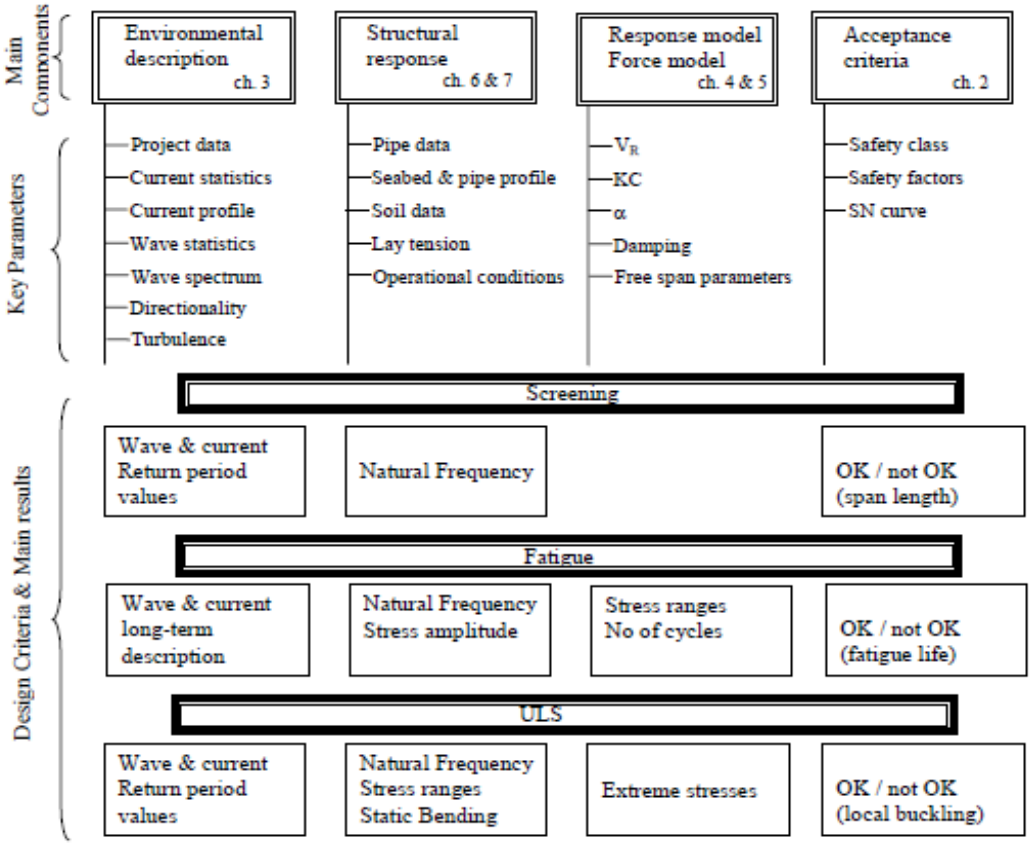

Figure 28 - Overview of main components in a free span assessment (DNV-RP-F105, 2006)

4.5 Assessment of Fatigue life

The assessment of fatigue life based on the guideline of DNV-RP-F105 as followed in this work focus on the damage made to the design life of the system, due to the VIV when the phenomenon of "Lock-in" happens. The damage made to the system through the vibrations that happens before "Lock-in" has not been accounted, as the associated amplitudes are not as significant as in case of resonance.

The fatigue life of the system can be assessed based on the S-N curve method with the assumption that the accumulated stress is linear as per Palmgren-Miner rule. When the long term stress distribution is expressed by a stress histogram, consisting of a convenient number of constant stress range blocks (S), each with a number of stress repetitions (n_i), the accumulated fatigue damage can then be calculated as per section.2 of DNV-RP-C203 as given in equation 4.5 (a) below,

$$D = \sum_{i=1}^{k} \frac{n_i}{N_i} = 1/\bar{a} * \sum_{i=1}^{k} n_i * S_i^{\,m} \ldots\ldots\ldots\ldots\ldots Eqn.\ 4.5\ (a)$$

Here,

$D = accumulated\ fatigue\ damage\ in\ years$

$\bar{a} = intercept\ of\ the\ design\ S-N\ curve\ with\ the \log N\ axis$

$m = negative\ inverse\ slope\ of\ the\ S-N\ curve$

$k = no.of\ stress\ blocks$

$n_i = no.of\ stress\ cycles\ of\ the\ stress\ range\ s_i\ per\ year$

$N_i = no.of\ stress\ cycles\ of\ the\ stress\ range\ s_i\ to\ failure$

$S_i = Stress\ range\ for\ the\ particular\ block\ as\ per\ either\ eqn.\ 4.2.2.1\ (a)\ or\ 4.2.2.2\ (a)$

The S-N curve based fatigue design follows the mean-minus-two-standard-deviation curves approach with the relevant experimental data obtained from fatigue tests. The S-N curves are thus associated with a 97.7% probability of survival. The design principle for the S-N curve is given in equation 4.5 (b) below,

$$\log N = \log \bar{a} - m \log S \ldots\ldots\ldots\ldots\ldots Eqn.\ 4.5\ (b)$$

The impact of the stress range on the number of cycles to failure of the concerned system includes the following parameters,

VIV ANALYSIS OF SUBSEA JUMPER SPOOLS

- Type of Environment the system is exposed to (air/seawater)
- Type of corrosion protection the system posses (cathode/free)
- Pipe-to-Pipe centre misalignment involved
- Uni-linear/bilinear type of S-N curve involved
- Stress concentration factor based on the type of weld involved

For the concerned system of subsea jumper, the corresponding parameters to define the S-N curve involved based on section.2 in DNV-RP-C203 is listed in table 6 below,

Table 6 - Parameters to define the Jumper S-N curve (DNV-RP-C203, 2010)

Parameter to define the S-N curve	
Parameter	**Value**
Environment exposed	Seawater
Corrosion Protection	Free to corrode
Misalignment	0.1*thickness (max)
S-N curve type	Uni-linear
S-N curve category	F1
Stress Concentration Factor (SCF)	1.0

The possible occurrence of the stress cycles of the system for the given stress range in a year is given by equation.4.5 (c),

$$n_i = \sum_{i=1}^{k} T_{year} * f_{vi} \dots\dots\dots\dots\dots Eqn.4.5(c)$$

Here,

$f_{vi} = Vibrating\ frequency\ for\ the\ particular\ mode\ (i)$

$T_{year} = Total\ exposure\ period\ in\ a\ year\ (secs)$

As, the long term distribution of the bottom current also follows the Rayleigh distribution, the equation 4.5 (c) above depends on the probability of occurrence of the current over the year. The modified stress cycle per year is given in equation 4.5 (d) below.

$$n_i = 31.54 * 10^6 \sum_{i=1}^{k} f_{vi} * P_i \dots\dots\dots\dots\dots Eqn.4.5(d)$$

Here,

$P_i = Probability\ of\ occurence\ of\ the\ i^{th}\ stress\ cycle$

Based on this S-N curve method, the fatigue life capacity (T_{life}) can formally be expressed as in equation.4.5 (e) below,

$$T_{life} = \frac{1}{\sum_{i=1}^{k} f_{vi} * {S_i}^{m} * \frac{P_i}{\bar{a}}} \dots\dots\dots\dots\dots Eqn.4.5\ (e)$$

But, the effect of utilization factor (η), should be accounted while calculating the actual service life of the system as mentioned in equation.4.3 (a) above.

From this chapter, we have understood the detailed information regarding the steps involved while performing a VIV analysis, with the help of the industrial available sources. It includes, the modal analysis of the system using the FEA tool ANSYS, modeling the system environment based on the extreme sea state condition considered, modeling the system VIV response based on the DNV-RP-F105 guidelines, selection of the conditions which require detailed fatigue life assessment and the detailed fatigue life assessment as per DNV-RP-C203 guidelines.

CHAPTER 5

ASSUMPTIONS

The analysis performed in the case study involves the following list of assumptions.

- The calculated fatigue damage is only with respect to the vortex induced vibration (VIV) phenomenon. All the other fatigue damage possibilities like, the pipeline thermal expansion, slugging and flow induced turbulence are not taken into consideration.
- Even though, the static analysis is performed to check the jumper configuration integrity, based on the minimum specified yield strength. All the other conditions like the collapse and reaction forces on the connector are assumed to be acceptable and within the limits.
- The displacement loads on the connector location are neglected. Because, the additional stress due to this effect can be compensated through the jumper configuration alteration.
- The current flow is assumed to be perpendicular and parallel to the jumper configuration for the out-of-plane and in-plane condition respectively.
- Any orientation of the current flow with respect to the jumper profile is neglected.
- The mode shapes are assumed to be either pure inline (or) cross-flow oscillations. The possible combination of these two oscillations based on a percentage is not considered.
- Only the tidal and wind induced current are considered to determine the total current flow on the surface and they are then extrapolated from the free surface to the pipe level. All the other possibilities of current like the subsurface, near shore and density driven components of the current flow are neglected.
- The tidal velocity at the free surface is assumed to be 1.5 Knots under all the case studies.
- The pipe level is assumed to be 1 meter above the seabed under all the case studies.
- The long-term distribution of the current that is considered under all the case studies is based on some realistic assumptions.
- The location parameter (γ) of the long term Weibull distribution is assumed to be zero.
- The duration of the storm is assumed as 3 hours in our case study.
- Since, the jumpers are assumed as the connectors between the wellhead and the manifold in our case study. The safety class of the jumper is assumed to be high.
- Since, the seabed bathymetry requirement is small, the safety class of the jumper in our case study is assumed to be well defined type.
- The bottom of the pipe is assumed to be at 838mm above the seabed. This shows that the presence of the trench will not affect the cross-flow VIV.
- The added mass effect for the inline type of oscillation is assumed to be equal to the volume of water displaced by the jumper. Because, the VIV amplitude relative to the inline oscillations in our case study is minimal.

VIV ANALYSIS OF SUBSEA JUMPER SPOOLS

- As mentioned in the section 4.5.2 of the DNV-RP-F105, the effect of the added mass coefficient for a reduced velocity of less than 2.5 can be neglected.
- As per the Palmgren-Minor rule, the linear cumulative damage is assumed in our case study, for the fatigue damage assessment based on the S-N curve.
- The Pipe-to-Pipe centre misalignment possible during fabrication of the jumper is assumed to a maximum value of 0.1 times the thickness or more.
- The probability of the current velocity occurrence on a long term basis is assumed in our case study.
- The service fluid inside the jumper system is assumed to be crude oil with a density of 830 kg/m3.
- The jumper system pipe material, its size and thickness are assumed to satisfy all its mechanical design requirements, like the allowable stress, erosion velocity and the system integrity check respectively.
- Based on the assumptions made with respect to the system safety classification, the fatigue life of the system should be 100 years (or) more, in order to satisfy the design life of 25 years.
- The jumper pipe size is assumed to be 300 NB and uniform throughout the system.
- The jumper system is assumed to be without any insulation and all the bends with a minimum radius of 3 times the outer diameter.
- The variation in the probability of the seabed current occurrence is assumed to vary only based on the tidal current variation at the free surface.
- As mentioned in the DNV-RP-F105, the effect of the screening factor on the Eigen frequency of the system, in order to identify the necessity for the detailed fatigue life analysis is not neglected.
- The possible fatigue damage during the installation of the jumper is not considered in the total fatigue cycles to failure of the system during service.

This chapter summarizes all the possible limitations that this work would face from a result accuracy perspective. It also helps us in identifying the possibilities of either improving this work through addressing the limitations stated (or) extending this background into similar systems in the future.

CHAPTER 6

SENSITIVITY ANALYSIS

For the subsea jumper system considered, the VIV sensitivity analysis is performed for the combination of conditions mentioned in the table 7 below.

Table 7 - Matrix of the Sensitivity Analysis performed

Jumper Configuration (m)	Case-1 (125 (m) Water Depth)		Case-2 (250 (m) Water Depth)		Case-3 (1000 (m) Water Depth)	
	In-Plane Current	Out-of-plane Current	In-Plane Current	Out-of-plane Current	In-Plane Current	Out-of-plane Current
30	X	X	X	X	X	X
34	X	X	X	X	X	X
38	X	X	X	X	X	X

The variation in the Eigen frequency, for the first three modes of excitation, with respect to the jumper configuration is represented in the figure 29 below. This is in accordance with the values in the tables C.2 and C.3 in the Annexure. C.

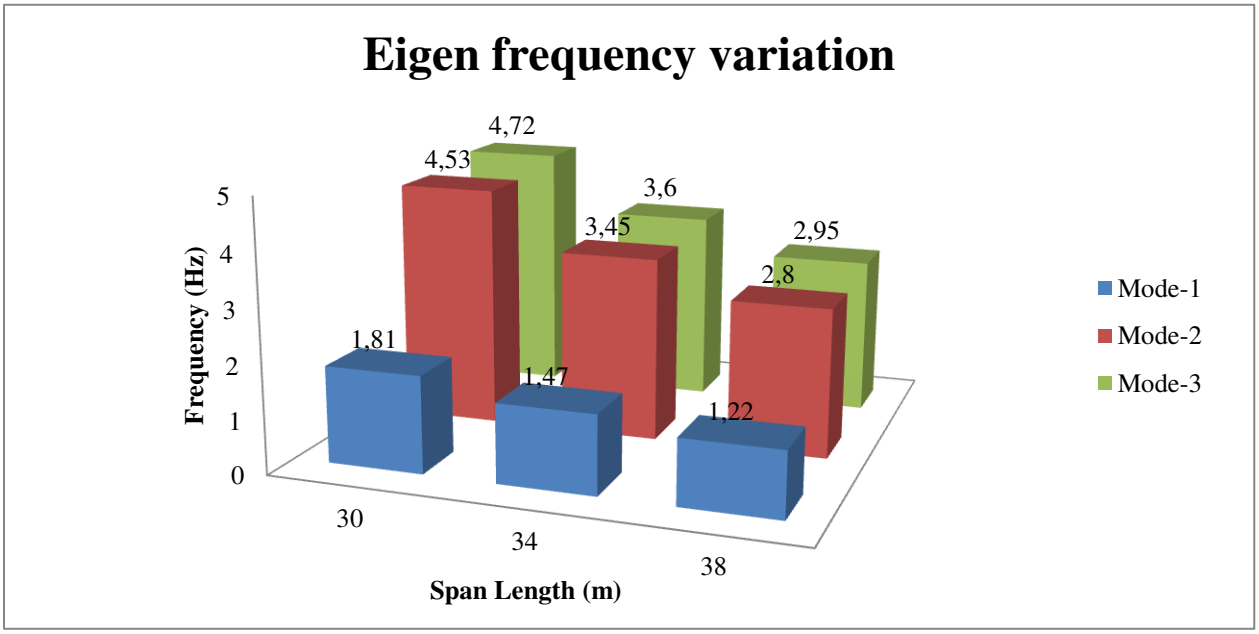

Figure 29 - Eigen frequency variations based on the mode number and the jumper length

VIV ANALYSIS OF SUBSEA JUMPER SPOOLS

The case specific sea bottom current on a long term distribution basis is represented in the figure 30 below. The components of the current velocity will include the wave induced and the tidal generated current and the corresponding values of the velocities are summarized in the tables B.11 and B.12 in the Annexure. B.

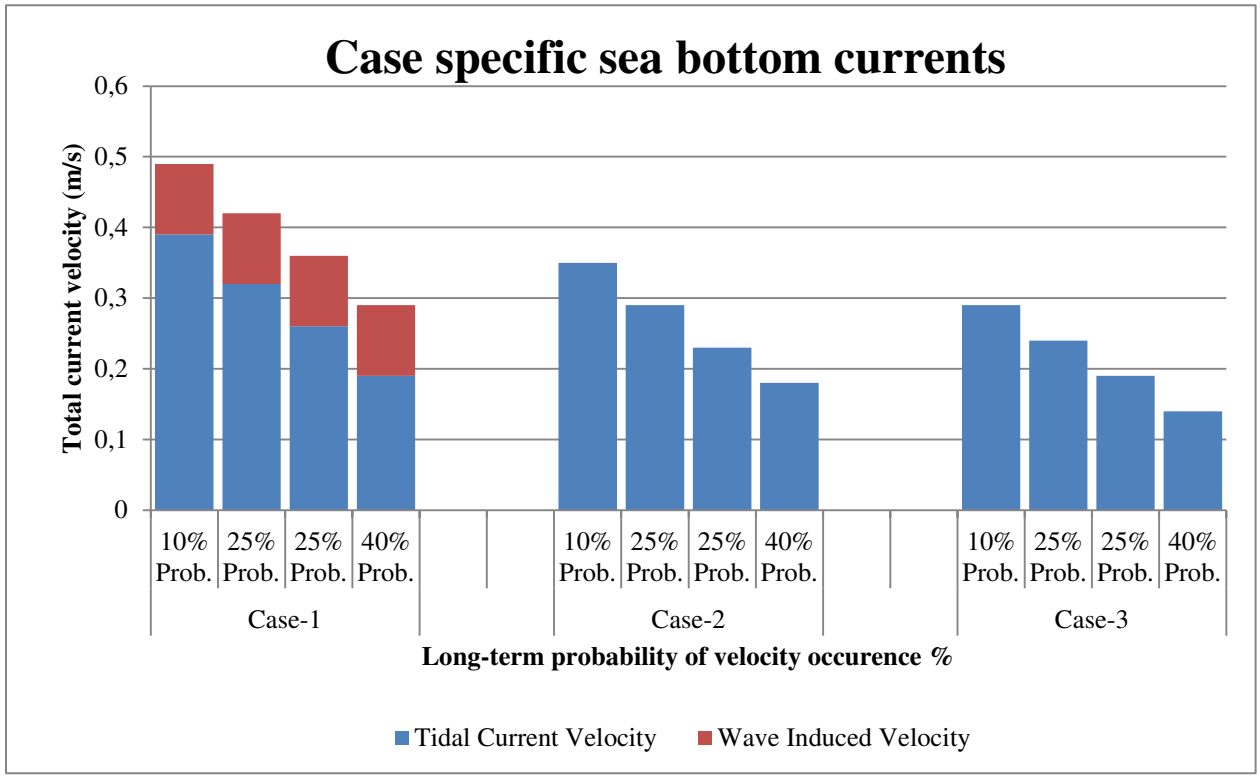

Figure 30 - Case specific sea bottom current velocities on a long-term distribution basis

The type of the jumper oscillation varies based on the type of current flow involved and also it is with respect to the corresponding mode number. This variation is represented in the table 8 below, and it is in accordance with the information represented in the tables C.2 and C.3 in the Annexure. C.

Table 8 - Variation in the jumper oscillation type based on current flow pattern

Mode No	Oscillation type	
	In-Plane Current flow	Out-of-Plane Current flow
1	Cross-flow	In-line
2	In-line	Cross-flow
3	Cross-flow	In-line

The reduced velocity variation based on the mode number, for all the three configurations of the jumpers is represented in the figure 31, 32 and 33. This variation depends on the probability of occurrence of the current velocity and the water depth of operation. These figures are based on the tables summarized in the Annexure. D.

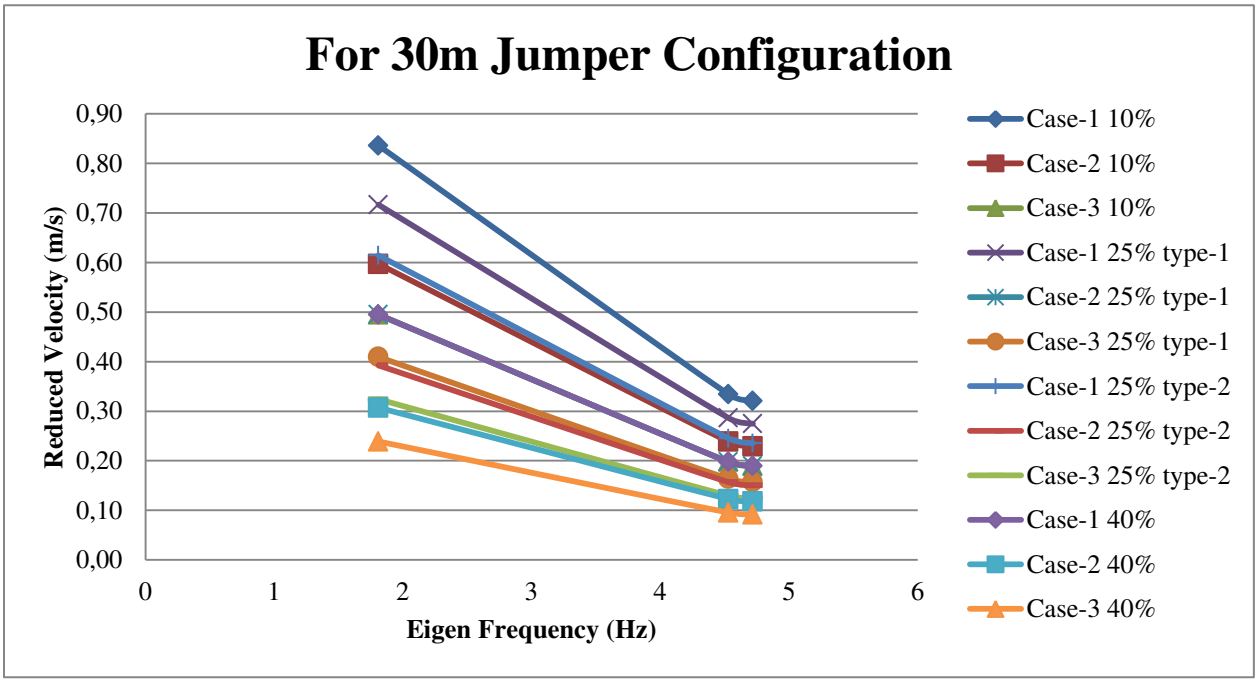

Figure 31 - Variation of Reduced Velocity (Vr) for the 30m Jumper profile

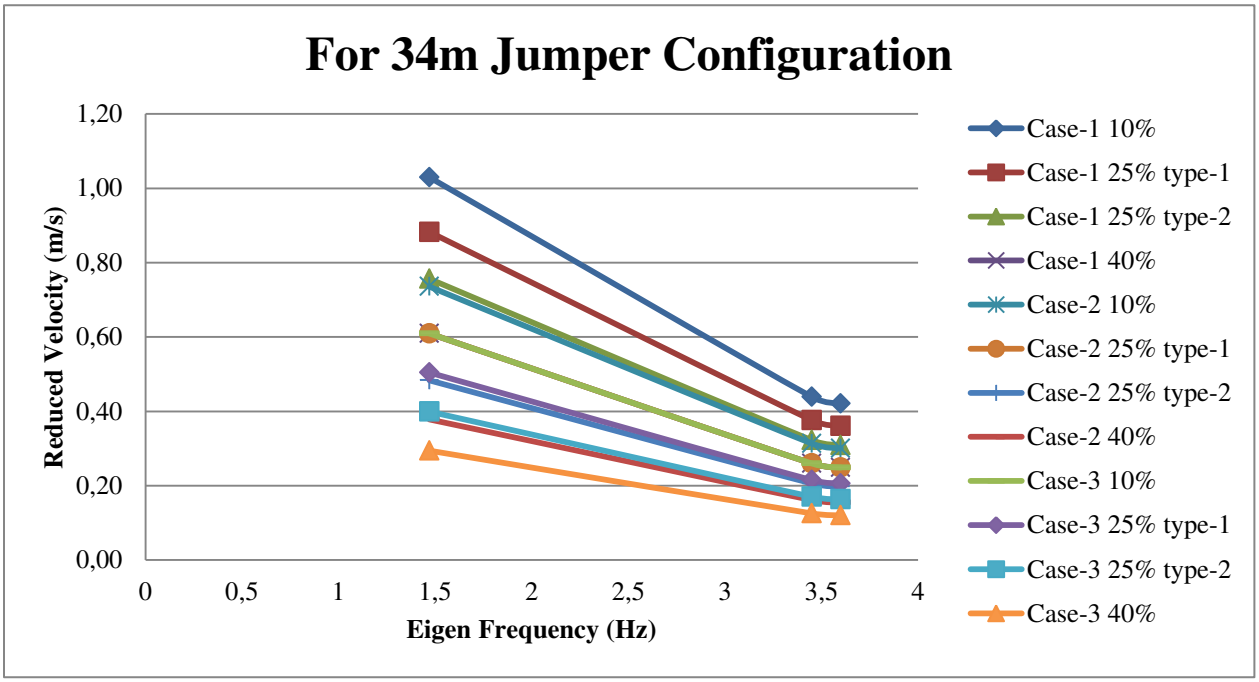

Figure 32 - Variation of Reduced Velocity (Vr) for the 34m Jumper profile

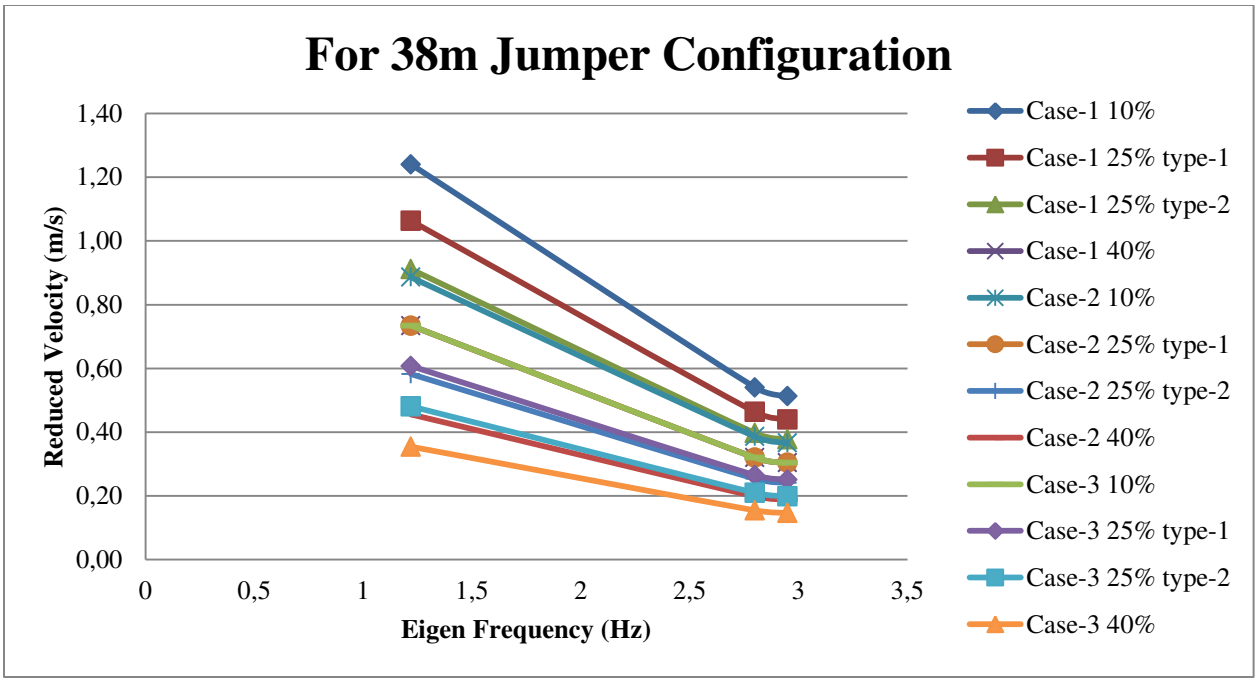

Figure 33 - Variation of Reduced Velocity (Vr) for the 38m Jumper profile

From the graphs in the figures 31, 32 and 33, we can observe that it is only the 1st mode of the excitation that makes the system more prone to the VIV "Lock-in" phenomenon. This can be observed from the tables represented in the Annexure. E. As the Eigen frequency increases with the consecutive modes, the value of the reduced velocity (Vr) gets reduced. This fits the higher modes of the system out of the VIV "Lock-in" zone. However, if the sea bottom current is strong enough, which can compensate for the frequency drop, it will then shift the system into the "Lock-in" zone. In addition, if the pipe bore diameter is small, then the increased flexibility of the system makes it more prone to "Lock-in" phenomenon and also it may lead to the multi-modal response characteristics.

Usually, the VIV response amplitude shows an increase with an increase in the reduced velocity, only up to a certain limit. Once, it has exceeded the limit, then the compensation from the reduced velocity stops, resulting in decreased amplitude due to the VIV stabilization phenomenon (from section 4.2.2). In our case study, this situation is not experienced due to the assumptions of seabed current, reasonable jumper configurations and optimal bore diameter.

Based on our observation from the figures 31, 32 and 33, the first mode of the jumper oscillation satisfies the "Lock-in" condition only under the in-line type of oscillation for the case-1 scenario. From the table-8, we infer that, only under the out-of-plane current condition, the 1st oscillation is in-line type. The amplitude of the in-line oscillation for the case-1 condition is shown in the figure 34 below. This depends on the jumper configuration, seabed current and the possibility of the "Lock-in" phenomenon. All the other cases, for which the reduced velocity does not satisfy the "Lock-in" condition, further detailed analysis of the fatigue life is not necessary. The figure

34 below is in accordance with the VIV response amplitudes specified in the tables F.3 and F.4 of the Annexure. F.

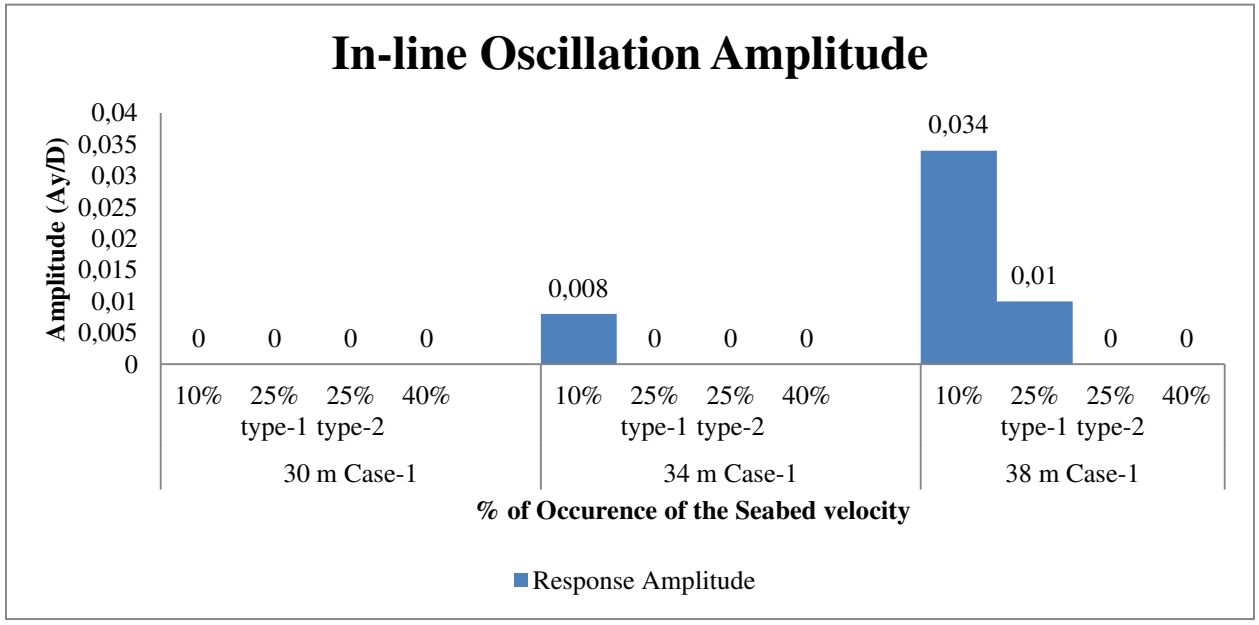

Figure 34 - Configurations specific In-line Oscillation amplitude

The unit amplitude stress for the different jumper configurations is represented in the figure 35 below. These stress values depend on the type of current flow and the nature of the oscillation involved as mentioned in the table F.2 of Annexure. F.

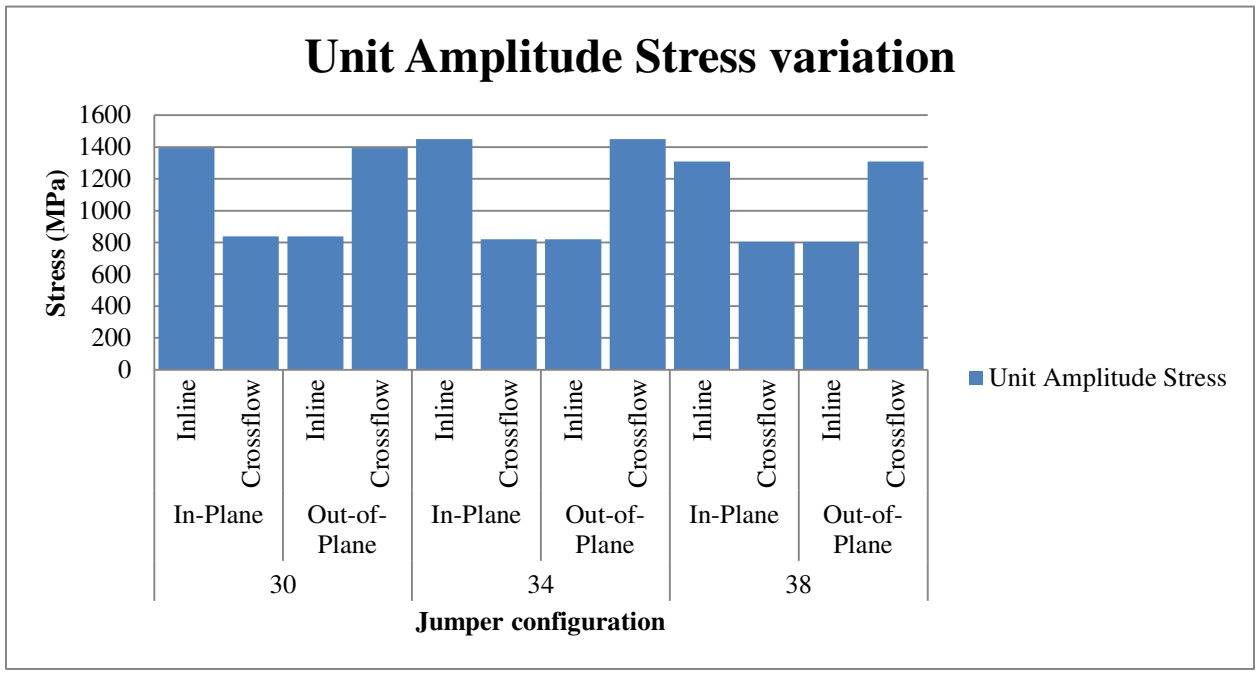

Figure 35 - Variation of the Unit Amplitude Stresses based on the jumper configurations

Based on the In-line oscillation amplitude values mentioned in the figure 34, their corresponding stresses range as per the table F.3 and F.4 of Annexure. F is represented in the figure 36 below. This stress range also depends on the unit amplitude stress and the current flow ratio.

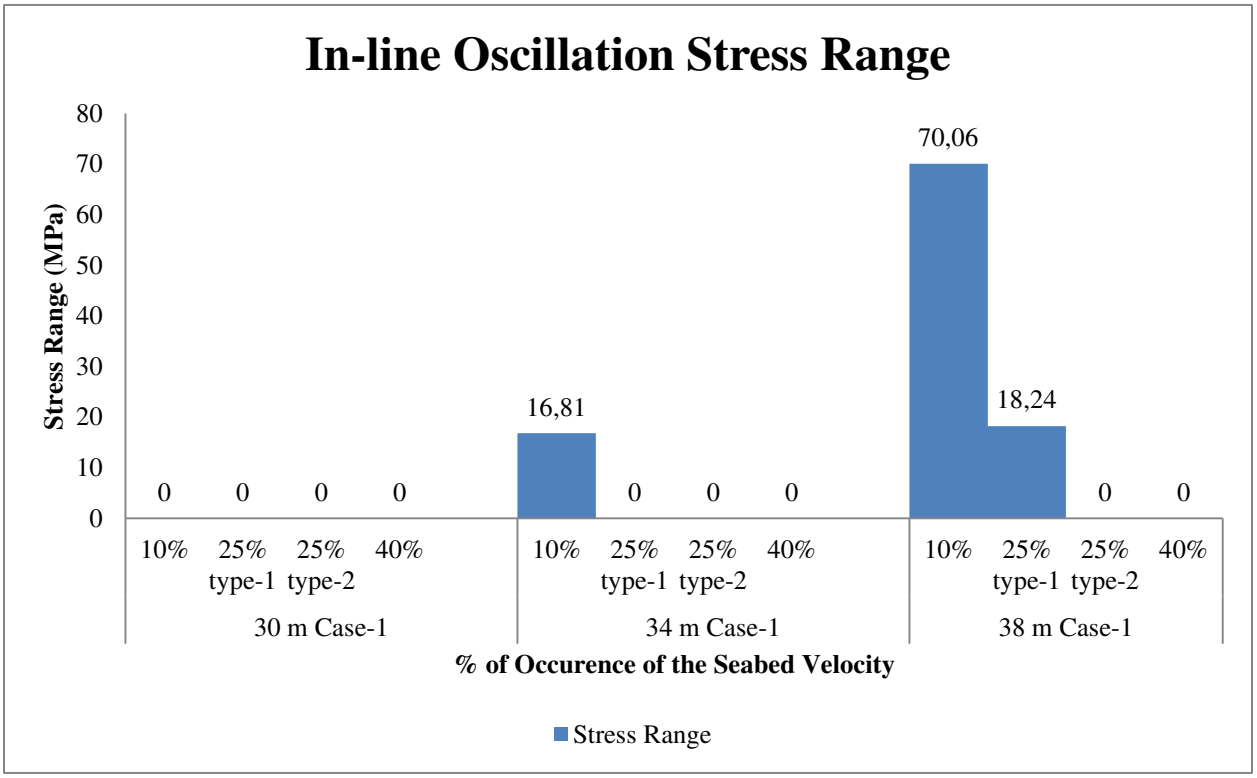

Figure 36 - Configurations specific In-line Oscillation Stress Range

From the stress range value mentioned in the figure 36 above, the number of fatigue cycles that the system can withstand, before the fatigue failure can be determined. This total cycle to the fatigue failure depends on the type of the hotspot welding and the type of the system corrosion protection. Even though, we know the total no. of cycles to the fatigue failure, it is the probability of occurrence of the fatigue cycles in a year that defines the fatigue life of the system before actual damage. However, the stress range of the system can be altered through variation in the following parameters,

- Unit amplitude stress (Based on the system flexibility and the Bore diameter)
- Oscillation amplitude (Based on the upstream velocity, system configuration and the Bore diameter)
- Current velocity ratio and
- Safety classification

With its impact on the total cycles that the system can accommodate before the fatigue failure (the higher the stress range, lower the cycles to failure). The fatigue life of the system can be

extended based on the probability of the fatigue cycle occurrence. This depends mainly on the sea bottom current variation, as all the other parameters confined to the system are fixed.

The required fatigue life of the system depends on two parameters. They are, the required design life of the system and the safety classification which depends on the location of the installation. In our case of study, the safety class is assumed to be high, as the jumper is assumed to be installed for connection between the wellhead and the manifold. Therefore, in order to attain the assumed design life of 25 years, the fatigue life of the system is supposed to be at least 100 years. The fatigue evaluation of the system depends on the following parameters,

- Jumper configuration
- Seabed current probability of occurrence
- Water depth of operation and
- Current flow direction

Since, all these parameters are related to one another, any change in one of the parameters, will influence the fatigue life of the system. This variation in the fatigue life of the system, both under the out-of-plane and in-plane current flow conditions are shown in the figures 37 and 38 respectively. But, this variation is based on the assumed probability of occurrence of the seabed current as mentioned in figure 36 above. The figure 37 and 38 below is in accordance with the tables from the Annexure. G. Those cases with the fatigue life of "Infinity" in the Annexure tables are represented as more than 100 years in the graphs here. This is because, as per our considered study case, minimum required fatigue life is 100 years.

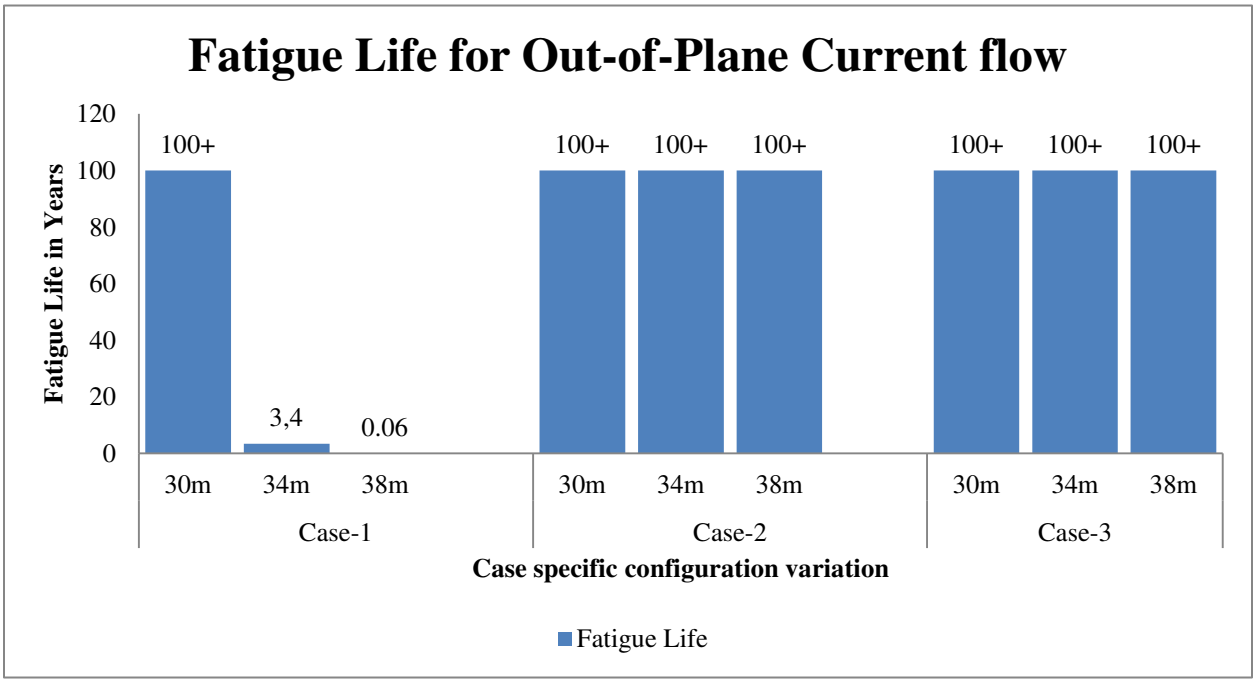

Figure 37 - Fatigue life variations for the Out-of-Plane current flow

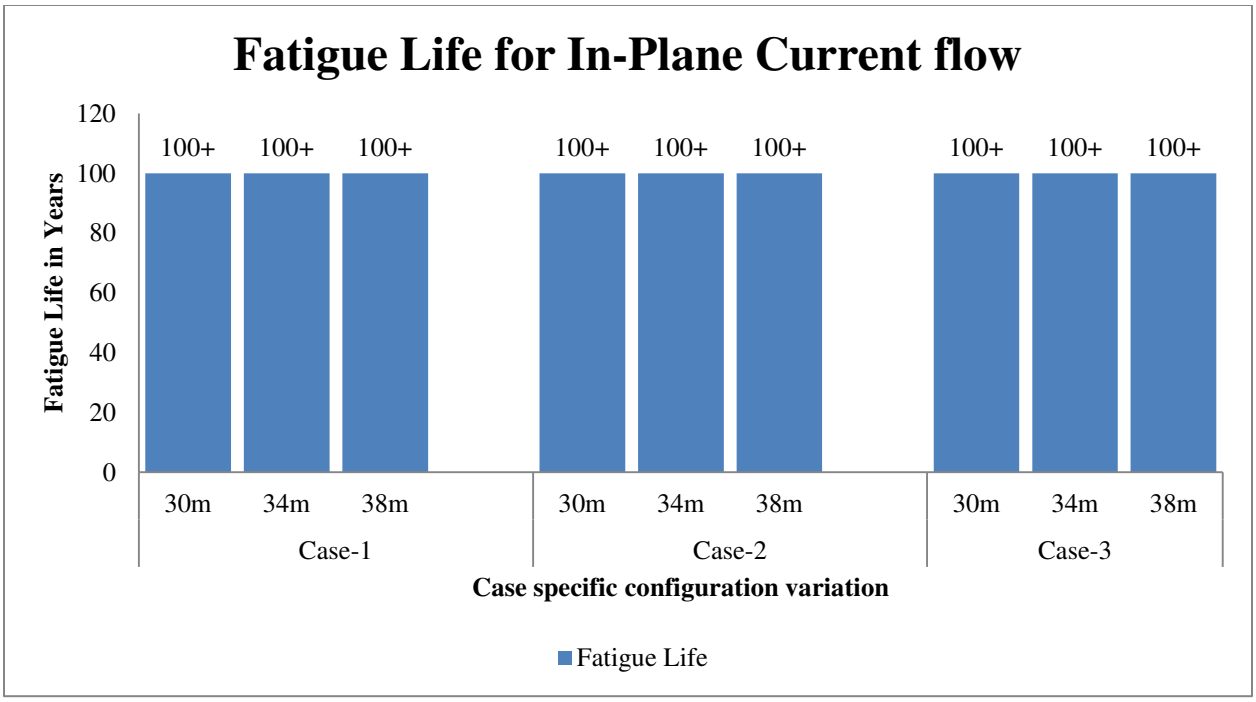

Figure 38 - Fatigue life variations for the In-Plane current flow

From the above figures 37 and 38, we can observe that it is only in the out-of-plane current flow condition, there is a possibility of reduced fatigue life. This happens only with the 34 and 38 (m) jumper configurations, under the case-1 condition of 125 meters of water depth. This is due to the presence of the strong seabed current in the case-1 condition than the other cases. Even though, the system characteristics remain the same in all the cases, it is the direction of the current flow and the seabed current velocity that influence the reduction in the system fatigue life.

The variation in the fatigue life of the system, based on the difference in the probability of the sea bottom current occurrence is examined further. This observation has been made only for the 34 and 38 (m) jumper configurations, for the case-1 condition. Since, all the other cases the system does not undergo any “lock-in” condition, they are not taken into account. It is based on the point of conservatism that, whenever there is a possibility of fatigue failure accounted from two different velocities, the one that can lead to the failure with the least no. of fatigue cycles is taken into account. This includes the possible probability of higher velocity occurrence at the nearest time period once after installation. It should also be noted that all these observations follow the safety factor of 0.25 as per DNV-RP-F105 section 2.6 based on the assumed safety class in our work.

The increase in the fatigue life of the system with the corresponding reduction in the probability of occurrence of the velocity shall be observed in figure 39, 40 and 41. All these figures are based on the tables summarized in the Annexure. H. For easy correspondence to the Annexure,

the variations in the probability are denoted as case-1 (a) to (f). It is also noted that only the changes in the velocities probability that has an impact on the lock-in zone occurrence will bring change in the fatigue life of the system.

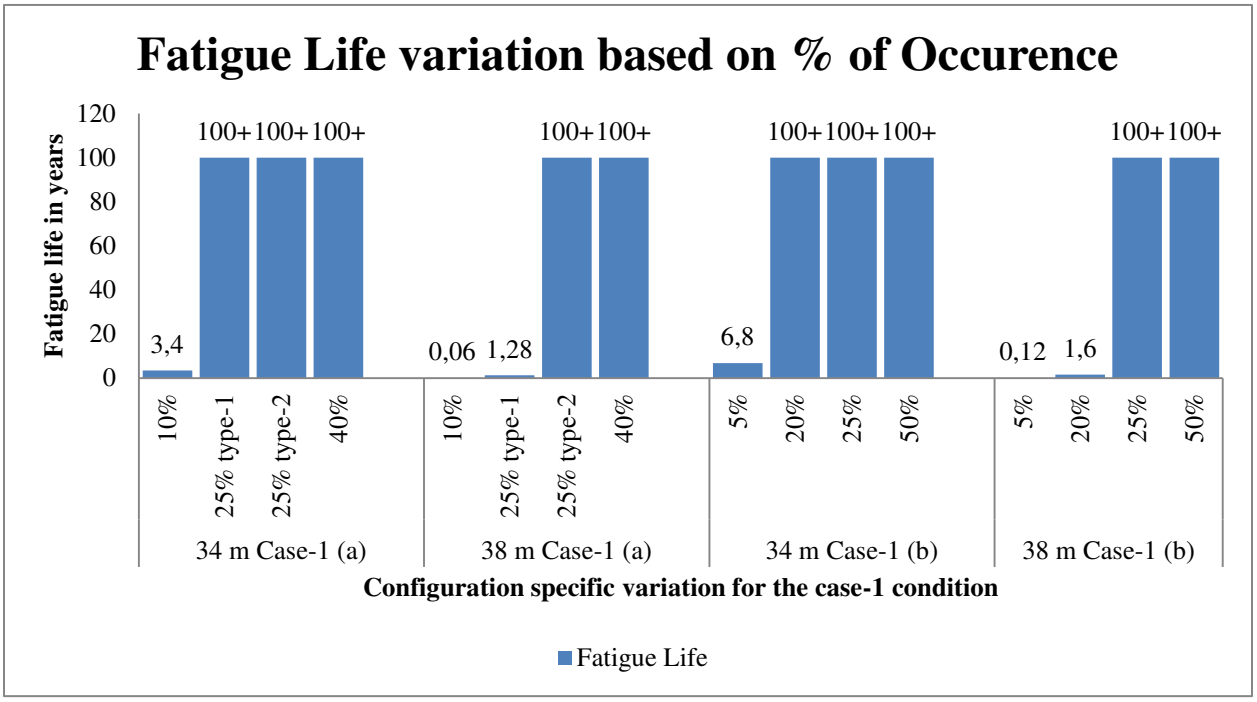

Figure 39 - Configurations specific fatigue life variation - 1

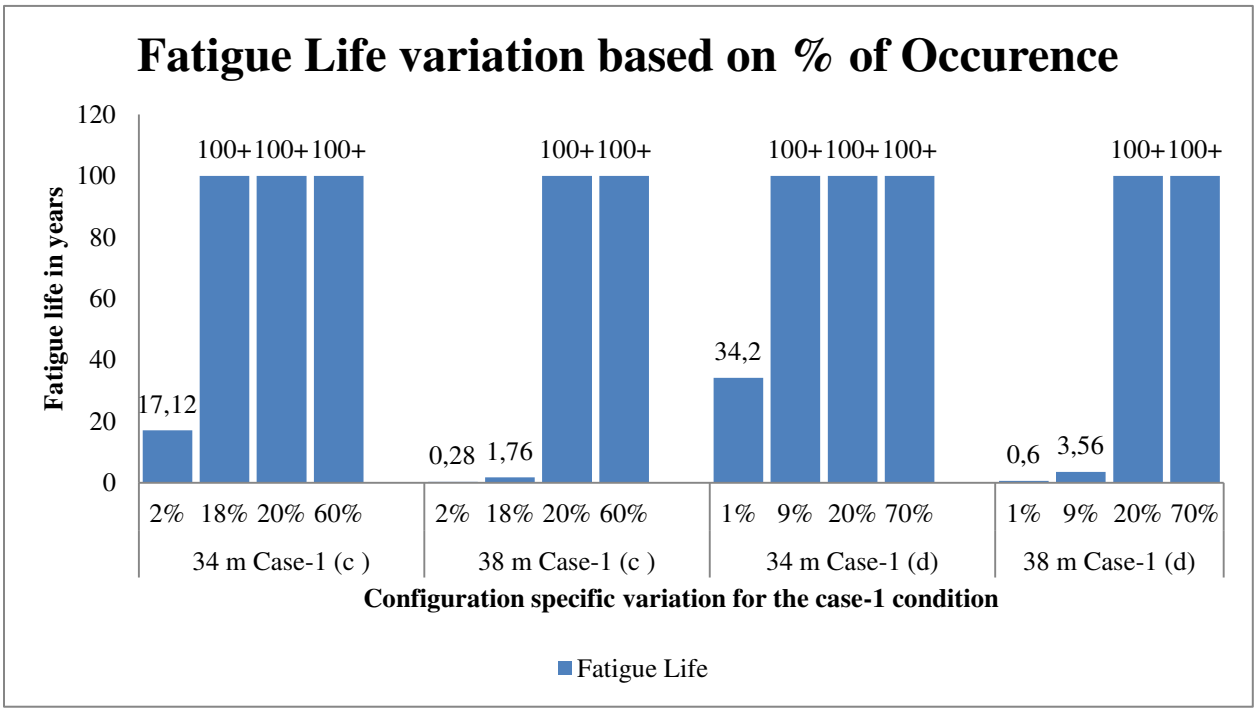

Figure 40 - Configurations specific fatigue life variation - 2

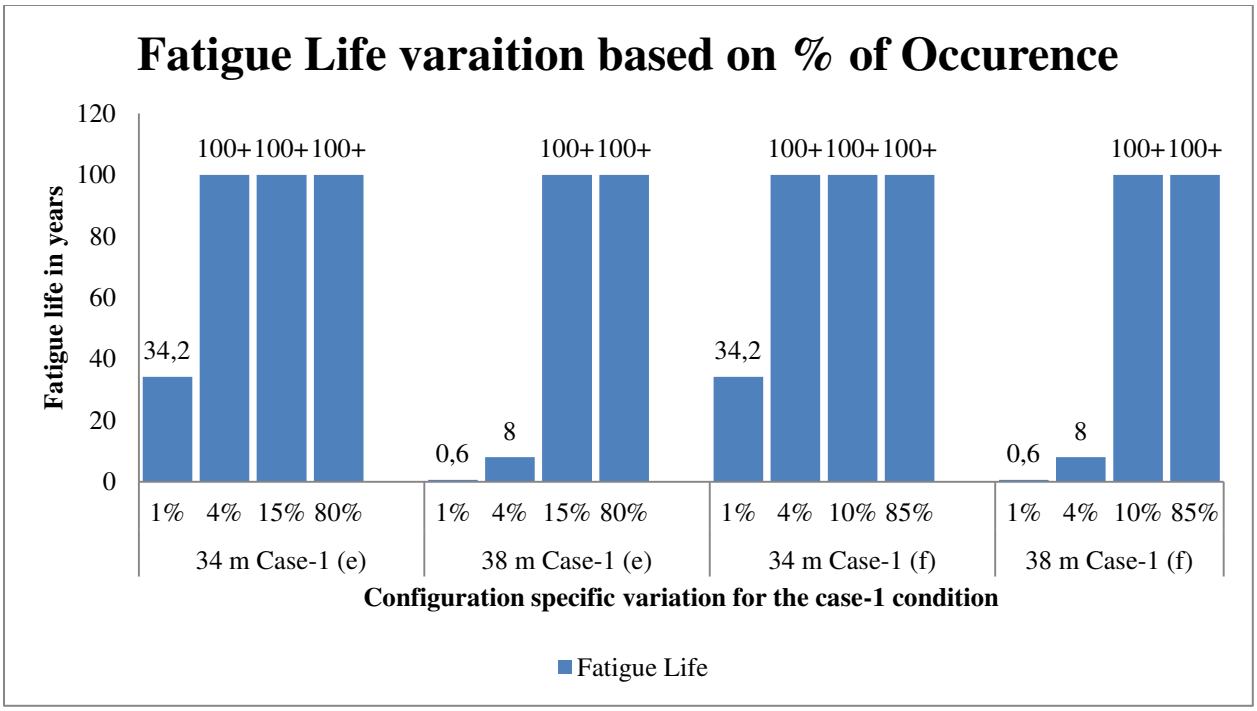

Figure 41 - Configurations specific fatigue life variation – 3

This chapter summarizes the sensitivity analysis performed in all the study case conditions considered in this work. The detailed calculations for each and every graph represented in this chapter, is summed up as tables in the appropriate Annexure. The major outcome of this chapter is, to observe the variation in the fatigue life of the system based on the configuration, water depth and the type of the current flow involved. These graphs also help us to understand that the system fatigue life can be extended for the same no. of fatigue failure cycles based on the variation in the annual probability of the fatigue cycle occurrence.

CHAPTER 7

DISCUSSION

Based on the sensitivity analysis performed, for the considered M-shaped profile of the rigid jumper, for three different configurations like the 30/34/38 meters of length, the following observations are discussed. The three different configurations, considered in our study, are based on the possible requirements from the assumed subsea layout as mentioned in Annexure. A. The analysis results depend on the seabed depth of operation of the jumper like the 125/250/1000 meters of water depth and the direction of the current flow, which can be either in-plane or out-of-plane.

7.1 Under In-Plane Current Condition

In the sensitivity analysis, whenever the considered jumper system is exposed to the assumed in-plane current flow, it will satisfy the condition of the demanded fatigue life. The demanded fatigue life in our case of study is 100 years or more, in order to meet the design life of 25 years. This result remains the same, irrespective of the jumper profile and the water depth of operation the system involves.

This is because under in-plane current flow the first mode of excitation of the system is the cross-flow type of oscillation. Since, the effective area of the jumper involved in the VIV is much less in comparison to that of the out-of-plane current condition, as mentioned in the figures.16 and 17, the possibility of the system to fall in the lock-in bandwidth is lesser. This reduces the chance of the system to experience the larger stress due to large amplitude of oscillation.

However, if the vertical doglegs of the system like V1, V3 and V5 as mentioned in the Annexure. A gets increased, then the Eigen frequency of the system gets reduced, this is due to the increased effective mass and length of the system. This reduction in the Eigen frequency can enhance the possibility of the lock-in to happen even under the in-plane current flow condition. The same result of increased lock-in possibility can be attained, if the current to which the system is exposed near the seabed is increased than the considered value as in our case study.

All the above discussed conditions that have its impact on the VIV occurrence are pertained only to our considered pipe size of 300 NB. Once the pipe size differs, the system flexibility requirement will change resulting in a different configuration than the one considered in our case study. This difference in the configuration, will impact on the Eigen frequency of the system through effective mass and length of the system variables involved. It also varies the fluid-surface contact area, which has its influence on the VIV generation strength. Hence, it can result

in a different limiting criterion for the VIV possibility, based on the jumper configuration from that of our 300 NB pipe size study case.

However, in our case study with the extreme environmental and system detail assumptions involved, the condition of the system design life of 25 years is satisfied. This can only be attained if the system fatigue life is 100 years (or) more as in our case. Under in-plane current condition, for all the three configurations, under all the three possible water depths of operation, the design life is met, because of the absence of the VIV lock-in phenomenon.

7.2 Under Out-of-Plane Current Condition

Since, the first mode of excitation under the out-of-plane current condition is the inline type of oscillation, the possibility for the jumper system to experience the lock-in phenomenon is much higher than in the in-plane current condition. This possibility would increase further with the increase in the unsupported length of the jumper configuration involved. But, based on the water depth of application, the critical length of the configuration that does not suffer any damage from the VIV phenomenon will change.

Based on our sensitive analysis study, we can observe that all the three possible configurations of the jumpers will satisfy the condition of 100 years (or) more fatigue life, under the 250 and 1000 meters of water depth scenario. But, this is not the case for 125 meters of water depth condition. The minimum decay of water particle velocity from the surface, results in a much higher seabed current velocity in the 125 meter condition, in comparison to the 250 and 1000 meters of water depth scenario.

This presence of the higher seabed current in the 125 meters of water depth scenario has resulted in a restricted critical jumper length of 30 meters, from the application perspective. The low frequency characteristics of the jumper based on the higher unsupported length have made the 34 and 38 meter jumper configuration more prone to the VIV phenomenon under this water depth condition.

Again, as mentioned in the section 7.1, the sensitivity analysis results are subjective to the considered assembly details of the jumper, with a pipe size of 300 NB and exposed to the assumed extreme environmental conditions. With any changes in these assumptions, the severity of the VIV phenomenon that the system is exposed to would differ.

Even, if the jumper configuration is exposed to the VIV phenomenon, it is the probability of occurrence of the VIV influencing current per year that defines the system survival time. This variation in the fatigue life based on the probability of occurrence per year can be observed in our case study plots. This variation in the fatigue life depends only on the velocity that influences VIV on the system. Since, in our case study the jumpers considered are assumed to be a connector between the wellhead and the manifold, the usage factor corresponding to a higher

class of safety is used. This demands a fatigue life of 100 years or more in order to satisfy the designed service life of 25 years.

Whenever, there are two different velocities that cause two different fatigue stresses in the system, then the fatigue life of the system is calculated based on the least possible fatigue life out of the two stresses. This involves the relationship between the S-N curve and the probability of occurrence per year. Since, the probability of the velocity occurrence will be different every year, a long term Rayleigh distribution of seabed velocity is usually considered to define the service life of the system.

Since, the 34 and 38 meters of jumper configuration experience the VIV effect, for the 125 meters of water depth scenario they do not satisfy the 100 years (or) more fatigue life requirement. This makes it clear that the 30 meter jumper configuration is the critical jumper length of the 125 meter water depth condition. However, as the jumper length is based on the seabed layout any length requirement of the jumper beyond 30 meters for the 125 meters water depth condition will require VIV mitigation measures to be considered. On the other hand, for the 250 and 1000 meters of water depth scenario, all the three configurations of jumpers can be successfully used, as they do meet the service life of the system.

7.3 Uncertainty

Even though, this sensitivity analysis aims to study the jumper fatigue life variation based on the difference in their configuration, water depth of operation and current flow conditions. The accuracy of our study results faces some uncertainty based on our assumptions listed in chapter 5. With the usage of real time site specific data, the accuracy of our realistic outcome can be improvised. But still the system fatigue life evaluation always remains case specific.

It should also be noted that, this fatigue life assessment focuses only on the fatigue damage from the VIV phenomenon, it does not include the fatigue damages from all other possibilities like, pipeline thermal expansion, slugging and flow induced turbulence. So, this result refers to the system total fatigue life, only if all other possibilities of fatigue damage are rectified. Any type of change that has its impact on the jumper characteristics like the fluid involved in the transportation, shape of the jumper, diameter of the pipe involved etc., will result in a different case specific critical length requirement. Moreover, any possibility of fatigue during the installation phase of the jumper will result in a corresponding reduction in the total fatigue cycles to failure during the service of the system.

Any type of update, on the standards used in our case study, may also account for the uncertainty associated with our study results. All the calculations had been performed based on the referred year of release of the standards.

CHAPTER 8

CONCLUSION AND RECOMMENDATION

The conclusion of this thesis work is divided into the following sections,

The subsea rigid jumpers, which are short rigid steel pipe sections that provide the interface between the subsea structures such as pipelines to manifolds, trees to flowlines and pipelines to risers, are not static elements as considered by many designers. In addition to satisfying the mechanical strength requirements like the pipeline thermal expansion, pipeline installation inaccuracies and lower reaction forces on the connection terminals, these jumpers should also satisfy the fatigue life requirements, in order to avoid any fatigue failure throughout the design life. The presence of the complex shape to meet its mechanical design requirements with larger unsupported lengths, results in the reduced Eigen frequency of the system making it more prone to VIV fatigue damage. The critical length of the jumper that defines the requirement for the VIV mitigation measure will change based on several factors like the jumper shape, jumper characteristics, seabed current, location of installation and the angle of the current flow.

For any typical jumper profile (like the Inverted-U, M (or) Z-shape), the fatigue failure cycles varies based on the direction of the current flow, seabed current condition, location of service and the Eigen frequency characteristics of the system. The influence of the direction of current flow upon the fatigue cycles of the system is based on the effective area of the jumper that is involved in the VIV phenomenon and also the possible type oscillation for the 1^{st} excitation mode. Even though, there are possibilities for the multi-modal response, the 1^{st} excitation mode is treated to be crucial in most of the cases due to the low Eigen frequency of the system and the lower seabed current velocity dependence. In case of the in-plane current condition, the 1^{st} mode of excitation is the cross-flow type with a lock-in velocity bandwidth of 2-16 m/s, whereas for the out-of-plane current condition it is the in-line type of oscillation with a lock-in velocity bandwidth of 0.91-4.3 m/s. This explains that the probability of the same system with the same current velocity condition to fall in the lock-in zone is much higher for the out-of-plane current flow than the in-plane current. However, this can be compensated based on the variation in the effective area that is involved in the vortex generation.

The phenomenon of multi-modal response can be possible for those systems with either much lower Eigen frequency characteristics (or) much stronger seabed current exposure. The presence of the stronger seabed current will influence the strength of the generated vortices. For the scenario with a stronger seabed current, the critical length (the maximum unsupported length without the possibility of VIV) of the jumper is reduced. Once we proceed from shallow water zone towards deep water depths, the possibility of strong seabed current is greatly reduced this is due to the exponential decay of the water particle velocity from the surface to the seabed. This

means that those systems that require VIV mitigation measure in the shallow water depth does not require any VIV mitigation measure in deeper water conditions.

For the same jumper system with the same direction of current flow and with the same seabed current velocity, the fatigue life requirement would differ based on the location of its installation. This is due to the difference in the safety factor which depends on the location uncertainty. Those systems that are close to the wellhead involve higher safety factor than those that are installed close to the platform.

Even though, all the above mentioned characteristics are related to one another in determining the total no. of fatigue cycles of the system for a considered case of study, it is the probability of occurrence of the stress range from one year that defines the fatigue life of the system. This means that, even if the no. of fatigue cycles to failure is less for a particular stress range, this will not be the fatigue life determining criterion of the system, if the probability of occurrence of that particular stress is the rarest. But, this influence of the probability of occurrence on the fatigue life of the system is only possible for those conditions that satisfy the lock-in criterion.

This work was carried out to address the present lack in the industry in order to perform the VIV analysis for the complex shaped jumper spools. But, the guidelines were used from the existing standard for pipelines DNV-RP-F105, since there is no specific standard been available in the industry for the subsea spools. Due to insufficient data on the methodology for carrying out this VIV analysis for the jumper spools, this work has confined its scope to only a typical M-shaped jumper profile with much of its time been spent on understanding the VIV phenomenon and the methodology it requires to perform the task involving some alteration from the existing guidelines for the pipeline. The methodology in this work primarily focuses on the possibility of the system to fall in the lock-in zone under respective excitation modes. This is because the amplitude of oscillation and its resulting stresses from the resonance condition are huge in comparison to other conditions. This will have a huge impact on the fatigue life of the system than in any other case. With the understanding of the VIV phenomenon and the methodology guideline from this work as the background skeleton, this work can be improved or extended further in the following paths.

- Rectifying the assumptions would improve the results accuracy of this work.
- Addition of the torsion component of stress induced in the vertical legs of the jumpers to the stress range wherever possible would result in a realistic study. This depends on the comparison of the torsion stress value to the bending stress before adding.
- The same methodology of this work can be extended further to all other possible shapes of the jumper spools to determine the ideal jumper profile that does not require any VIV mitigations even under the severe environmental case.
- Through comparison of the different jumper profile results, any extension of the existing standard DNV-RP-F105 to make it applicable also for the jumper spools can be done.

CHAPTER 9

REFERENCE

Abeele, F. V., Voorde, J. V., and Goes, P. (2008). Numerical Modelling of Vortex Induced Vibrations in Submarine Pipelines. *COMSOL Conference*. Hannover.

Achenbach, E., and Heinecke, E. (1981). On vortex shedding from smooth and rough cylinders in the range of Reynolds numbers $6x10^3$ to $5x10^6$. *Journal of fluid mechanics*, 109, 239-251.

Bai, Y., and Bai, Q. (2005). *Subsea Pipelines and Risers*. Kidlington: Elsevier.

Bai, Y., and Bai, Q. (2012). *Subsea Engineering Handbook*. Burlington: Gulf Professional Publishing.

Bishop, R. E. D. and Hassan, A. Y. (1964). The lift and drag forces on a circular cylinder oscillating in a flowing fluid. *Proceeding of the Royal Society of London*, Series A 277, 51-75.

Blevins, R. D. (2001). *Flow Induced Vibrations*. Florida: Krieger Publishing Company.

Carruth, A. L., and Cerkovnik, M. E. (2007). Jumper VIV – New Issues for New Frontiers. *17th International Offshore and Polar Engineering Conference*. Houston, Texas.

Coder, D. W. (1982). The Strouhal Number of Vortex Shedding from Marine Risers in Currents at Super-Critical Reynolds Number. *14th Annual Offshore Technology Conference*. Paper 4318.

DNV-OS-J101. (2014). Det Norske Veritas Offshore Standards, Design of Offshore Wind Turbine Structures. Oslo, Norway.

DNV-RP-C203. (2010). Det Norske Veritas Recommended Practice, Fatigue Design of Offshore Steel Structures. Oslo, Norway.

DNV-RP-F105. (2006). Det Norske Veritas Recommended Practice, Free Spanning Pipelines. Oslo, Norway.

Griffin, O.H., and Ramberg, S. E. (1974). The Vortex Street Wakes of Vibrating Cylinders. *Journal of Fluid Mechanics*, 66, 553-576.

Gudmestad, O. T. (2015). *Marine Technology and Operations (Theory and Practice).* Southampton: WIT Press.

Guo, B., Song, S., Chacko, J., and Ghalambor, A. (2005). *Offshore Pipelines.* Burlington: Gulf Professional Publishing.

Jauvtis, N., and Williamson, C. (2003). Vortex Induced Vibration of a Cylinder with Two Degrees of Freedom. *Journal of Fluids and Structures*, 17, pp. 1035-1042.

Kenny, J. P. (1993). Structural analysis of pipeline spans. *Offshore Technology Information*. HMSO.

Keulegan, G. H. and Carpenter, L. H. (1958). Forces on cylinders and plates in an oscillating fluid. *Journal of Research of the National Bureau Standards*, 60, No. 5, 423-440.

Koopman, G. H. (1967). The Vortex Wakes of Vibrating Cylinders at low Reynolds Numbers. *Journal of Fluid Mechanics*, 28, 501-512.

Lienhard, I. H. (1966). *Synopsis of lift, drag and vortex frequency data for rigid circular cylinders.* Washington: Washington State University.

Massey, B. S. (1979). *Mechanics of Fluids*. New York: Van Nostrand Reinhold.

Newman, J. N. (1977). *Marine Hydrodynamics*. Massachusetts: The Massachusetts Institute of Technology.

Ongoren, A., and Rockwell, D. (1988). Flow Structure from on Oscillatory Cylinder. *Journal of Fluid Mechanics*, 191, 197-245.

Palmer, A. C., and King, R. A. (2004). *Subsea Pipeline Engineering*. Oklahoma: PennWell Corporation.

Perry, A. E., Chong, M. S., and Lim, T. T. (1982). The vortex shedding process behind two dimensional bluff bodies. *Journal of fluid mechanics*, 116, 77-90.

Prandtl, L. (1904). Uber Flussigkeitsbewegungen bei sehr kleiner reibung. Verhandlg. III. Intern. Math. Kongr. Heidelberg, 484-491.

Roshko, A. (1954). *On the Drag and Vortex Shedding Frequency of Two Dimensional Bluff Bodies*. National Advisory Committee for Aeronautics Report.

Sarpkaya, T. (1978). Fluid forces on oscillating cylinders. *Journal of Waterway, Port, Costal and Ocean Division*, 104(WW4), 275-290.

Schlichting, H. (1968). *Boundary Layer Theory*. New York: McGraw- Hill Book Company.

Skop, R. A., Griffin, O. M., and Ramberg, S. E. (1977). Strumming Predictions for the SEACON II Experimental Mooring. *Offshore Technology Conference*. Paper OTC 2491, May 1977.

Stansby, P. K. (1976). The Locking on of Vortex Shedding due to the Cross Stream Vibration of Circular Cylinder in Uniform and Shear Flow. *Journal of Fluid Mechanics*, 74, 641-665.

Strouhal, V. (1878). Ueber eine besondere Art der Tonerregung. *In: Annalen der Physik und Chemie. Leipzig,* NF. Bd. V, H. 10, S. 216-251.

Tanida, Y., Okajima, A., and Watanabe, Y. (1973). Stability of a Circular Cylinder Oscillating in Uniform Flow or Wake. *Journal of Fluid Mechanics*, 61, 769-784.

Torum, A., and Anand, N. M. (1985). Free Span Vibrations of Submarine Pipelines in Steady flows – Effect of Free Stream Turbulence on Mean Drag Coefficient. *Journal of Energy Resource Technology*, 107, 415-420.

Vandiver, J. K. (1983). Drag Coefficients of Long Flexible Cylinders. *Offshore Technology Conference*, Paper OTC 4490, May 1977.

Williamson, C. H. K. and Roshka, A. (1988). Vortex formation in the wake of an oscillating cylinder. *Journal of Fluid and Structures*, 2, 355-381.

Wootton, L. R. (1991). Vortex-Induced Forces. *Dynamics of Marine Substructure*, London.

Zdravkovich, M. M. (1982). Review and classification of various aerodynamic and hydrodynamic means for suppressing vortex shedding. *Journal of Wind Engineering and Industrial Aerodynamics*, 7, 145-189.

ANNEXURES

ANNEXURE – A

JUMPER MODELLING

A.1 CONSIDERED SEABED LAYOUT OF STUDY

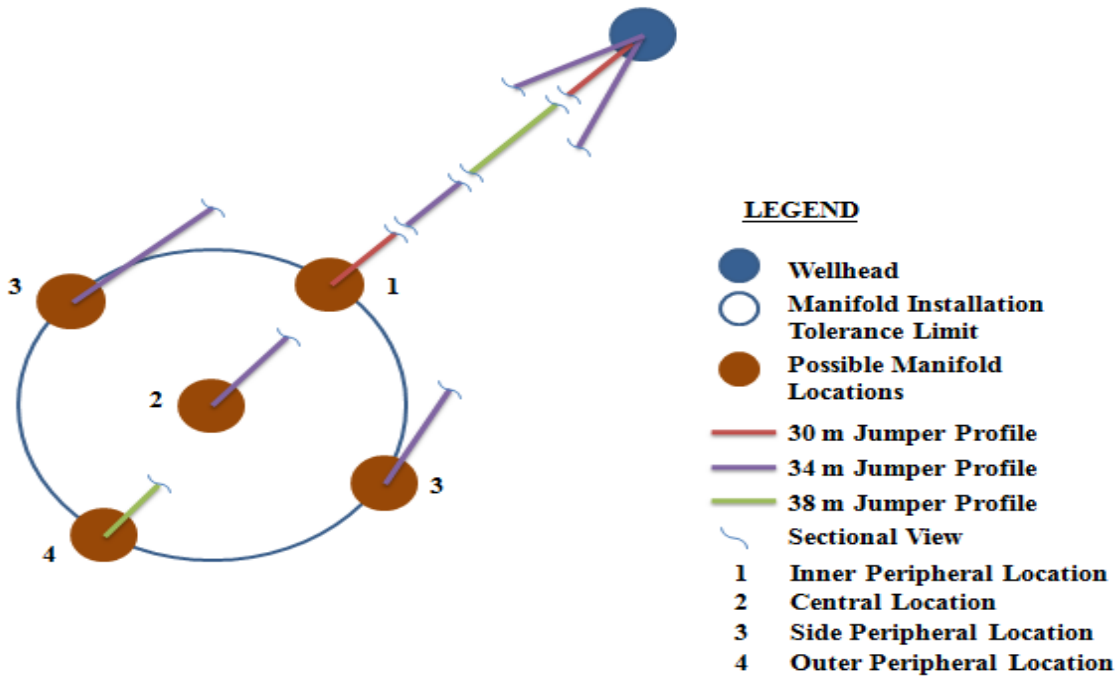

A.2 CONSIDERED JUMPER PROFILE

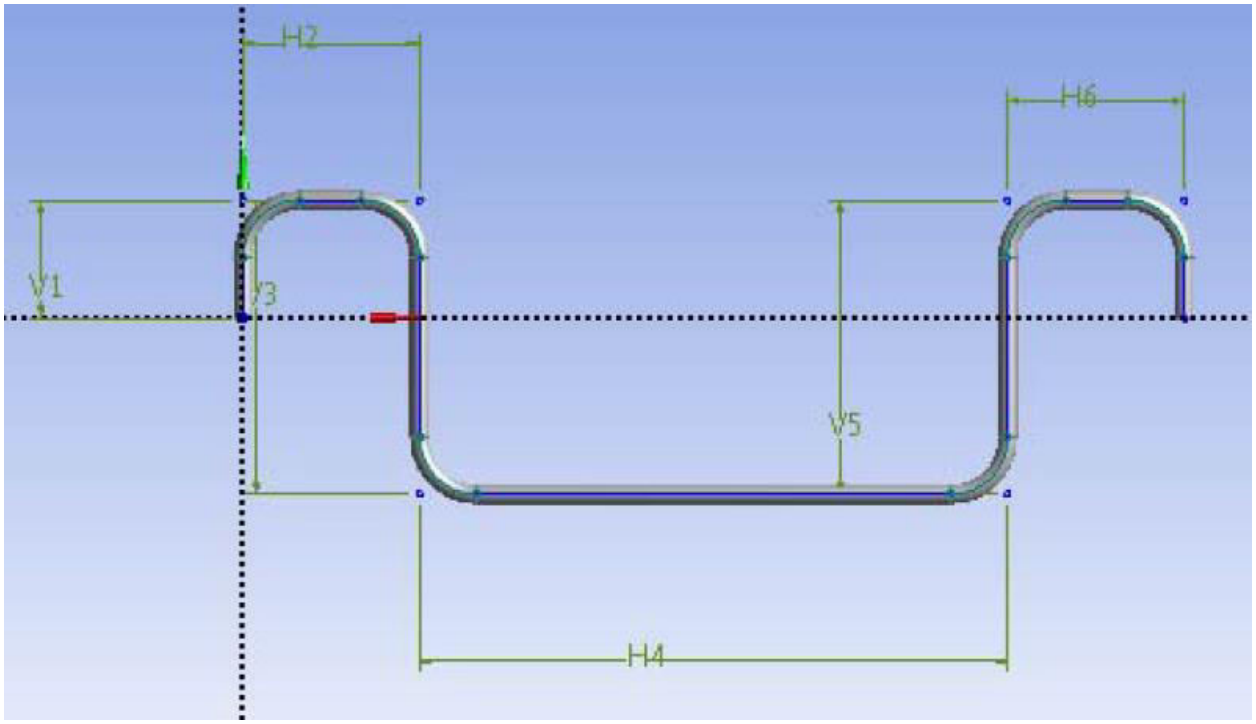

A.3 POSSIBLE JUMPER CONFIGURATIONS BASED ON THE SEABED INSTALLATION TOLERENCE

Equipment Installation Location	Span Length of Jumper (m)
Wellhead to Inner Peripheral Location	30
Wellhead to Central & Side Peripheral Location	34
Wellhead to Outer Peripheral Location	38

A.4 JUMPER SEGMENT LENGTH DETAILS FOR EACH POSSIBLE CONFIGURATIONS

Jumper Span Length (m)	Segment Length Details (m)					
	V1	H2	V3	H4	V5	H6
30	2	3	5	10	5	3
34				14		
38				18		

A.5 JUMPER MATERIAL, DIMENSIONAL & OPERATIONAL PARAMETER DETAILS

Type	Unit	Value
Pipe O.D	mm	323.80
Wall Thickness	mm	21.44
Jumper Material	-	UNS 32750
SMYS	Mpa	550.00
Material Density	Kg/m3	7800.00
Insulation Thickness	mm	Zero
Poisson Ration	No Unit	0.3
Young's Modulus	GPa	200
Cladding Thickness	mm	Zero
Maximum Operating Pressure	MPa	175
Maximum Operating Temperature	Deg. C	30
Fluid in Service	-	Oil-Gas-Water
Density of Service Fluid	Kg/m3	830
Density of Sea Water	Kg/m3	1025
Jumper Boundary Condition	-	Flanged on both sides

ANNEXURE – B

ENVIRONMENT MODELLING

B.1 FREQUENCY TABLE FOR THE COMBINATION OF Hs &Tp (Gudmestad, 2015)

Time Period Interval (s)			3	4	5	6	7	8	9	10	11	12	13	14	15	16	17	18	19	20	Height Interval Sum	Cumulative Height Observation	Alternative CDF	ln(-ln(1-F(x)))	Average Period (s)
			4	5	6	7	8	9	10	11	12	13	14	15	16	17	18	19	20	21					
Interval Height (m)		ln (h)																							
0	0.5	-0.693	1	3	12	17	10	12	5	6	3	1	1								71	71	0.009	-4.746	7.627
0.5	1	0.000	16	68	121	133	96	91	78	38	24	8	2	1	1						677	748	0.091	-2.349	7.324
1	1.5	0.405	6	63	151	170	226	171	156	79	67	41	17	4	2	1					1154	1902	0.232	-1.334	8.075
1.5	2	0.693		11	127	230	227	186	168	113	81	64	45	17	3	1	2		1	1	1277	3179	0.387	-0.714	8.639
2	2.5	0.916		2	41	146	216	202	146	128	88	50	33	31	10	5	1	1	1	2	1103	4282	0.521	-0.305	9.173
2.5	3	1.099			11	69	184	204	119	94	106	73	45	29	19	6	4	2		1	966	5248	0.639	0.019	9.753
3	3.5	1.253				22	92	207	120	102	61	71	47	33	19	6	3				783	6031	0.734	0.282	10.155
3.5	4	1.386				8	44	162	119	92	57	74	40	22	14	8	3	1			644	6675	0.813	0.516	10.427
4	4.5	1.504					16	103	114	75	60	43	18	18	10	5	5				467	7142	0.870	0.712	10.541
4.5	5	1.609				1	3	44	76	45	51	29	27	9	10	10	8	2			315	7457	0.908	0.869	11.233
5	5.5	1.705						18	60	69	50	23	13	10	5	4	4	1			257	7714	0.939	1.030	11.138
5.5	6	1.792					1	8	32	40	31	17	10	13	3	6	4	4			169	7883	0.960	1.168	11.725
6	6.5	1.872							6	28	21	22	6	10	2	4	2	2	2	1	106	7989	0.973	1.281	12.472
6.5	7	1.946							2	20	18	21	14	2	4						81	8070	0.983	1.399	12.080
7	7.5	2.015								3	9	15	13	3	1	1	1				46	8116	0.988	1.490	12.848
7.5	8	2.079									8	12	4	3	3						30	8146	0.992	1.570	12.867
8	8.5	2.140								3	5	11	4	5	3						31	8177	0.996	1.692	12.887
8.5	9	2.197									3	3	4	4	1						15	8192	0.997	1.787	13.300
9	9.5	2.251										1	4	2	3		1		1		12	8204	0.999	1.919	14.917
9.5	10	2.303										3	1								4	8208	0.999	2.002	12.750
10	10.5	2.351										1									1	8209	0.999	2.032	12.500
10.5	11	2.398								1						1		1			3	8212	0.999	2.199	15.167
11	11.5	2.442																			0	8212	0.999	2.199	
11.5	12	2.485																			0	8212	0.999	2.199	
12	12.5	2.526																			0	8212	0.999	2.199	
12.5	13	2.565																			0	8212	0.999	2.199	
13	13.5	2.603																			0	8212	0.999	2.199	
13.5	20																				0	8212	0.999	2.199	
Total			23	147	463	796	1115	1408	1201	936	743	583	348	216	113	58	38	14	5	5	**8212**				

B.2 3-PARAMETRIC WEIBULL DISTRIBUTION FOR THE FREQUENCY TABLE

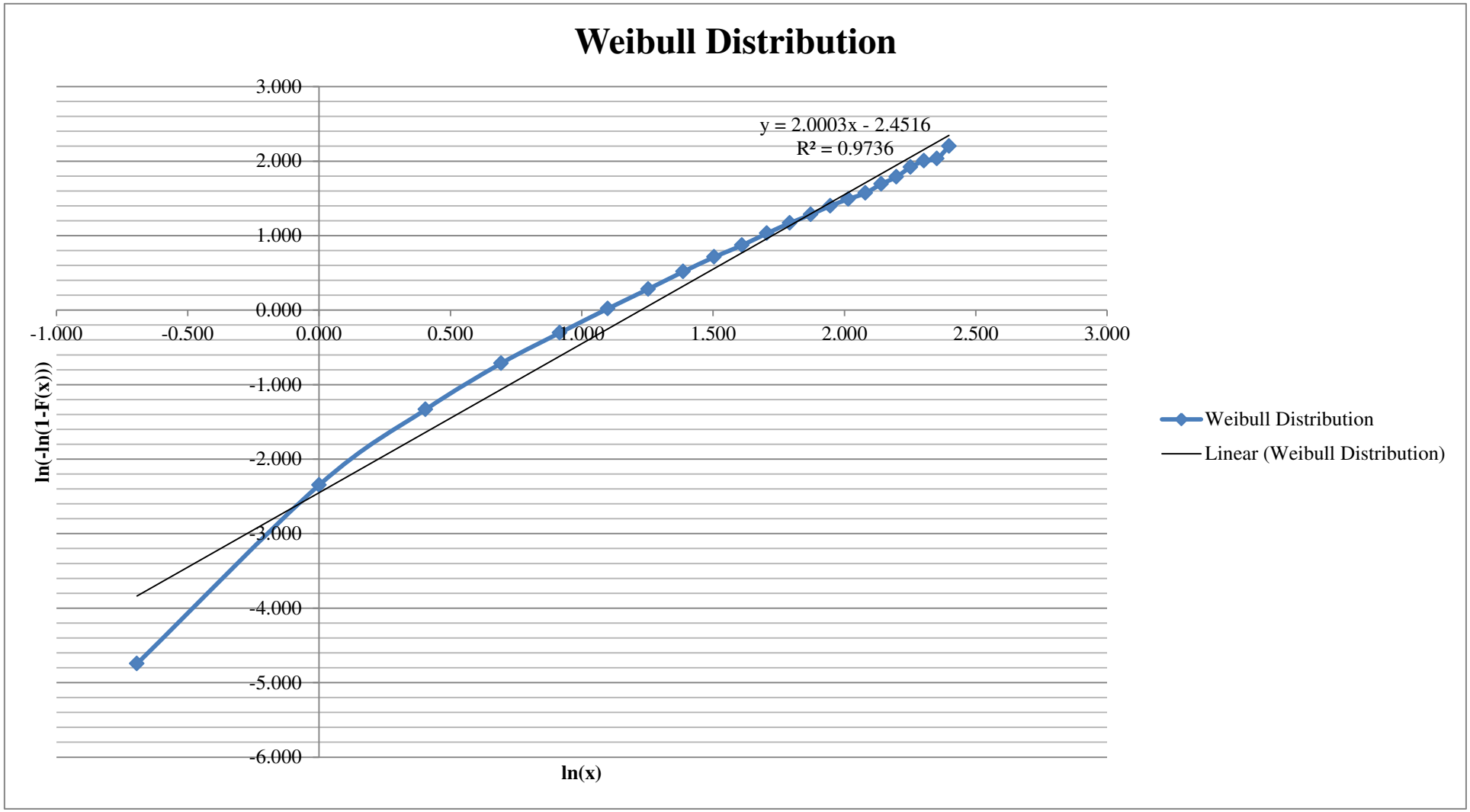

B.3 EXTREME SEA STATE SIGNIFICANT WAVE HEIGHT

Inputs		
Description	**Value**	**Unit**
Considered Period of Exceedance	100	Years
Type of Sea Storm Observation	3	Hours
Total no. of observation possible	292000	No's
Extreme value in Y-axis for 100 year condition	2.533	No Unit
Slope of Linear Weibull Distribution	2	No Unit
Constant of Linear Weibull Distribution	-2.451	No Unit
Ln (h)	2.492	No Unit
Extreme Sea State Significant Height in 100 years	12.08	meters
Results		
Description	**Value**	**Unit**
Significant wave height of extreme sea state	**12**	**meters**

B.4 EXTREME SEA STATE SIGNIFICANT WAVE HEIGHT & PEAK PERIOD RELATION

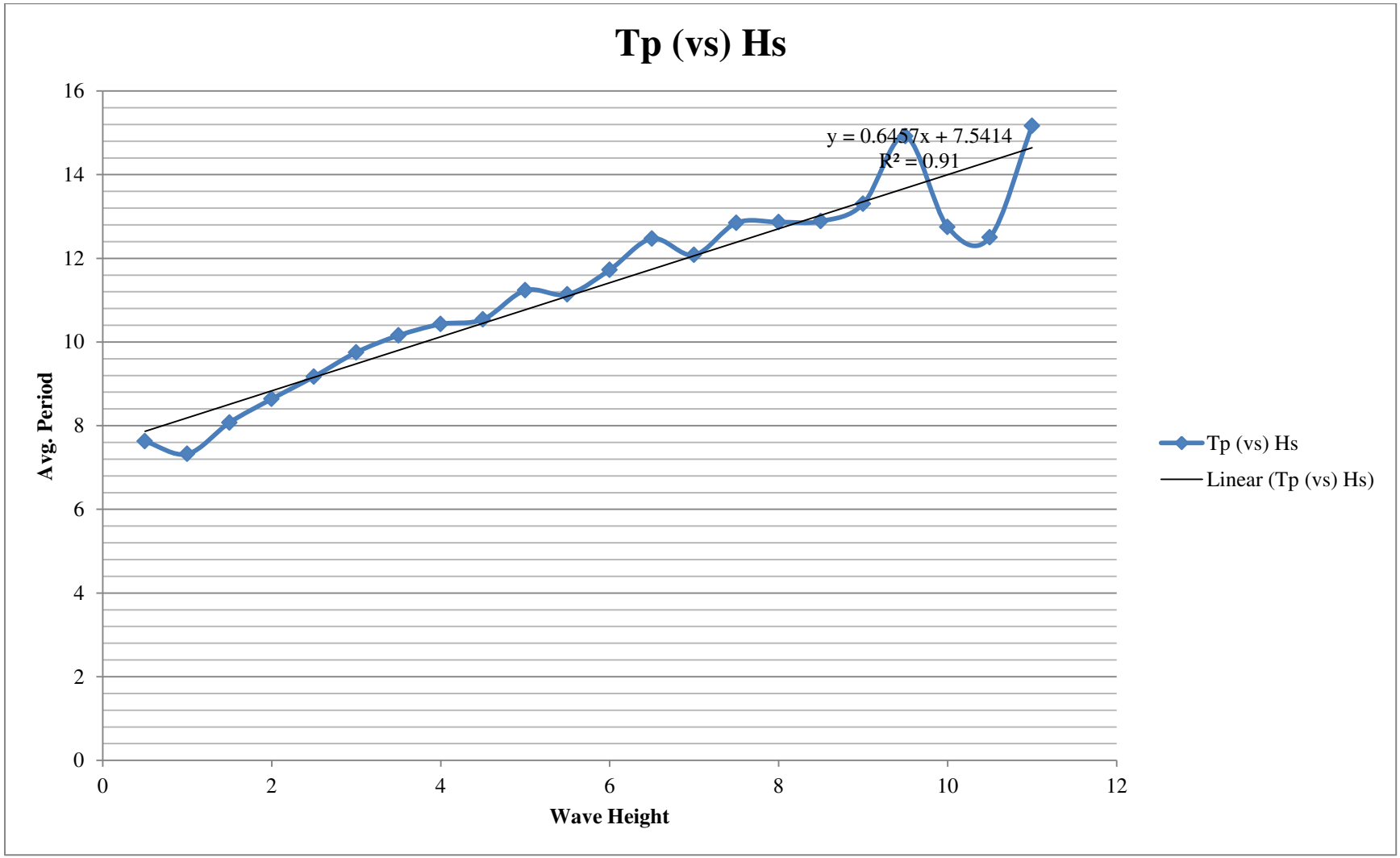

B.5 EXTREME SEA STATE PEAK WAVE PERIOD

Inputs		
Description	**Value**	**Unit**
Considered Period of Exceedance	100	Years
Type of Sea Storm Observation	3	Hours
Total no. of observation possible	292000	No's
Extreme Sea State Wave Height	12	m
Slope of Linear Tp (vs) Hs	0.645	No Unit
Constant of Linear Tp (vs) Hs	7.541	No Unit
Results		
Description	**Value**	**Unit**
Wave Period of extreme sea state	**15**	**sec**

B.6 EXTREME SEA STATE ZERO UP-CROSSING PERIOD & CHARACTERISTIC HIGHEST WAVE CREST

Inputs		
Description	**Value**	**Unit**
Extreme Sea State Wave Height	12	meters
Extreme Sea State Peak Wave Period	15	sec
Extreme Sea State Angular Frequency	0.42	rad/sec
Peak Shape Factor	2.16	No Unit
Type of Sea Storm Observation	3	Hours
Number of waves observed during the storm period	982	No's
Results		
Description	**Value**	**Unit**
Zero Up Crossing Period of extreme sea state	**11**	**sec**
Characteristic Highest Wave Crest	**11**	**meter**

B.7 WAVE INDUCED CURRENT VELOCITY @ PIPE LEVEL

Case - 1				**Case - 2**				**Case - 3**			
Water Depth = 125 Meters				**Water Depth = 250 Meters**				**Water Depth = 1000 Meters**			
Extreme Sea State Wave Amplitude	ξ_0	11	m	Extreme Sea State Wave Amplitude	ξ_0	11	m	Extreme Sea State Wave Amplitude	ξ_0	11	m
Extreme Sea State Wave Period	T	11	sec	Extreme Sea State Wave Period	T	11	sec	Extreme Sea State Wave Period	T	11	sec
Water Depth	d	125	m	Water Depth	d	250	m	Water Depth	d	1000	m
Pipe Elevation	z	124	m	Pipe Elevation	z	249	m	Pipe Elevation	z	999	m
Acceleration due to Gravity	g	9.81	m/s^2	Acceleration due to Gravity	g	9.81	m/s^2	Acceleration due to Gravity	g	9.81	m/s^2
Calculation of Wave Length (L) in Meters using Dispersion Equation				**Calculation of Wave Length (L) in Meters using Dispersion Equation**				**Calculation of Wave Length (L) in Meters using Dispersion Equation**			
Wave Length	L	189.00	m	Wave Length	L	189.00	m	Wave Length	L	189.00	m
ω2		0.3259	hertz^2	ω2		0.3259	hertz^2	ω2		0.3259	hertz^2
g.k		0.3260	hertz^2	g.k		0.3260	hertz^2	g.k		0.3260	hertz^2
tanh (kd)		0.9995	No unit	tanh (kd)		1.0000	No unit	tanh (kd)		1.0000	No unit
g.k.tanh (kd)		0.3258	hertz^2	g.k.tanh (kd)		0.3260	hertz^2	g.k.tanh (kd)		0.3260	hertz^2
Wave Length	**L**	**189**	**m**	**Wave Length**	**L**	**189**	**m**	**Wave Length**	**L**	**189**	**m**
Calculation of the water type (Shallow/Intermediate/Deep)				**Calculation of the water type (Shallow/Intermediate/Deep)**				**Calculation of the water type (Shallow/Intermediate/Deep)**			
Ratio	d/L	0.66	No Unit	Ratio	d/L	1.32	No Unit	Ratio	d/L	5.29	No Unit
Water Depth Type		**Deep**		**Water Depth Type**		**Deep**		**Water Depth Type**		**Deep**	

B.7 WAVE INDUCED CURRENT VELOCITY @ PIPE LEVEL (CONTINUES)

Case - 1			**Case - 2**			**Case - 3**		
Calculation of Horizontal Water Particle velocity @ the pipe level			**Calculation of Horizontal Water Particle velocity @ the pipe level**			**Calculation of Horizontal Water Particle velocity @ the pipe level**		
ξ0.k.g	3.59	m/s^2	ξ0.k.g	3.59	m/s^2	ξ0.k.g	3.59	m/s^2
ω	0.57	hertz	ω	0.57	hertz	ω	0.57	hertz
kz @ wave crest	0.37	No unit	kz @ wave crest	0.37	No unit	kz @ wave crest	0.37	No unit
kz @ pipe level	-4.12	No unit	kz @ pipe level	-8.27	No unit	kz @ pipe level	-33.19	No unit
e^kz @ wave crest	1.44	No unit	e^kz @ wave crest	1.44	No unit	e^kz @ wave crest	1.44	No unit
e^kz @ pipe level	0.02	No unit	e^kz @ pipe level	0.00	No unit	e^kz @ pipe level	0.00	No unit
Horizontal Particle Velocity (u) @ wave crest	9.05	m/s	Horizontal Particle Velocity (u) @ wave crest	9.05	m/s	Horizontal Particle Velocity (u) @ wave crest	9.05	m/s
Horizontal Particle Velocity (u) @ pipe level	**0.10**	**m/s**	**Horizontal Particle Velocity (u) @ pipe level**	**0.00**	**m/s**	**Horizontal Particle Velocity (u) @ pipe level**	**0.00**	**m/s**

B.8 DECAY OF THE VELOCITY ALONG THE WATER DEPTH FOR CASE-1

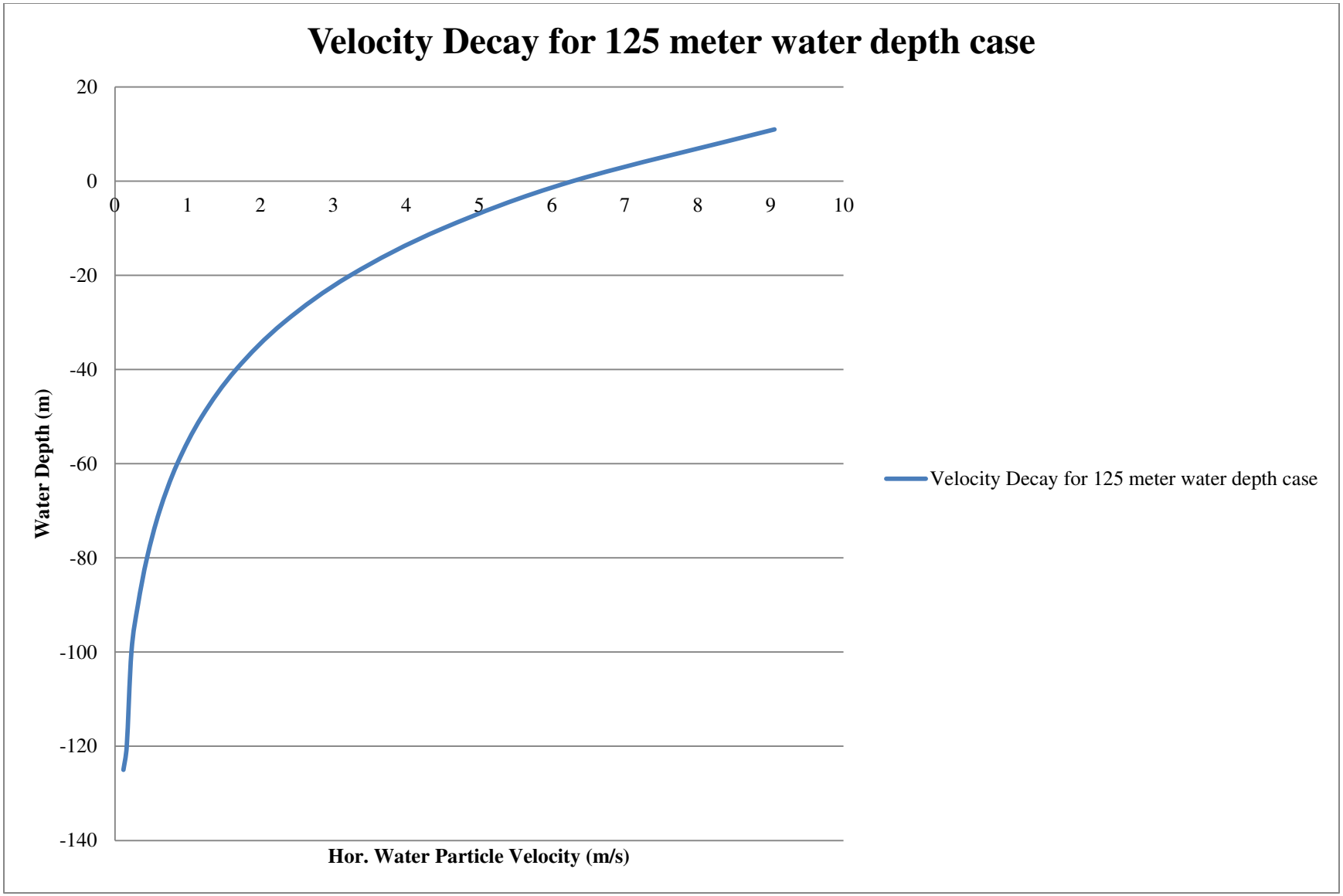

B.9 DECAY OF THE VELOCITY ALONG THE WATER DEPTH FOR CASE-2

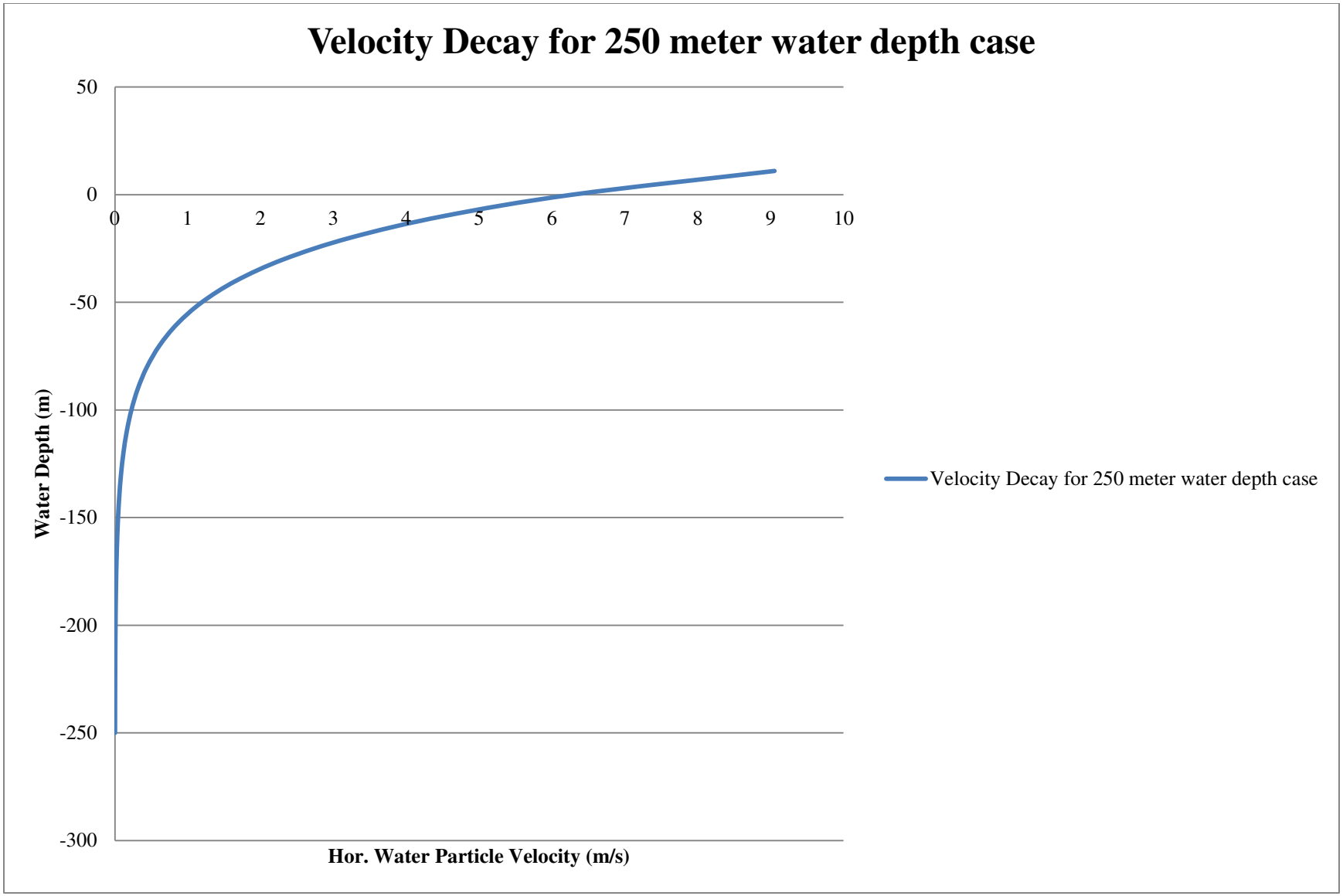

B.10 DECAY OF THE VELOCITY ALONG THE WATER DEPTH FOR CASE-3

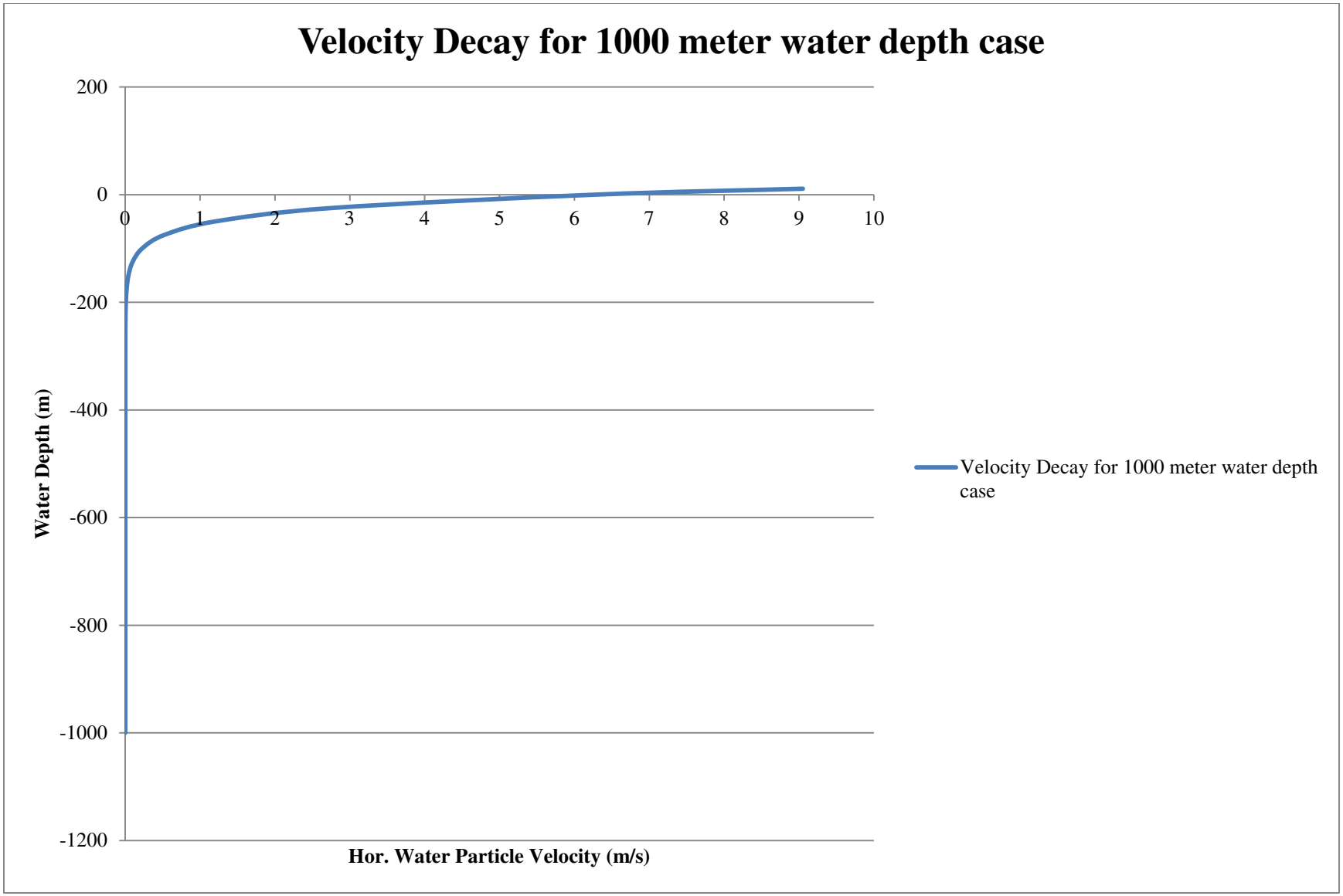

B.11 CASE SPECIFIC TIDAL VELOCITY @ PIPE LEVEL DETAILS

Tidal Current Details for Case-1				**Tidal Current Details for Case-2**				**Tidal Current Details for Case-3**			
Tidal Velocity @ the sea surface	Knots	1.5	Assumed	Tidal Velocity @ the sea surface	Knots	1.5	Assumed	Tidal Velocity @ the sea surface	Knots	1.5	Assumed
Water depth considered	m	125	Water Depth	Water depth considered	m	250	Water Depth	Water depth considered	m	1000	Water Depth
Pipe level	m	124	Pipe Level	Pipe level	m	249	Pipe Level	Pipe level	m	999	Pipe Level
Tidal Velocity @ Pipe level	**m/s**	**0.39**	**DNV OS J101**	**Tidal Velocity @ Pipe level**	**m/s**	**0.35**	**DNV OS J101**	**Tidal Velocity @ Pipe level**	**m/s**	**0.29**	**DNV OS J101**
Wave Velocity @ Pipe level	**m/s**	**0.10**	**From Extreme State**	**Wave Velocity @ Pipe level**	**m/s**	**0.00**	**From Extreme State**	**Wave Velocity @ Pipe level**	**m/s**	**0.00**	**From Extreme State**
Total Current Details for Case-1				**Total Current Details for Case-2**				**Total Current Details for Case-3**			
Total Velocity @ Pipe level	**m/s**	**0.49**		**Total Velocity @ Pipe level**	**m/s**	**0.35**		**Total Velocity @ Pipe level**	**m/s**	**0.29**	

B.12 LONG-TERM CASE SPECIFIC CURRENT VELOCITY DISTRIBUTION

Case-1		**Case-2**		**Case-3**	
Current Speed (m/s)	**Occurrence (%)**	**Current Speed (m/s)**	**Occurrence (%)**	**Current Speed (m/s)**	**Occurrence (%)**
0.29	40	0.18	40	0.14	40
0.36	25	0.23	25	0.19	25
0.42	25	0.29	25	0.24	25
0.49	10	0.35	10	0.29	10

ANNEXURE – C

RESPONSE MODELLING

C.1 GENERALIZED INPUT OF JUMPER PROPERTIES & SAFETY FACTOR DETAILS IRRESPECTIVE OF THE STUDY CASE

JUMPER PROPERTIES			
Type	**Unit**	**Value**	**Comments**
Pipe O.D	mm	323.80	
Wall Thickness	mm	21.44	
Jumper Material	-	UNS 32750	
SMYS	Mpa	550.00	
Material Density	Kg/m3	7800	
Jumper Total Length	m	30/34/38	Profile Specific
Concrete coated	-	No	
Jumper effective Mass per unit length	Kg/m	294.70	Pipe + Content + Displaced Water

SAFETY FACTOR DETAILS			
Type	**Unit**	**Value**	**Comments (DNV-RPF105)**
γk	No Unit	1.30	Based on Section 2.6
γs	No Unit	1.30	Based on Section 2.6
$\gamma on,IL$	No Unit	1.10	Based on Section 2.6
$\gamma on,CF$	No Unit	1.20	Based on Section 2.6
γf	No Unit	1.15	Based on Section 2.6

C.2 MODAL ANALYSIS RESULTS BASED ON THE JUMPER PROFILE UNDER IN-PLANE CURRENT FLOW CONDITION

MODAL ANALYSIS RESULTS FOR THE 30m JUMPER PROFILE		
Mode No	**Mode Type**	**Natural Frequency (Hz)**
1	Cross-Flow	1.81
2	In-Line	4.53
3	Cross-Flow	4.72

MODAL ANALYSIS RESULTS FOR THE 34m JUMPER PROFILE		
Mode No	**Mode Type**	**Natural Frequency (Hz)**
1	Cross-Flow	1.47
2	In-Line	3.45
3	Cross-Flow	3.60

MODAL ANALYSIS RESULTS FOR THE 38m JUMPER PROFILE		
Mode No	**Mode Type**	**Natural Frequency (Hz)**
1	Cross-Flow	1.22
2	In-Line	2.80
3	Cross-Flow	2.95

C.3 MODAL ANALYSIS RESULTS BASED ON THE JUMPER PROFILE UNDER OUT-OF-PLANE CURRENT FLOW CONDITION

MODAL ANALYSIS RESULTS FOR THE 30m JUMPER PROFILE		
Mode No	**Mode Type**	**Natural Frequency (Hz)**
1	In-Line	1.81
2	Cross-Flow	4.53
3	In-Line	4.72

MODAL ANALYSIS RESULTS FOR THE 34m JUMPER PROFILE		
Mode No	**Mode Type**	**Natural Frequency (Hz)**
1	In-Line	1.47
2	Cross-Flow	3.45
3	In-Line	3.60

MODAL ANALYSIS RESULTS FOR THE 38m JUMPER PROFILE		
Mode No	**Mode Type**	**Natural Frequency (Hz)**
1	In-Line	1.22
2	Cross-Flow	2.80
3	In-Line	2.95

C.4 TIDAL CURRENT & ENVIRONMENTAL INPUTS FOR THE CASE-1 CONDITION (125 m WATER DEPTH)

TIDAL CURRENT DETAILS			
Type	**Unit**	**Value**	**Comments**
Tidal Velocity @ the sea surface	Knots	1.5	Assumed
Water depth considered	m	125	
Pipe level	m	124	
Tidal Velocity @ Pipe level	m/s	0.39	DNV OS J-101

ENVIRONMENTAL DETAILS			
Type	**Unit**	**Value**	**Comments**
Sea Water Density	Kg/m3	1025	Density for about 4 deg condition
Current Velocity	m/s	0.39	Based on Tidal Current details
Sea Water Viscosity	m2/s	0.000001	Usually defined value for the seawater
Flow angle relative to pipe axis	deg	90.00	Flow assumed normal to the pipe axis
Wave Velocity @ Pipe level	m/s	0.10	
Wave Frequency	Hz	0.09	
Turbulence Intensity	No Unit	0.05	Based on Section 3.2.11
Soil Damping	No Unit	0.00	Based on Section 7.3.1
Seabed Gap from Pipe Bottom	mm	838	Correction factor based on the seabed proximity
Safety Class	High & Well defined		Assumed

C.5 TIDAL CURRENT & ENVIRONMENTAL INPUTS FOR THE CASE-2 CONDITION (250 m WATER DEPTH)

TIDAL CURRENT DETAILS			
Type	**Unit**	**Value**	**Comments**
Tidal Velocity @ the sea surface	Knots	1.50	Assumed
Water depth considered	m	250	
Pipe level	m	249	
Tidal Velocity @ Pipe level	m/s	0.35	DNV OS J-101

ENVIRONMENTAL DETAILS			
Type	**Unit**	**Value**	**Comments**
Sea Water Density	Kg/m3	1025	Density for about 4 deg condition
Current Velocity	m/s	0.35	Based on Tidal Current details
Sea Water Viscosity	m2/s	0.000001	Usually defined value for the seawater
Flow angle relative to pipe axis	deg	90.00	Flow assumed normal to the pipe axis
Wave Velocity @ Pipe level	m/s	0.00	
Wave Frequency	Hz	0.09	
Turbulence Intensity	No Unit	0.05	Based on Section 3.2.11
Soil Damping	No Unit	0.00	Based on Section 7.3.1
Seabed Gap from Pipe Bottom	mm	838	Correction factor based on the seabed proximity
Safety Class	High & Well defined		Assumed

C.6 TIDAL CURRENT & ENVIRONMENTAL INPUTS FOR THE CASE-3 CONDITION (1000 m WATER DEPTH)

TIDAL CURRENT DETAILS			
Type	**Unit**	**Value**	**Comments**
Tidal Velocity @ the sea surface	Knots	1.50	Assumed
Water depth considered	m	1000	
Pipe level	m	999	
Tidal Velocity @ Pipe level	m/s	0.29	DNV OS J-101

ENVIRONMENTAL DETAILS			
Type	**Unit**	**Value**	**Comments**
Sea Water Density	Kg/m3	1025	Density for about 4 deg condition
Current Velocity	m/s	0.29	Based on Tidal Current details
Sea Water Viscosity	m2/s	0.000001	Usually defined value for the seawater
Flow angle relative to pipe axis	deg	90.00	Flow assumed normal to the pipe axis
Wave Velocity @ Pipe level	m/s	0.00	
Wave Frequency	Hz	0.09	
Turbulence Intensity	No Unit	0.05	Based on Section 3.2.11
Soil Damping	No Unit	0.00	Based on Section 7.3.1
Seabed Gap from Pipe Bottom	mm	838	Correction factor based on the seabed proximity
Safety Class	High & Well defined		Assumed

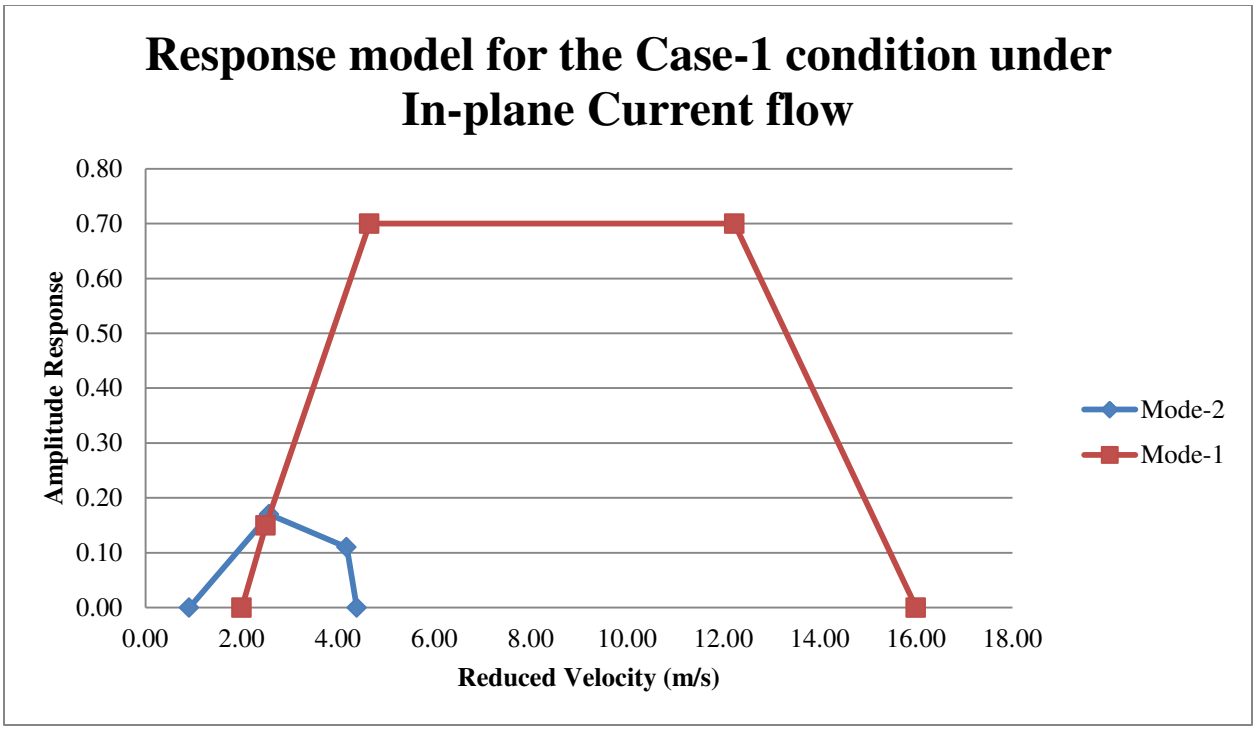

C.7 TYPICAL RESPONSE MODEL UNDER IN-PLANE CURRENT FLOW CONDITION FOR CASE-1

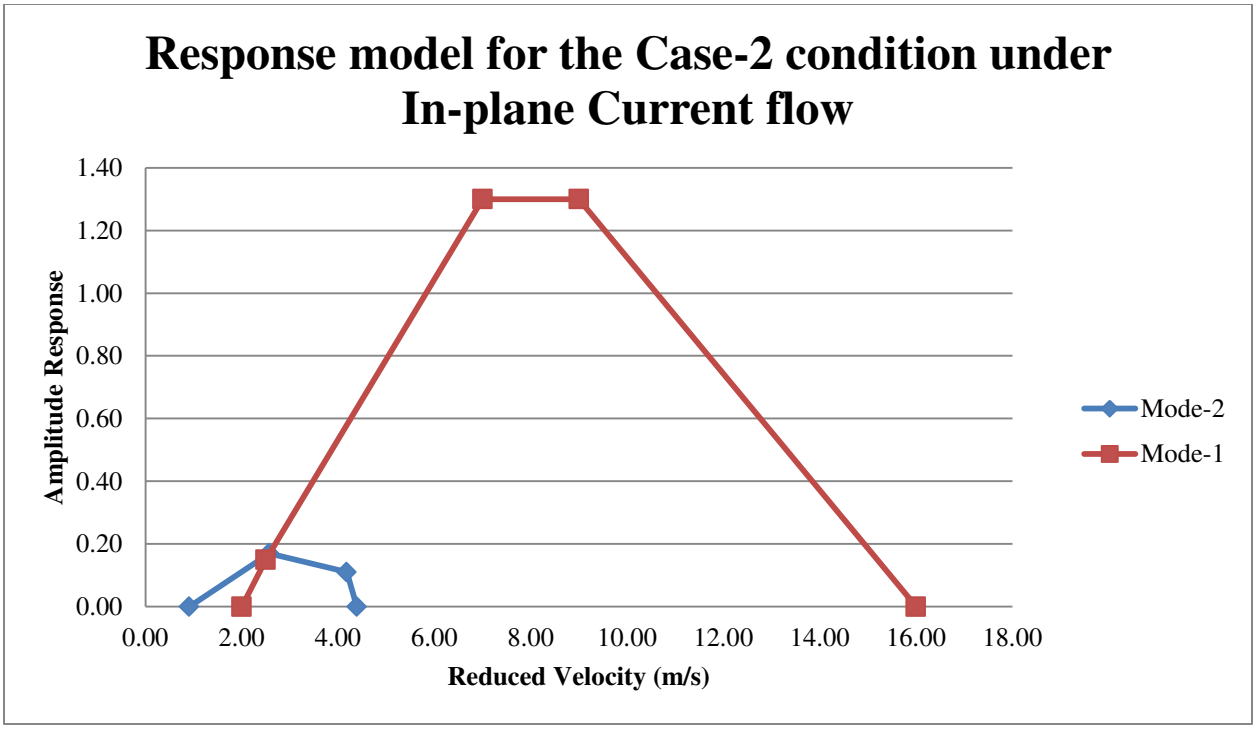

C.8 TYPICAL RESPONSE MODEL UNDER IN-PLANE CURRENT FLOW CONDITION FOR CASE-2

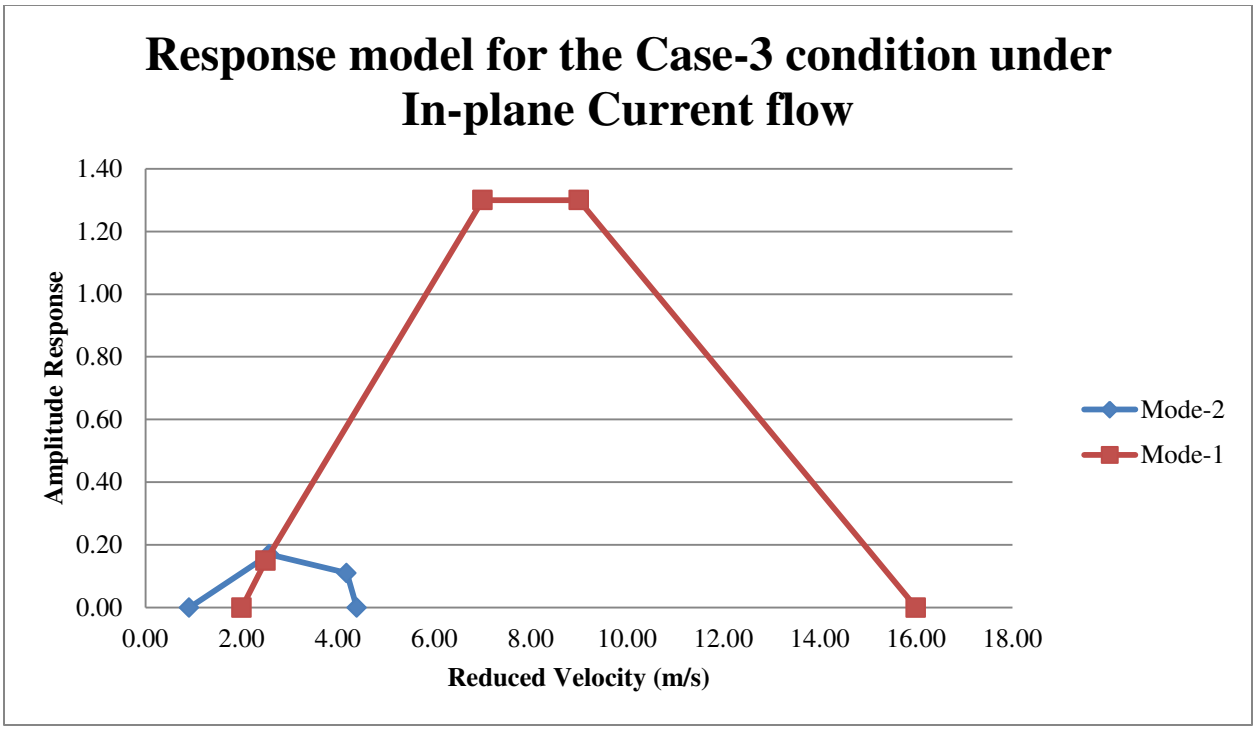

C.9 TYPICAL RESPONSE MODEL UNDER IN-PLANE CURRENT FLOW CONDITION FOR CASE-3

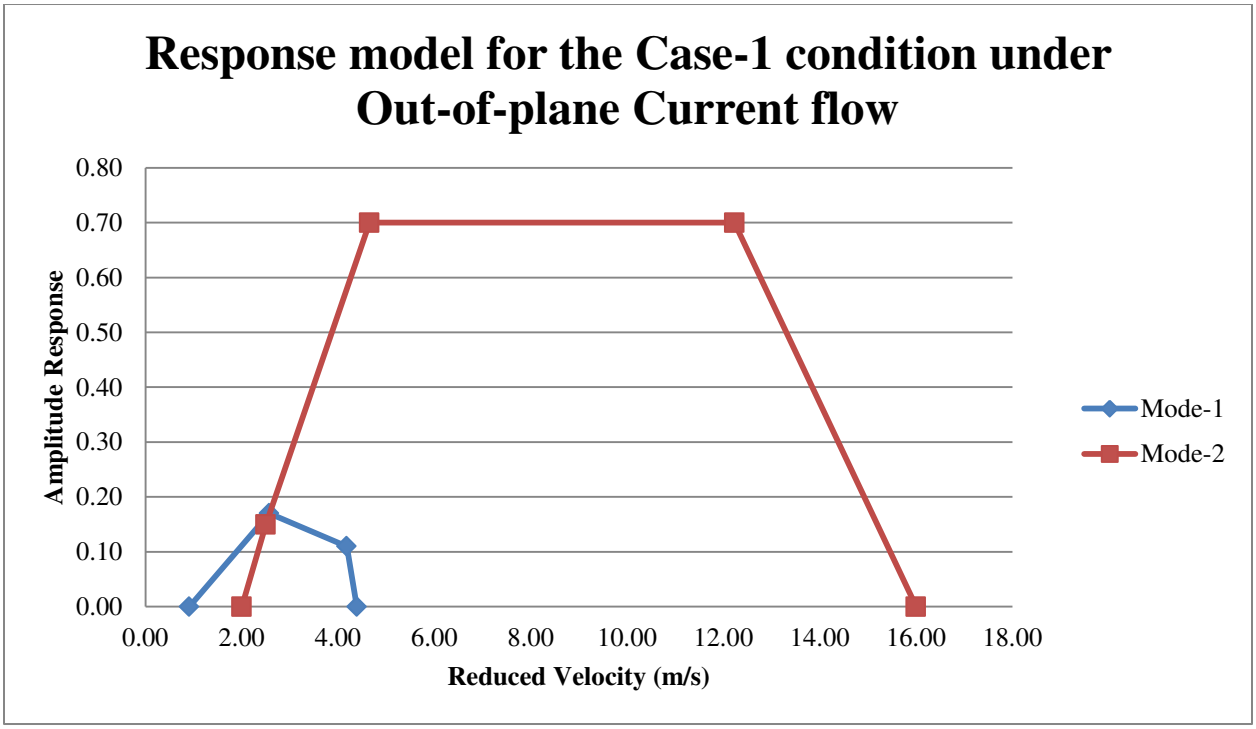

C. 10 TYPICAL RESPONSE MODEL UNDER OUT-OF-PLANE CURRENT FLOW CONDITION FOR CASE-1

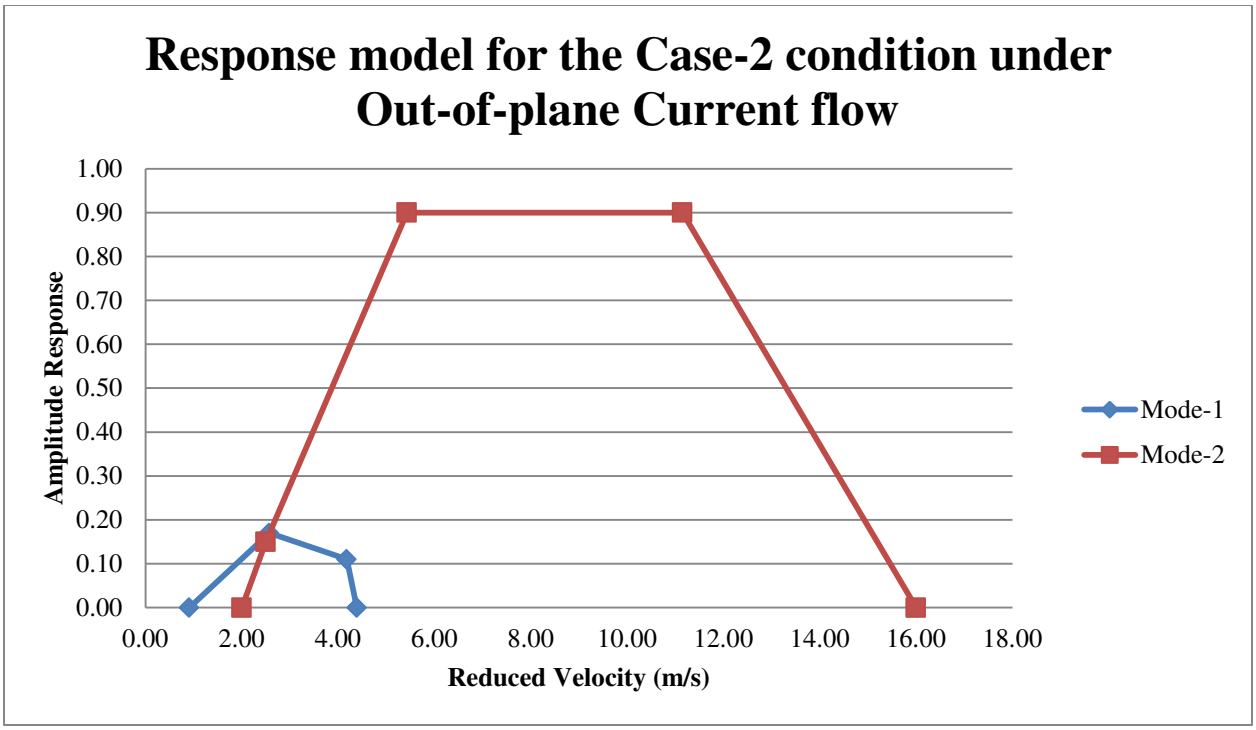

C. 11 TYPICAL RESPONSE MODEL UNDER OUT-OF-PLANE CURRENT FLOW CONDITION FOR CASE-2

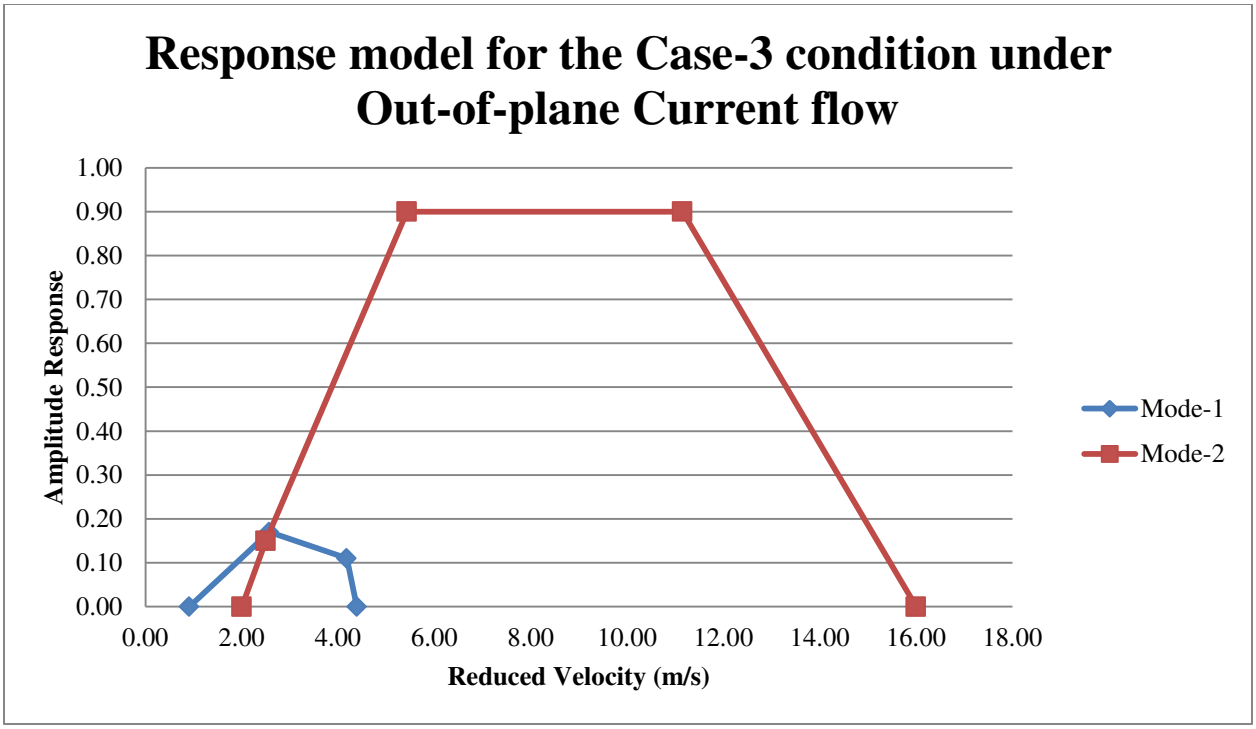

C. 12 TYPICAL RESPONSE MODEL UNDER OUT-OF-PLANE CURRENT FLOW CONDITION FOR CASE-3

ANNEXURE – D

PROFILE SPECIFIC REDUCED VELOCITY (Vr) VARIATION BASED ON THE PROBABILITY OF THE SEABED CURRENT CONDITION

D.1 REDUCED VELOCITY FOR 30 METER JUMPER CONFIGURATION UNDER CASE-1

Case Study	Probability of Occurrence	Seabed Current Velocity	Eigen Frequency	Pipe Diameter	Reduced Velocity
No's	%	m/s	Hz	m	m/s
1	10	0.49	1.81	0.3238	0.84
			4.53		0.33
			4.72		0.32
	25% type-1	0.42	1.81		0.72
			4.53		0.29
			4.72		0.27
	25% type-2	0.36	1.81		0.61
			4.53		0.25
			4.72		0.24
	40	0.29	1.81		0.49
			4.53		0.20
			4.72		0.19

D.2 REDUCED VELOCITY FOR 30 METER JUMPER CONFIGURATION UNDER CASE-2

Case Study	Probability of Occurrence	Seabed Current Velocity	Eigen Frequency	Pipe Diameter	Reduced Velocity
No's	%	m/s	Hz	m	m/s
2	10	0.35	1.81	0.3238	0.60
			4.53		0.24
			4.72		0.23
	25% type-1	0.29	1.81		0.49
			4.53		0.20
			4.72		0.19
	25% type-2	0.23	1.81		0.39
			4.53		0.16
			4.72		0.15
	40	0.18	1.81		0.31
			4.53		0.12
			4.72		0.12

D.3 REDUCED VELOCITY FOR 30 METER JUMPER CONFIGURATION UNDER CASE-3

Case Study	Probability of Occurrence	Seabed Current Velocity	Eigen Frequency	Pipe Diameter	Reduced Velocity
No's	%	m/s	Hz	m	m/s
3	10	0.29	1.81	0.3238	0.49
			4.53		0.20
			4.72		0.19
	25% type-1	0.24	1.81		0.41
			4.53		0.16
			4.72		0.16
	25% type-2	0.19	1.81		0.32
			4.53		0.13
			4.72		0.12
	40	0.14	1.81		0.24
			4.53		0.10
			4.72		0.09

D.4 REDUCED VELOCITY FOR 34 METER JUMPER CONFIGURATION UNDER CASE-1

Case Study	Probability of Occurrence	Seabed Current Velocity	Eigen Frequency	Pipe Diameter	Reduced Velocity
No's	%	m/s	Hz	m	m/s
1	10	0.49	1.47	0.3238	1.03
			3.45		0.44
			3.6		0.42
	25% type-1	0.42	1.47		0.88
			3.46		0.37
			3.6		0.36
	25% type-2	0.36	1.47		0.76
			3.46		0.32
			3.6		0.31
	40	0.29	1.47		0.61
			3.45		0.26
			3.6		0.25

D.5 REDUCED VELOCITY FOR 34 METER JUMPER CONFIGURATION UNDER CASE-2

Case Study	Probability of Occurrence	Seabed Current Velocity	Eigen Frequency	Pipe Diameter	Reduced Velocity
No's	%	m/s	Hz	m	m/s
2	10	0.35	1.47	0.3238	0.74
			3.45		0.31
			3.6		0.30
	25% type-1	0.29	1.47		0.61
			3.45		0.26
			3.6		0.25
	25% type-2	0.23	1.47		0.48
			3.45		0.21
			3.6		0.20
	40	0.18	1.47		0.38
			3.45		0.16
			3.6		0.15

D.6 REDUCED VELOCITY FOR 34 METER JUMPER CONFIGURATION UNDER CASE-3

Case Study	Probability of Occurrence	Seabed Current Velocity	Eigen Frequency	Pipe Diameter	Reduced Velocity
No's	%	m/s	Hz	m	m/s
3	10	0.29	1.47	0.3238	0.61
			3.45		0.26
			3.6		0.25
	25% type-1	0.24	1.47		0.50
			3.45		0.21
			3.6		0.21
	25% type-2	0.19	1.47		0.40
			3.45		0.17
			3.6		0.16
	40	0.14	1.47		0.29
			3.45		0.13
			3.6		0.12

D.7 REDUCED VELOCITY FOR 38 METER JUMPER CONFIGURATION UNDER CASE-1

Case Study	Probability of Occurrence	Seabed Current Velocity	Eigen Frequency	Pipe Diameter	Reduced Velocity
No's	%	m/s	Hz	m	m/s
1	10	0.49	1.22	0.3238	1.24
			2.8		0.54
			2.95		0.51
	25% type-1	0.42	1.22		1.06
			2.8		0.46
			2.95		0.44
	25% type-2	0.36	1.22		0.91
			2.8		0.40
			2.95		0.38
	40	0.29	1.22		0.73
			2.8		0.32
			2.95		0.30

D.8 REDUCED VELOCITY FOR 38 METER JUMPER CONFIGURATION UNDER CASE-2

Case Study	Probability of Occurrence	Seabed Current Velocity	Eigen Frequency	Pipe Diameter	Reduced Velocity
No's	%	m/s	Hz	m	m/s
2	10	0.35	1.22	0.3238	0.89
			2.8		0.39
			2.95		0.37
	25% type-1	0.29	1.22		0.73
			2.8		0.32
			2.95		0.30
	25% type-2	0.23	1.22		0.58
			2.8		0.25
			2.95		0.24
	40	0.18	1.22		0.46
			2.8		0.20
			2.95		0.19

D.9 REDUCED VELOCITY FOR 38 METER JUMPER CONFIGURATION UNDER CASE-3

Case Study	Probability of Occurrence	Seabed Current Velocity	Eigen Frequency	Pipe Diameter	Reduced Velocity
No's	%	m/s	Hz	m	m/s
3	10	0.29	1.22	0.3238	0.73
			2.8		0.32
			2.95		0.30
	25% type-1	0.24	1.22		0.61
			2.8		0.26
			2.95		0.25
	25% type-2	0.19	1.22		0.48
			2.8		0.21
			2.95		0.20
	40	0.14	1.22		0.35
			2.8		0.15
			2.95		0.15

ANNEXURE – E

FLOW SPECIFIC VIV “LOCK-IN” PHENOMENON CHECK

E.1 VIV LOCK-IN CHECK FOR THE IN-PLANE CURRENT CONDITION

Span Length (m)	Water Depth (m)	Mode No.	Eigen Frequency (Hz)	Oscillation Type	Reduced Velocity (m/s)	Lock-in Velocity (m/s)	Lock-in Possibility
30	125	1	1.81	Cross-Flow	0 - 0.84	2 - 16.0	No
		2	4.53	In-Line	0 - 0.33	0.91 - 4.3	No
	250	1	1.81	Cross-Flow	0 - 0.60	2 - 16.0	No
		2	4.53	In-Line	0 - 0.24	0.91 - 4.3	No
	1000	1	1.81	Cross-Flow	0 - 0.50	2 - 16.0	No
		2	4.53	In-Line	0 - 0.20	0.91 - 4.3	No
34	125	1	1.47	Cross-Flow	0 - 1.03	2 - 16.0	No
		2	3.45	In-Line	0 - 0.44	0.91 - 4.3	No
	250	1	1.47	Cross-Flow	0 - 0.74	2 - 16.0	No
		2	3.45	In-Line	0 - 0.31	0.91 - 4.3	No
	1000	1	1.47	Cross-Flow	0 - 0.61	2 - 16.0	No
		2	3.45	In-Line	0 - 0.26	0.91 - 4.3	No
38	125	1	1.22	Cross-Flow	0 - 1.24	2 - 16.0	No
		2	2.80	In-Line	0 - 0.54	0.91 - 4.3	No
	250	1	1.22	Cross-Flow	0 - 0.89	2 - 16.0	No
		2	2.80	In-Line	0 - 0.39	0.91 - 4.3	No
	1000	1	1.22	Cross-Flow	0 - 0.73	2 - 16.0	No
		2	2.80	In-Line	0 - 0.32	0.91 - 4.3	No

E.2 VIV LOCK-IN CHECK FOR THE OUT-OF-PLANE CURRENT CONDITION

Span Length (m)	Water Depth (m)	Mode No.	Eigen Frequency (Hz)	Oscillation Type	Reduced Velocity (m/s)	Lock-in Velocity (m/s)	Lock-in Possibility
30	125	1	1.81	In-Line	0 - 0.84	0.91 – 4.3	No
		2	4.53	Cross-Flow	0 - 0.33	2 - 16	No
	250	1	1.81	In-Line	0 - 0.60	0.91 – 4.3	No
		2	4.53	Cross-Flow	0 - 0.24	2 - 16	No
	1000	1	1.81	In-Line	0 - 0.50	0.91 – 4.3	No
		2	4.53	Cross-Flow	0 - 0.20	2 - 16	No
34	125	1	1.47	In-Line	0 - 1.03	0.91 – 4.3	Yes
		2	3.45	Cross-Flow	0 - 0.44	2 - 16	No
	250	1	1.47	In-Line	0 - 0.74	0.91 – 4.3	No
		2	3.45	Cross-Flow	0 - 0.31	2 - 16	No
	1000	1	1.47	In-Line	0 - 0.61	0.91 – 4.3	No
		2	3.45	Cross-Flow	0 - 0.26	2 - 16	No
38	125	1	1.22	In-Line	0 - 1.24	0.91 – 4.3	Yes
		2	2.80	Cross-Flow	0 - 0.54	2 - 16	No
	250	1	1.22	In-Line	0 - 0.89	0.91 – 4.3	No
		2	2.80	Cross-Flow	0 - 0.39	2 - 16	No
	1000	1	1.22	In-Line	0 - 0.73	0.91 – 4.3	No
		2	2.80	Cross-Flow	0 - 0.32	2 - 16	No

ANNEXURE – F

CONFIGURATION SPECIFIC FATIGUE STRESS RANGE EVALUATION

The following stress range evaluation is based on the oscillation type involved in the system based on the current flow direction considered. It is also based on the relation between the pure inline, pure cross-flow & the cross-flow induced inline amplitude as detailed in figure F.1 below. There are also some conditions specified in the DNV-RP-F105 Appendix A, related to the applicability of the considered oscillations for the fatigue stress evaluation.

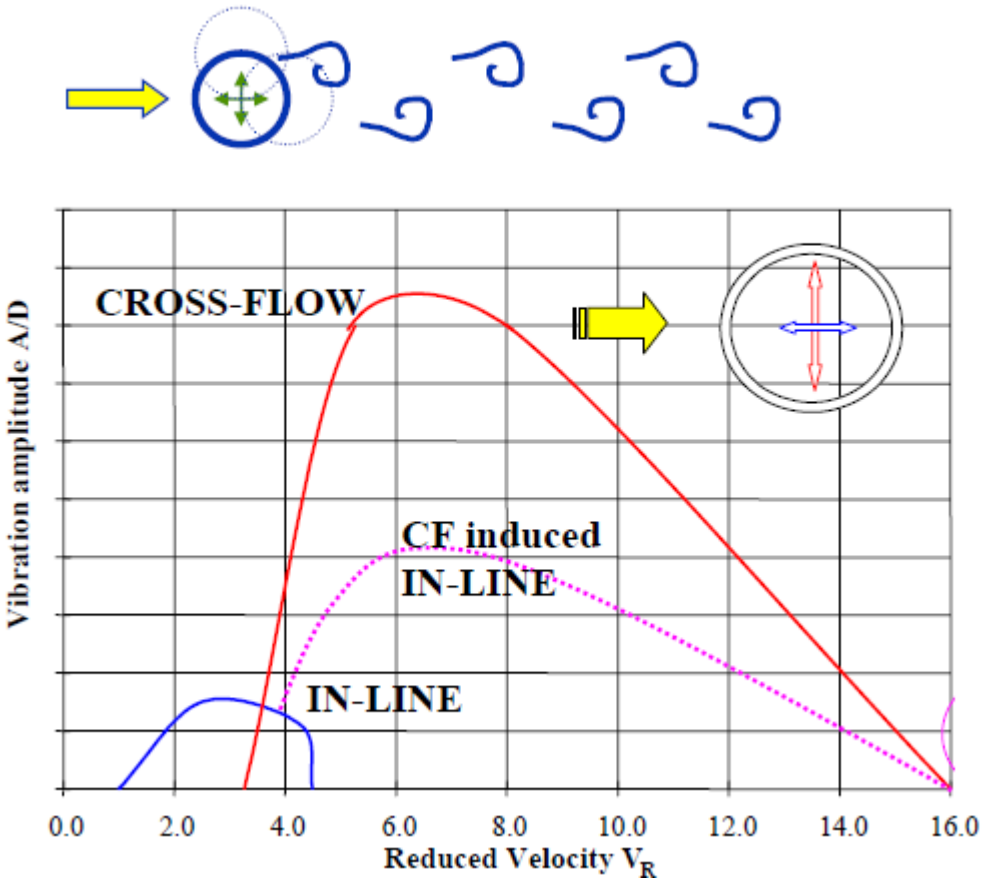

F.1 RELATION BETWEEN THE INLINE, CROSS-FLOW & CROSS-FLOW INDUCED INLINE AMPLITUDES.

Conditions to be considered in the stress calculation based on DNV-RP-F105 Appendix. A:-

i. Potential IL induced cross-flow response is neglected for an IL response mode with a reduced velocity of 2-3.
ii. The effect of the cross-flow induced IL motion also needs to be considered whenever relevant.
iii. The possible responses include dominant pure inline & cross-flow with the possibility of IL induced cross-flow & cross-flow induced IL whenever applicable.

Out of all the possible combinations between the jumper profile & the water depth of operation, only the jumpers with a span length of 34 & 38 meters experience the “Lock-in” phenomenon

under 125 meters of water depth. Even this will happen only under the out-of-plane current flow condition. This is because of the strong current existence & the lower Eigen frequency from the increased unsupported length of the jumper.

The stress range tables of the 34 & 38 meter jumpers profile, for the above mentioned scenario are given in the table F.3 & F.4 below.

F.2 UNIT AMPLITUDE STRESS VARIATION

For 30 m Jumper Configuration			
Current Flow type	**Mode No.**	**Type of Oscillation**	**Unit Amplitude Stress**
In-Plane / Out-of-Plane	No's	In-Line / Cross-Flow	Mpa
In-Plane	1	Cross-Flow	838.32
	2	In-line	1392.9
Out-of-Plane	1	In-line	838.32
	2	Cross-Flow	1392.9
For 34 m Jumper Configuration			
Current Flow type	**Mode No.**	**Type of Oscillation**	**Unit Amplitude Stress**
In-Plane / Out-of-Plane	No's	In-Line / Cross-Flow	Mpa
In-Plane	1	Cross-Flow	819.81
	2	In-line	1450
Out-of-Plane	1	In-line	819.81
	2	Cross-Flow	1450
For 38 m Jumper Configuration			
Current Flow type	**Mode No.**	**Type of Oscillation**	**Unit Amplitude Stress**
In-Plane / Out-of-Plane	No's	In-Line / Cross-Flow	Mpa
In-Plane	1	Cross-Flow	803.43
	2	In-line	1307.8
Out-of-Plane	1	In-line	803.43
	2	Cross-Flow	1307.8

F.3 EVALUATION OF STRESS RANGE FOR THE 34 m JUMPER UNDER OUT-OF-PLANE CURRENT

Amplitude Reduction Factor due to Damping			0.9805	No Unit		Current Flow Ratio Correction Factor			0.986	No Unit
Safety Factor			1.3	No Unit		Competing Modes Reduction Factor			1	No Unit
Span Length (m)	**In-Line Mode Unit Stress Amplitude (Mpa)**	**Cross-Flow Mode Unit Stress Amplitude (Mpa)**	**Water Depth (m)**	**Current Velocity (m/s)**	**Maximum Inline VIV Response Amplitude (No Unit)**	**Maximum Cross-Flow VIV Response Amplitude (No Unit)**	**Stress Range due to pure cross-flow response (Mpa)**	**Stress Range due to pure inline response (Mpa)**	**Stress Range due to inline induced crossflow response (Mpa)**	**Total Stress Range for the considered case (Mpa)**
34	819.81	1450	125	0.29	0	0	0	0	0	0
				0.36	0	0	0	0	0	0
				0.42	0	0	0	0	0	0
				0.49	0.008	0	0	16.81	0	16.81

F.4 EVALUATION OF STRESS RANGE FOR THE 38 m JUMPER UNDER OUT-OF-PLANE CURRENT

Amplitude Reduction Factor due to Damping			0.9805	No Unit		Current Flow Ratio Correction Factor			0.986/0.873	No Unit
Safety Factor			1.3	No Unit		Competing Modes Reduction Factor			1	No Unit
Span Length (m)	**In-Line Mode Unit Stress Amplitude (Mpa)**	**Cross-Flow Mode Unit Stress Amplitude (Mpa)**	**Water Depth (m)**	**Current Velocity (m/s)**	**Maximum Inline VIV Response Amplitude (No Unit)**	**Maximum Cross-Flow VIV Response Amplitude (No Unit)**	**Stress Range due to pure cross-flow response (Mpa)**	**Stress Range due to pure inline response (Mpa)**	**Stress Range due to inline induced crossflow response (Mpa)**	**Total Stress Range for the considered case (Mpa)**
38	803.43	1307.8	125	0.29	0	0	0	0	0	0
				0.36	0	0	0	0	0	0
				0.42	0.01	0	0	18.24	0	18.24
				0.49	0.034	0	0	70.06	0	70.06

ANNEXURE – G

CURRENT FLOW BASED EVALUATION OF THE FATIGUE LIFE

G.1 EVALUATION OF THE FATIGUE LIFE FOR THE IN-PLANE CURRENT FLOW CONDITION

Characteristic Fatigue Strength Constant (a)			74757.14	No Unit	Fatigue Exponent (m)			3	No Unit
Span Length (m)	**Water Depth (m)**	**Mode No**	**Eigen Frequency (Hz)**	**Oscillation Type**	**Stress Range (Mpa)**	**Stress Concentration Factor (SCF) (No Unit)**	**Number of Cycles to Failure (N)**	**Number of Cycles per Year (n)**	**Fatigue life of the system (Years)**
30	125	1	1.81	Cross-Flow	0	1.00	Infinity	0	Infinity
		2	4.53	In-Line	0		Infinity	0	Infinity
	250	1	1.81	Cross-Flow	0		Infinity	0	Infinity
		2	4.53	In-Line	0		Infinity	0	Infinity
	1000	1	1.81	Cross-Flow	0		Infinity	0	Infinity
		2	4.53	In-Line	0		Infinity	0	Infinity
34	125	1	1.47	Cross-Flow	0		Infinity	0	Infinity
		2	3.45	In-Line	0		Infinity	0	Infinity
	250	1	1.47	Cross-Flow	0		Infinity	0	Infinity
		2	3.45	In-Line	0		Infinity	0	Infinity
	1000	1	1.47	Cross-Flow	0		Infinity	0	Infinity
		2	3.45	In-Line	0		Infinity	0	Infinity
38	125	1	1.22	Cross-Flow	0		Infinity	0	Infinity
		2	2.80	In-Line	0		Infinity	0	Infinity
	250	1	1.22	Cross-Flow	0		Infinity	0	Infinity
		2	2.80	In-Line	0		Infinity	0	Infinity
	1000	1	1.22	Cross-Flow	0		Infinity	0	Infinity
		2	2.80	In-Line	0		Infinity	0	Infinity

G.2 EVALUATION OF THE FATIGUE LIFE FOR THE OUT-OF-PLANE CURRENT FLOW CONDITION

Characteristic Fatigue Strength Constant (a)			74757.14	No Unit	Fatigue Exponent (m)			3	No Unit
Span Length (m)	**Water Depth (m)**	**Mode No**	**Eigen Frequency (Hz)**	**Oscillation Type**	**Stress Range (Mpa)**	**Stress Concentration Factor (SCF) (No Unit)**	**Number of Cycles to Failure (N) x10^6**	**Number of Cycles per Year (n) x10^6**	**Fatigue life of the system (Years)**
30	125	1	1.81	In-line	0	1.00	Infinity	0	Infinity
		2	4.53	Cross-Flow	0		Infinity	0	Infinity
	250	1	1.81	In-line	0		Infinity	0	Infinity
		2	4.53	Cross-Flow	0		Infinity	0	Infinity
	1000	1	1.81	In-line	0		Infinity	0	Infinity
		2	4.53	Cross-Flow	0		Infinity	0	Infinity
34	125	1	1.47	In-line	16.81		15.74	4.64	3.4
		2	3.45	Cross-Flow	0		Infinity	0	Infinity
	250	1	1.47	In-line	0		Infinity	0	Infinity
		2	3.45	Cross-Flow	0		Infinity	0	Infinity
	1000	1	1.47	In-line	0		Infinity	0	Infinity
		2	3.45	Cross-Flow	0		Infinity	0	Infinity
38	125	1	1.22	In-line	88.30		0.22	3.85	0.06
		2	2.80	Cross-Flow	0		Infinity	0	Infinity
	250	1	1.22	In-line	0		Infinity	0	Infinity
		2	2.80	Cross-Flow	0		Infinity	0	Infinity
	1000	1	1.22	In-line	0		Infinity	0	Infinity
		2	2.80	Cross-Flow	0		Infinity	0	Infinity

ANNEXURE – H

VARIATION OF THE FATIGUE LIFE UNDER OUT-OF-PLANE CURRENT FLOW CONDITION BASED ON THE PROBABILITY OF OCCURRENCE VARIATION

H.1 VARIATION ON THE OCCURRENCE OF THE CURRENT AT THE 125 (m) WATER DEPTH CASE

Case-1 (a)		Case-1 (b)		Case-1 (c)		Case-1 (d)		Case-1 (e)		Case-1 (f)	
Current Velocity (m/s)	Occurrence (%)	Current Velocity (m/s)	Occurrence (%)	Current Velocity (m/s)	Occurrence (%)	Current Velocity (m/s)	Occurrence (%)	Current Velocity (m/s)	Occurrence (%)	Current Velocity (m/s)	Occurrence (%)
0.29	40	0.29	50	0.29	60	0.29	70	0.29	80	0.29	85
0.36	25	0.36	25	0.36	20	0.36	20	0.36	15	0.36	10
0.42	25	0.42	20	0.42	18	0.42	9	0.42	4	0.42	4
0.49	10	0.49	5	0.49	2	0.49	1	0.49	1	0.49	1

H.2 EVALUATION OF FATIGUE LIFE BASED ON THE PROBABILITY OF OCCURRENCE

Water Depth (m)	Span Length (m)	Mode No	Eigen Frequency (Hz)	Oscillation Type	Stress Range (Mpa)	Stress Concentration Factor (SCF) (No Unit)	Number of Cycles to Failure (N) x10^6	Number of Cycles per Year (n) x10^6	Fatigue life of the system (Years)
Case-1 (a)									
125	34	1	1.47	In-Line	16.81	1	15.74	4.64	3.4
		2	3.45	Cross-Flow	0		Infinity	0	Infinity
	38	1	1.22	In-Line	88.30		0.22	3.85	0.06
		2	2.80	Cross-Flow	0		Infinity	0	Infinity
Case-1 (b)									
125	34	1	1.47	In-Line	16.81	1	15.74	2.32	6.8
		2	3.45	Cross-Flow	0		Infinity	0	Infinity
	38	1	1.22	In-Line	88.30		0.22	1.92	0.12
		2	2.80	Cross-Flow	0		Infinity	0	Infinity
Case-1 (c)									
125	34	1	1.47	In-Line	16.81	1	15.74	0.92	17.12
		2	3.45	Cross-Flow	0		Infinity	0	Infinity
	38	1	1.22	In-Line	88.30		0.22	0.77	0.28
		2	2.80	Cross-Flow	0		Infinity	0	Infinity

H.2 EVALUATION OF FATIGUE LIFE BASED ON THE PROBABILITY OF OCCURRENCE (CONTINUES)

Water Depth (m)	Span Length (m)	Mode No	Eigen Frequency (Hz)	Oscillation Type	Stress Range (Mpa)	Stress Concentration Factor (SCF) (No Unit)	Number of Cycles to Failure (N) x10^6	Number of Cycles per Year (n) x10^6	Fatigue life of the system (Years)
Case-1 (d)									
125	34	1	1.47	In-Line	16.81	1	15.74	0.46	34.2
		2	3.45	Cross-Flow	0		Infinity	0	Infinity
	38	1	1.22	In-Line	88.30		0.22	0.38	0.60
		2	2.80	Cross-Flow	0		Infinity	0	Infinity
Case-1 (e)									
125	34	1	1.47	In-Line	16.81	1	15.74	0.46	34.2
		2	3.45	Cross-Flow	0		Infinity	0	Infinity
	38	1	1.22	In-Line	88.30		0.22	0.38	0.60
		2	2.80	Cross-Flow	0		Infinity	0	Infinity
Case-1 (f)									
125	34	1	1.47	In-Line	16.81	1	15.74	0.46	34.2
		2	3.45	Cross-Flow	0		Infinity	0	Infinity
	38	1	1.22	In-Line	88.30		0.22	0.38	0.60
		2	2.80	Cross-Flow	0		Infinity	0	Infinity